OCEAN DRILLING PROGRAM

LEG 182 PRELIMINARY REPORT

GREAT AUSTRALIAN BIGHT: CENOZOIC COOL-WATER CARBONATES

Dr. David Feary
Co-Chief Scientist
Australian Geological Survey Organisation
G.P.O. Box 378
Canberra, ACT 2601
Australia

Dr. Albert C. Hine
Co-Chief Scientist
Department of Marine Science
University of South Florida, St. Petersburg
140 7th Avenue South
St. Petersburg, FL 33701
U.S.A.

Dr. Mitchell J. Malone
Staff Scientist
Ocean Drilling Program
Texas A&M University Research Park
1000 Discovery Drive
College Station, TX 77845-9547
U.S.A.

Dr. Jack Baldauf
Deputy Director of
Science Operations
ODP/TAMU

Dr. Mitchell J. Malone
Leg Project Manager
Science Services
ODP/TAMU

January 1999

This informal report was prepared from the shipboard files by the scientists who participated in the cruise. The report was assembled under time constraints and is not considered to be a formal publication which incorporates final works or conclusions of the participating scientists. The material contained herein is privileged proprietary information and cannot be used for publication or quotation.

Preliminary Report No. 82

First Printing 1999

Distribution

Electronic copies of this publication may be obtained from the ODP Publications Homepage on the World Wide Web at http://www-odp.tamu.edu/publications.

D I S C L A I M E R

This publication was prepared by the Ocean Drilling Program, Texas A&M University, as an account of work performed under the international Ocean Drilling Program, which is managed by Joint Oceanographic Institutions, Inc., under contract with the National Science Foundation. Funding for the program is provided by the following agencies:

Australia/Canada/Chinese Taipei/Korea Consortium for the Ocean Drilling
Deutsche Forschungsgemeinschaft (Germany)
Institut Français de Recherche pour l'Exploitation de la Mer (France)
Ocean Research Institute of the University of Tokyo (Japan)
National Science Foundation (United States)
Natural Environment Research Council (United Kingdom)
European Science Foundation Consortium for the Ocean Drilling Program (Belgium, Denmark, Finland, Iceland, Italy, The Netherlands, Norway, Spain, Sweden, and Switzerland)
Marine High-Technology Bureau of the State Science and Technology Commission of the People's Republic of China

The following scientists were aboard *JOIDES Resolution* for Leg 182 of the Ocean Drilling Program:

David A. Feary
Co-Chief Scientist
Australian Geological Survey Organisation
GPO Box 378
Canberra, ACT 2601
Australia
Internet: dfeary@agso.gov.au
Work: 61-2-6249-9798
Fax: 61-2-6249-9980

Albert C. Hine
Co-Chief Scientist
Department of Marine Science
University of South Florida, St. Petersburg
140 7th Avenue South
St. Petersburg, FL 33701
U.S.A.
Internet: hine@seas.marine.usf.edu
Work: 813-553-1161
Fax: 813-553-1189

Mitchell J. Malone
Staff Scientist
Ocean Drilling Program
Texas A&M University Research Park
1000 Discovery Drive
College Station, TX 77845
U.S.A.
Internet: mitchell_malone@odp.tamu.edu
Work: 409-845-5218
Fax: 409-845-0876

Miriam Andres
Sedimentologist
Geologisches Institut
Eidgenössische Technische Hochschule - Zentrum
Sonneggstrasse 5
Zürich 8092
Switzerland
Internet: miriam@erdw.ethz.ch
Work: 41-1-632-4818
Fax: 41-1-632-1080

Christian Betzler
Sedimentologist
Geologische-Paläontologisches Institut
Johann Wolfgang Geothe-Universität Frankfurt am Main
Senskenberganlage 32-34
Postfach 11-19-32
Frankfurt-am-Main 60054
Federal Republic of Germany
Internet: betzler@em.uni-frankfurt.d400.de
Work: 49-69-798-23107
Fax: 49-69-798-22958

Gregg R. Brooks
Sedimentologist
Department of Marine Science
Eckerd College
4200 54th Avenue South
St. Petersburg, FL 33711
U.S.A.
Internet: brooksgr@eckerd.edu
Work: 813-864-8992
Fax: 813-864-7964

Charlotte A. Brunner
Paleontologist (planktonic foraminifers)
Center for Marine Science
University of Southern Mississippi
Building 1103, Room 102
Stennis Space Center, MS 39529
U.S.A.
Internet: cbrunner@sunfish.st.usm.edu
Work: 228-688-3402
Fax: 228-688-1121

Michael Fuller
Paleomagnetist
Hawaii Institute of Geophysics and Planetology-SOEST
University of Hawaii
2525 Correa Road
Honolulu, HI 96822
U.S.A.
Internet: mfuller@soest.hawaii.edu
Work: 808-956-4038, Fax: 808-956-3188

Roberto S. Molina Garza
Paleomagnetist
Department of Earth and Planetary Sciences
University of New Mexico
Northrop Hall
Albuquerque, NM 87131-1116
U.S.A.
Internet: molina@unm.edu
Work: 505-277-5261
Fax: 505-277-8843

Ann E. Holbourn
Paleontologist (benthic foraminifers)
Department of Paleontology
Natural History Museum
Cromwell Road
London SW7 5BD
United Kingdom
Internet: a.holbourn@nhm.ac.uk
Work: 44-171-938-9046
Fax: 44-171-938-9277

Mads Huuse
LDEO Logging Trainee
Department of Earth Sciences
Aarhus Universitet
Finlandsgade 8
Aarhus N 8200
Denmark
Internet: mhuuse@geoserver1.aau.dk
Work: 45-8942-4343
Fax: 45-8610-1003

Alexandra R. Isern
JOIDES Logging Scientist/Physical Properties Specialist
Division of Geology and Geophysics
University of Sydney
Building F05
Sydney, NSW 2006
Australia
Internet: aisern@mail.usyd.edu.au
Work: 61-2-9351-3998
Fax: 61-2-9351-0184

Noel P. James
Sedimentologist
Department of Geological Sciences
Queen’s University at Kingston
Kingston, ON K7L 3N6
Canada
Internet: james@geol.queensu.ca
Work: 613-545-2597
Fax: 613-545-6592

Bryan C. Ladner
Paleontologist (nannofossils)
Department of Geology
Florida State University
108 Carraway Building
Tallahassee, FL 32306-4100
U.S.A.
Internet: ladner@quartz.gly.fsu.edu
Work: 850-644-5860
Fax: 850-644-4214

Qianyu Li
Paleontologist (planktonic foraminifers)
Department of Geology and Geophysics
University of Adelaide
Adelaide, South Australia 5005
Australia
Internet: qli@geology.adelaide.edu.au
Work: 61-8-8303-5826
Fax: 61-8-8303-4347

Hideaki Machiyama
Sedimentologist
Deep Sea Research Department
Oceanic Crust Dynamics Research
Japan Marine Science and Technology Center
2-15 Natsushimacho
Yokosuka, Kanagawa 237
Japan
Internet: bucci@jamstec.go.jp
Work: 81-468-67-3395
Fax: 81-468-67-3409

David J. Mallinson
Physical Properties Specialist/Stratigraphic Correlator
Department of Marine Science
University of South Florida, St. Petersburg
140 Seventh Avenue South
St. Petersburg, FL 33701
U.S.A.
Internet: davem@seas.marine.usf.edu
Work: 813-553-3927
Fax: 813-553-1189

Hiroki Matsuda
Sedimentologist
Department of Earth Sciences
Kumamoto University
2-39-1 Kurokami
Kumamoto, Kumamoto 860
Japan
Internet: hmat@sci.kumamoto-u.ac.jp
Work: 81-96-342-3424
Fax: 81-96-342-3411

Richard M. Mitterer
Organic Geochemist
Programs in Geosciences
University of Texas at Dallas
P.O. Box 830688
Richardson, TX 75083-0688
U.S.A.
Internet: mitterer@utdallas.edu
Work: 972-883-2462
Fax: 972-883-2537

Cécile Robin
Physical Properties Specialist
Laboratoire de Géologie de Bassins Sédimentaires
Université Pierre et Marie Curie
4 Place Jussieu
Paris Cedex 05 75252
France
Internet: robin@ccr.jussieu.fr
Work: 33-1-4427-2760
Fax: 33-1-4427-4965

Joellen L. Russell
Physical Properties Specialist
Scripps Institution of Oceanography
University of California, San Diego
Marine Physical Laboratory
9500 Gilman Drive
La Jolla, CA 92093-0208
U.S.A.
Internet: jlrussel@ucsd.edu
Work: 619-534-2582
Fax: 619-456-9079

Samir Shafik
Paleontologist (nannofossils)
Marine Geoscience and Petroleum Geology Program
Australian Geological Survey Organisation
GPO Box 378
Canberra, ACT 2601
Australia
Internet: sshafik@agso.gov.au
Work: 61-6-249-9436
Fax: 61-6-249-9981

J. A. (Toni) Simo
Sedimentologist
Department of Geology and Geophysics
University of Wisconsin-Madison
1215 West Dayton Street
Madison, WI 53706
U.S.A.
Internet: simo@geology.wisc.edu
Work: 608-262-5987
Fax: 608-262-0693

Peter L. Smart
Physical Properties Specialist
Department of Geography
University of Bristol
University Road
Bristol BS8 1SS
United Kingdom
Internet: smartpl@gma.bris.ac.uk
Work: 44-1179-288305
Fax: 44-1179-287878

Guy H. Spence
LDEO Logging Scientist
Department of Geology
University of Leicester
Borehole Research
Leicester LE1 7RH
United Kingdom
Internet: ghs2@leicester.ac.uk
Work:
Fax: 44-116-252-3918

Finn C. Surlyk
Sedimentologist
Geologisk Institut
Københavns Universitet
Øster Voldgade 10
København K 1350
Denmark
Internet: finns@geo.geol.ku.dk
Work: 45-3532-2453
Fax: 45-3314-8322

Peter K. Swart
Inorganic Geochemist
Rosenstiel School of Marine and Atmospheric Science
University of Miami
4600 Rickenbacker Causeway
Miami, FL 33149
U.S.A.
Internet: pswart@rsmas.miami.edu
Work: 305-361-4103
Fax: 305-361-4632

Ulrich G. Wortmann
Inorganic Geochemist
Department of Geology
Eidgenössische Technische Hochschule - Zentrum
Sonneggstrasse 5
Zûrich 8092
Switzerland
Internet: uliw@bonk.ethz.ch
Work: 41-632-3694
Fax: 41-632-1080

(This page is intentionally left blank)

SCIENTIFIC REPORT

(This page is intentionally left blank)

ABSTRACT

Sediments recovered in the Great Australian Bight during Leg 182 record carbonate deposition in a middle- and high-latitude setting against the background of an evolving Southern Ocean and northward drift of the Australian continent. Approximately 3.5 km of sediments was recovered from nine sites, in water depths ranging from 202 to 3875 m. Most drilling took place on the shelf edge and upper slope, in 202–784 m water depth, through a mainly carbonate succession.

Two distinct groups of strata, Eocene–middle Miocene and Pleistocene in age, form the upper Cenozoic component of the continental margin, separated by a thin, upper middle Miocene–Pliocene interval characterized by slumps, sediment gravity-flow deposits, or unconformities. Such erosion, corrosion, and/or mass wasting and redeposition processes reflect periods of margin instability, seismicity, or lowered sea level.

The older succession consists of Eocene shallow-water terrigenous sands and carbonates that deepen upward into Oligocene and early-middle Miocene pelagic ooze and chalk. The carbonate component was poorly recovered because of irregular selective silicification, with available cored material indicating a sequence dominated by nannofossil chalk with abundant sponge spicules and characterized by stained hardgrounds and numerous omission surfaces. The high-quality downhole logs collected through all poorly recovered intervals will enable more detailed postcruise lithological analysis for this part of the succession. In contrast, the middle Eocene–early Oligocene succession was well recovered on the continental rise at Site 1128 in 3875 m water depth, and it contains an excellent expanded (>350 m) siliceous biogenic record of proto Circum-Antarctic Current evolution.

The younger Pleistocene package is a spectacular, extraordinarily thick (> 500 m), seaward-dipping wedge of carbonate sediment on the shelf-edge/uppermost slope that prograded seaward onto the Eyre Terrace and downlaps onto older sediments. Rates of accumulation exceed 40 cm/k.y., equivalent to many shallow-water tropical carbonates and twice the rate of Bahamian slope sedimentation. These green and gray carbonate strata are surprisingly uniform in composition, made up of fine carbonate sand and silt composed of skeletal fragments, mainly delicate bryozoans, ostracodes, benthic and planktonic foraminifer tests, tunicate sclerites, nannofossils, and siliceous sponge spicules. The facies transition upslope into shallower water is marked by the presence of numerous spectacular bryozoan-rich buildups. These mounds, in water depths of ~200–350 m, are characterized by numerous and diverse bryozoans, with intervening bioclastic sand and mud. These are among the first modern analogs of similar mounds that were an important component of carbonate depositional regimes in earlier Phanerozoic time.

One of the surprising discoveries of Leg 182 was the presence of a brine, varying in salinity between 80 and 105, within and underlying seven drill sites. The Cl^- distribution at three sites (1127, 1129, and 1131) suggests that the top of the brine has an essentially uniform depth below sea level and, therefore, crosscuts sequence boundaries. Although the origin of the brine has not yet been established, pore fluids in the Pleistocene portion of the sediments from the shallow water sites possess a Na^+/Cl^- ratio greater than that of seawater, suggesting that fluids in these sediments were involved in the dissolution of NaCl. It is likely that further postcruise study of the nature and distribution of this brine will shed light on lowstand shelf evaporative processes and the nature of fluid flow within cool-water carbonate margin sediments. Because of high sedimentation rates and their location at the edge of a broad continental shelf, the shallow water sites initially contained a high concentration of organic material. The brine underlying and within the Pleistocene succession contains up to three times normal sulfate concentrations and, with sufficient organic material, was therefore able to produce significant amounts of hydrogen sulfide. In addition, the relatively low iron concentration in these carbonate sediments means that the H_2S was not sequestered as iron sulfides. Consequently, H_2S concentrations were able to reach high levels, >150,000 ppm at one site. The oxidation of organic material also had an important influence on carbonate recrystallization, which is occurring at higher rates than previously thought possible for cool-water carbonates.

INTRODUCTION

Carbonate sediments and sedimentary rocks contain a particularly sensitive record of paleoceanographic and biostratigraphic evolution. The focus of the Ocean Drilling Program (ODP) carbonate drilling on continental margins has largely been in warm-water environments. There is a complete sedimentary realm whose nature and history have not yet been investigated— that of continental margin cool-water carbonates. These biogenic sediments, formed where seawater temperatures rarely rise above 20°C, commonly mantle continental margins in middle and high latitudes. They are untapped storehouses of information regarding the evolution of global climates, eustacy, and marine biology.

The southern Australian continental margin is the ideal location to study cool-water carbonate facies and evolution. The shelf has been the site of cool-water carbonate sedimentation since Eocene time, resulting in an almost 1-km-thick succession. It is now the largest area on the globe composed of such sediments. In addition, slight tectonic tilting during the late Miocene has led to subaerial exposure of Eocene–middle Miocene strata in extensive, shallow basins. These sediments form a more compressed and less continuous section than the section offshore, yet

they have allowed the development of actualistic models for the formation and development of cool-water carbonates. These models can be tested and greatly expanded by drilling.

A critically important benefit of drilling in the Great Australian Bight is that, because the shelf is latitudinally parallel to the southern margin of the Australian plate, the sediments contain a record of the development of the Southern Ocean. In particular, the region offers the potential to collect high-resolution stable isotopic and biostratigraphic profiles to clarify several important stages in the evolution of the Southern Ocean.

Drilling in the Great Australian Bight provided essential and original information on the contrast between the sedimentologic, paleontologic, paleoceanographic, and climatic records from warm- and cool-water realms. It will also allow the development of well-constrained and greatly needed models that can be used in the interpretation of older Mesozoic and Paleozoic continental margin carbonate systems.

Background

Tectonic Setting

The southern margin of the Australian continent is a divergent, passive continental margin that formed during the protracted period of extension and rifting that led to the separation of Australia and Antarctica in the Cretaceous and that evolved during the subsequent northward drift of the Australian continent. The initial extension phase before breakup in the mid-Cretaceous (96 Ma), together with the subsequent period of slow spreading until the middle Eocene (49 Ma), resulted in deep continental margin basins filled with as much as 12 km of mainly terrigenous clastic sediments (Willcox et al., 1988; Davies et al., 1989). These basins broadly correspond to the sites of modern upper slope terraces (e.g., the Eyre Terrace at 400–1600 m depth in the western Great Australian Bight; Fig. 1). The onset of faster spreading in the middle Eocene also corresponded with the establishment of fully marine conditions and the initiation of carbonate sedimentation in the widening "gulf" between Australia and Antarctica. Carbonate sedimentation continued throughout the remainder of the Cenozoic as the gulf evolved first into a broad, open seaway and then into the modern Southern Ocean. Cenozoic sedimentation resulted in an extensive, relatively thin (up to 800 m; Feary and James, 1998) Eucla Basin succession deposited in a predominantly platform-sag to platform-edge tectonic regime (Stagg et al., 1990).

Throughout the Cenozoic, the western Great Australian Bight portion of Australia’s southern continental margin has been particularly stable, with geohistory analysis of the Jerboa-1 exploration well indicating minimal Tertiary subsidence (Hegarty et al., 1988). Slight regional tilting (<1°?) during the middle Miocene resulted in uplift and exposure of the Nullarbor Plain and restriction of Neogene sedimentation to the modern outer shelf and upper slope.

Cenozoic Stratigraphy of the Eucla Basin

The Eucla Basin extends inland as far as 350 km from the present coastline and seaward some 200 km to the modern shelf edge and upper slope. Inland, the Eucla Basin succession thins and feathers out against Precambrian basement; it then gradually thickens southward to its thickest point beneath the modern shelf edge (Fig. 2). The Eucla Basin succession is entirely carbonate, apart from the basal siliciclastic sequence both offshore (Sequence 7) and onshore (Hampton Sandstone), and a thin, transgressive, paleovalley-filling and strandline succession of terrigenous clastics on the inland margins of the basin.

The succession is basically divisible into two mega-sequences: a Mesozoic (Late Jurassic?–Cenomanian; Stagg et al., 1990) siliciclastic-dominated syn- to early postrift section, and a Cenozoic (Paleocene–Holocene) predominantly carbonate-dominated section. These two sections are separated by a major, basinwide unconformity. The subject of the bulk of this drilling leg is the upper succession, which makes up an overall sigmoid-shaped series of sequences reaching a maximum thickness beneath the present-day outer shelf (Fig. 2). The stratigraphy of the lower, Mesozoic succession can be derived from the sequence intersected in the Jerboa-1 exploration well (Fig. 1); however, little information on the upper, Cenozoic section was obtained from this hole.

The extensive erosional unconformity at the top of the synrift section forms an easily recognizable and mappable surface. Seven unconformity-bounded seismic sequences have been recognized overlying this unconformity (Fig. 2) (Feary and James, 1998). One of the most striking elements of this seismic stratigraphic analysis is the identification of numerous mound-shaped structures interpreted as biogenic mounds (Feary and James, 1995), that are present throughout the Cenozoic succession. These structures are likely to preserve a detailed record of cool-water faunal community relationships and potentially to provide an analog for cool-water mounds recognized in the rock record, but for which no modern analogs have previously been identified.

The ages assigned to this succession precruise were extremely tentative and are based on (1) correlation of Sequence 6B with the onshore Eucla Group (Fig. 2); (2) the similarity in depositional style between the Sequence 7 progradational wedge and Paleocene?–early Eocene progradational sequences elsewhere along Australia's southern margin; and (3) the division of the remainder of the sequences into a reasonable time-stratigraphic framework. On this basis, the offshore sequences can be placed in the following stratigraphic framework (based on Feary and James, 1998):

Sequence 7: Paleocene–middle Eocene progradational siliciclastic wedge deposited in a depositional sag, representing initial transgressive sedimentation;

Sequence 6A: middle-late Eocene to early-middle Miocene deep-water carbonates forming a multilobed sediment apron;

Sequence 6B: cool-water ramp carbonates with biogenic mounds (middle-late Eocene to Oligocene), overlain by an upper, warm-water, flat-topped platform rimmed by the early?-middle Miocene "Little Barrier Reef" (Feary and James, 1995);

Sequence 5: small late-middle Miocene lowstand sediment wedge with restricted distribution, lying at the foot of the steepest part of the progradational carbonate shelf escarpment zone;

Sequence 4: extensive late Miocene aggradational deep-water carbonate ramp sequence;

Sequence 3: latest Miocene and early Pliocene highstand aggradational deep-water carbonate ramp sequence;

Sequence 2: thick succession of highstand, Pliocene–Pleistocene, cool-water carbonates with spectacular clinoform ramp geometry that forms most of the modern outer shelf and contains large deep-water biogenic mounds; and

Sequence 1: thin Quaternary deep-water drape.

Existing Data

Present knowledge of the western Great Australian Bight margin is based on extensive, high-quality seismic reflection data, together with a single oil exploration drill hole, which provide little information about the Cenozoic succession. The original Leg 182 drilling proposals (James and Feary, 1993; Feary et al., 1994) were based on detailed seismic stratigraphic interpretation (Feary and James, 1998) of a grid of 2350 km of high-quality, regional 2-D seismic reflection lines. These lines were collected and processed by the Japan National Oil Corporation (JNOC) in 1990 and 1991, over an area of 155,000 km^2 on the continental shelf and upper slope of the western Great Australian Bight. An additional 1380 km of moderate-quality, regional 2-D seismic lines, collected by Esso Australia in 1979 and reprocessed by JNOC, were also used to fill gaps in the JNOC dataset. The 1996 seismic-site survey cruise (Feary, 1995) collected high-resolution, 80-channel generator-injector (GI) gun seismic data as 0.5-nmi-spaced grids centered on each site, together with tie-lines between sites. These data permitted minor refinements of some site locations to avoid potential safety concerns.

Jerboa-1 was drilled by Esso/Hematite in 1980 as a wildcat oil exploration well in a water depth of 761 m, above a prominent tilted basement fault block located in the southern half-graben of the Eyre Sub-basin (Bein and Taylor, 1981). Jerboa-1 penetrated 1738 m of a Cenozoic and Cretaceous sedimentary section before bottoming in Precambrian metabasalt basement and did not encounter any significant hydrocarbon shows. The top 232 m was washed down and cased so that only 145 m of Tertiary section was actually drilled and logged. No cores were cut in this interval, so lithologic and biostratigraphic inferences are based on cuttings and downhole logs. Thermal modeling and vitrinite data (Stagg et al., 1990) indicate that the entire sedimentary section at Jerboa-1 is thermally immature (R_v = < 0.65%).

SCIENTIFIC OBJECTIVES

Leg 182 drilling in the Great Australian Bight was designed around six fundamental scientific topics to be addressed:

1. *The paleoceanographic history of a carbonate-dominated, mid-latitude continental margin and adjacent basin during evolution of the Southern Ocean.* Because the Southern Ocean is one of the major controlling influences on global circulation and climate, it is imperative that the oceanic history of this region be refined as much as possible. However, the paleoceanographic development of this area is not nearly as well known at present as that of the high-latitude North Atlantic (Kennett and Barron, 1992). Although there are numerous paleoceanographic problems that can be answered by the Leg 182 drilling transect, four stand out as critical:
   (a) *The relationship between circulation patterns in the deep ocean and on the shelf during times of warm vs. cold ocean conditions.* The stratigraphic record in the Southern Ocean is punctuated with numerous breaks in sedimentation that are attributed to erosive periods related to increased circulation during initiation of the Circum-Antarctic Current (Miller et al., 1987; Kennett and Barker, 1990). Although such hiatuses are thought to develop on deep margins during times of lower sea level and to correlate with unconformities on the continental shelf, there are apparently continuous onshore sequences of Oligocene shelf carbonates that were deposited concurrently with erosion or nondeposition of the entire Oligocene succession on the adjacent ocean floor.
   (b) *The precise timing and nature of the opening of the Tasman Gateway.* Subsidence of the Tasman Rise, which permitted initiation of the cold Circum-Antarctic circulation and thermal isolation of Antarctica, is one of the most important developments in Cenozoic paleoceanography (Kennett, 1982). The history of this event is poorly constrained because so much of the oceanic record is missing as a result of seafloor erosion. The Leg 182 shelf-to-basin transect is sufficiently proximal to the Tasman Rise that it should contain an excellent record of the paleoceanographic development of this seaway.
   (c) *The evolution and effect of the Leeuwin Current.* The first evidence for the existence of the Leeuwin Current occurred in middle Eocene time, when currents from the Indian Ocean were deflected into the elongate proto-Great Australian Bight embayment. In support of this, the record of warm-water intervals is more common in the west than it is in the east, implying that the source of the water is from the west.

Studies of Quaternary cores from the Great Australian Bight suggest a complex interplay between the Leeuwin Current and the West Wind Drift. This interplay appears to have had dramatic effects on primary productivity, as the Leeuwin Current is a source of warm oligotrophic waters, whereas the West Wind Drift causes upwelling of cooler eutrophic waters.

(d) *The relationship between primary productivity and cool-water carbonate development.* The Leg 182 shelf-to-basin transect should contain an important record of paleoproductivity linked to upwelling. Such periods should be recorded in the biota by low species diversity, high numbers of individuals, increased sedimentation rates, and distinctive changes in stable-isotopic and trace-element compositions.

2. *The formulation of models for carbonate sedimentation on continental margins bathed predominantly by cool oceanic waters.* The deposition and accumulation of platform (neritic) carbonate sediments under cool-water (~<20°C) conditions is poorly understood compared to warm-water carbonates, primarily because the database is so small (Nelson, 1988; James and Kendall, 1992). Yet because of their dominantly skeletal composition, nutrient-dependent biology, and low diagenetic potential, cool-water carbonates record the history of oceanic change in ways that are profoundly different from tropical carbonates. In hydrodynamic terms, cool-water carbonate shelves are hybrids, possessing some of the characteristics of both terrigenous clastic shelves and warm-water carbonate shelves. Sediments are produced on the shelf, in contrast to terrigenous clastic shelves where sediment is transported onto the shelf from the hinterland. Without the elevated rim that typifies warm-water carbonate shelves, however, the sediments are subject to the full sweep of oceanic waves and swells, because they are on terrigenous clastic shelves. Cenozoic exposures of inner-shelf facies in Australia suggest that storm- and wave-dominated processes tend to control deposition. By contrast, many contemporaneous deposits in New Zealand are clearly tide dominated. Are the models of wave-dominated shelf deposition developed onshore applicable throughout the Cenozoic? All seismic profiles across the southern margin of Australia indicate that a large proportion of the youngest part of the succession is made up of prograding clinoforms (James and von der Borch, 1991; Feary and James, 1998). Such clinoforms seem to be a signature of cool-water platforms and ramps and are postulated to be a product of accumulation dynamics (Boreen and James, 1993). There is little information regarding the composition of these deposits. Specifically, are they produced by in-place, enhanced bioproduction along the shelf edge, or are they made up of finer grained material produced on the shelf and swept offshore to accumulate below the wavebase?
3. *Determination of the Southern Ocean basin sea-level record, and the effect of sea-level fluctuations on stratigraphic packaging and early diagenesis of cool-water carbonates.*

The Eucla margin is rich in biogenic carbonate sediments that respond in a sensitive way to variations in sea level and contain vital geochemical information needed for linking sea-level changes to paleoceanography. This information can be utilized to address two major questions of global and temporal significance.

(a) *What is the detailed sea-level history of the Southern Ocean basin, and can it be linked to paleoceanographic variations?* The southern Australian neritic shelf record, derived largely from onshore successions in which the marine record is preserved only in highstand systems tracts, appears to be at odds with the global model (Haq et al., 1987) during several critical periods. Is this because the sediments were deposited in cool water? Through the use of a combination of physical stratigraphy and proxy paleoenvironmental parameters in a much more expanded section than exists onshore, the well-preserved Eocene–Oligocene and early to middle Miocene successions will allow a thorough testing of this part of the sea-level curve and resolution of specific eustatic events. The late Miocene–Pliocene sequence is unknown onshore except for the early Pliocene highstand, so this will be the first clear record of this component of the sea-level record in the region.

(b) *How do cool-water carbonate platforms respond to changes in sea level?* Carbonate platforms, with their chemically metastable sediments born largely in place, are particularly responsive to changes in seawater temperature and chemistry and variations in sea state and sea level. To date, most information on carbonate platforms comes from rimmed, warm-water platforms (Kendall and Schlager, 1981; Sarg, 1988). There is almost no information on the manner in which cool-water carbonate platforms respond to changes in these critical parameters at a variety of different time scales. Specifically, we require information to describe how different segments of the shelf react during different parts of the sea-level cycle and to determine whether cold- and warm-water carbonate platforms have basically different depositional geometries as a result of the different ways the carbonate factory responds to sea-level changes.

4. *The circulation patterns of shallow subsurface fluids in an area of low hydraulic gradient and minimal recharge.* The Eucla margin is one of the few modern shelves where the onshore recharge zone is an areally vast, flat-lying karst (the Nullarbor Plain). The high primary depositional permeability of winnowed grainstones of the Eucla Shelf and the lack of early cementation suggest that significant ground-water circulation may occur, at least at shallow depths. The drive for such a circulation may come from temperature contrasts between cool ocean waters and ground waters warmed by geothermal heat flux (and possibly volcanics) within the shelf, concentrating waters on the shelf margin (Simms, 1984). Alternatively, despite inland aridity, recharge occurring over the vast continental hinterland may drive brackish to saline waters southward to discharge through

the flooded shelf. Such a circulation has been recognized by James (1992) and is associated with cave development on the Nullarbor Plain (James et al., 1989). In contrast to the long-lived nature of the above systems, differences in sea-surface elevation, on and off the shelf, associated with regional wave buildup (Feary, 1995), current flow (Rockford, 1986), and atmospheric pressure system changes may cause pumping of marine waters into and out of the platform (Marshall, 1986).

5. *Early seafloor and shallow burial diagenesis and dolomitization of calcite-dominated sediments.* Cool-water carbonates exhibit a radically different pattern of diagenesis from that of tropical aragonitic carbonates. Slow sedimentation permits seafloor lithification by intermediate Mg-calcite cements, but these appear to be volumetrically limited and localized to omission surfaces and hardgrounds, which are ubiquitous in the inner platform. Indeed, both shallow-marine and meteoric cements appear to be very sparse, with magnesium being lost from high-Mg calcite to low-Mg calcite during grain recrystallization. Sparse calcium-rich dolomites may be present (Reeckmann, 1988; Bone et al., 1992), and at some locations replacement can be pervasive (James et al., 1993), although the fine subtidal evaporation-related dolomites typical of tropical platforms are absent. It is not known whether dolomitization is episodic, as recognized in other present-day platforms (Vahrenkamp, et al. 1991; McKenzie et al., 1993), or occurred over extended time periods. The Eucla margin carbonates will provide an opportunity to determine the present-day associations among ground-water circulation, fluid geochemistry, and diagenetic products, and by inference from the temporal and spatial distribution of ancient diagenetic components, those that occurred under different conditions in the past. This has the potential to provide fundamental insights into the diagenesis of cool-water, open-shelf carbonates, which are direct analogs for the comparable carbonate platforms that were ubiquitous during Paleozoic and other times.
6. *The pace and style of evolution of mid-latitude oceanic and neritic biotas.* The Leg 182 drilling transect offers the opportunity for pioneering analysis of the Cenozoic evolution of cool-water calcareous biota, with direct applicability to studies of ancient carbonate platforms presently lacking modern analogs. Linked information from the neritic and oceanic high- to mid-latitude carbonate realm should produce an unmatched record of paleobiological information. Specifically, the patterns and modes of speciation and diversification of coeval shallow- and deep-water benthic organisms as well as contemporaneous planktonic biota should be revealed. By comparing these results with those from Antarctica and the northeast Australian shelf, the geography of such processes and their relationship to physiochemical factors should be discernible.

SYNTHESIS AND RESULTS

Lithostratigraphy

Sediments recovered during Leg 182 record carbonate deposition in a mid- and high-latitude setting against the background of an evolving Southern Ocean and northward drift of the Australian continent. Sediment in 3875 m of water at the toe of slope (Site 1128) chronicles the change from early Paleogene time, when a humid onshore climate flushed large amounts of terrigenous clastic sediment into the deep sea, to Neogene time, when increasing continental aridity promoted mostly marine carbonate deposition. Green Eocene siliciclastic sands and silts that accumulated largely below the carbonate compensation depth (CCD) in a poorly oxygenated, bathyal setting become finer grained upward, with much of the deep-water late Eocene represented by clay deposition (Fig. 3). Initiation of the contemporary Southern Ocean circulation system, and thus the modern global ocean, is signaled by a gradual change to lower Oligocene brown clay and carbonate, as this part of the seafloor became ventilated and the CCD deepened. The deep-water Neogene record is one of pink pelagic carbonate ooze punctuated by white planktonic foraminiferal turbidites. Early-middle Miocene time is represented by a major hiatus and sediment gravity-flow deposits.

Most drilling took place on the upper slope and outermost shelf, in 202–784 m of water, through a mainly carbonate succession (Figs. 3, 4). Two distinct groups of strata, Eocene–middle Miocene and late Miocene–Quaternary in age, form the upper part of the continental margin. The older succession is stratigraphically equivalent to and roughly coeval with most of the Eucla Group, exposed onshore in the Eucla Basin beneath the Nullarbor Plain. Sediments are a package of Eocene shallow-water terrigenous sands and carbonates that deepens upward into Oligocene and early-middle Miocene pelagic ooze and chalk (Fig. 3). Although recovery was generally poor through the Oligocene and Miocene interval because of silicification (Site 1134 is an exception for the Miocene), recovered carbonates are characterized by stained hardgrounds and numerous omission surfaces. The younger, wholly Neogene succession is a large, seaward-dipping wedge of carbonate sediment that downlaps onto the older sediments and has been prograding seaward onto the Eyre Terrace since late Miocene time. The contact between the two successions is represented, particularly the late Miocene and especially the Pliocene, by slumps, sediment gravity-flow deposits, or unconformities. Such erosion, corrosion, and/or mass-wasting and redeposition processes reflect periods of margin instability, seismicity, or lowered sea level.

The most astonishing discovery of Leg 182 was that the huge wedge of slope sediment prograding onto the Eyre Terrace is nearly entirely Pleistocene in age (Figs. 3, 4). This deposit, formed by carbonate produced on the outer shelf and upper slope and swept seaward, is more than 500 m thick in the center (Fig. 4), where rates of accumulation exceed 40 cm/k.y., equivalent to many shallow-water tropical carbonates and twice the rate of Bahamian slope sedimentation. The green and gray material is surprisingly uniform in composition, made up of

fine carbonate sand and silt that was reworked in place by generations of burrowing organisms, leading to multitiered trace fossil assemblages. Particles are all skeletal fragments, mainly delicate bryozoans, ostracodes, benthic and planktonic foraminifer tests, tunicate sclerites, nannofossils, and siliceous sponge spicules. The deposit grades from mud and sand at the top downward to partially lithified sediment in the middle, and finally to hard limestone at the base. Sediment below 400 mbsf is usually neomorphosed with numerous fossil molds, or partially altered to sucrosic dolomite.

The facies transition upslope into shallower water is marked by the presence of numerous bryozoan-rich buildups (Figs. 3, 4). These mounds, in water depths of ~200–350 m, are dominantly muddy and characterized by the prolific growth of numerous and diverse bryozoans. The mounds in particular have seafloor relief of as much as 20 m and extend laterally many hundreds of meters. These are among the first modern analogs to similar mounds that were an important part of the carbonate depositional systems in earlier, Phanerozoic time.

Biostratigraphy

Age of Sediments and Hiatuses

The Cenozoic sequence penetrated at Leg 182 sites mainly represents the Pleistocene, Miocene, Oligocene, and Eocene. Biostratigraphic data indicate that these Cenozoic successions are mostly hiatus bound (Fig. 5). The Pliocene and the later part of the middle Miocene successions are either missing or highly condensed. Other intervals of the Miocene and Oligocene are also missing, though unmatched between sites along the eastern and western transects.

A greatly expanded Pleistocene section was recovered at shallow-water sites from the eastern transect (Sites 1129, 1131, and 1127). The longest at Site 1129 exceeds 540 mbsf, with an average accumulation rate of more than 300 m/m.y. (Fig. 6). In contrast, the Pleistocene sections from the western transect only extend down to ~250 mbsf at Sites 1130, and ~230 mbsf at Site 1132. The biostratigraphic units, however, are similar between eastern and western transect sites. The Pleistocene section is underlain by a thin upper Miocene interval, which in turn disconformably overlies a unit of mainly early-middle Miocene age. The absence of many Pliocene to later middle Miocene biozones from Sites 1127, 1129, and 1130 signifies a hiatus of at least 7 m.y. between the Pleistocene–Pliocene and the middle Miocene. This major unconformity was detected at all other sites as two shorter hiatuses of ~3 m.y. each at the middle/late Miocene and late Miocene/Pliocene–Pleistocene boundaries. They are more clearly recorded as disconformities capping the upper Miocene section at Sites 1126, 1134, and 1133 in intermediate water depths, and at shallow-water Sites 1130 and 1132 along the western transect (Fig. 5). Thus, it is reasonable to speculate that the unconformity at the Pleistocene–Pliocene/middle Miocene boundary, as observed at eastern sites, probably resulted

from at least two major events that subsequently almost completely erased the sedimentation record of the later middle Miocene–Pliocene.

The late Miocene succession is better represented in the west, especially at Site 1130 and at deep-water sites. The middle Miocene, mainly the early part, is present at all sites except Sites 1128 and 1130. It also represents the oldest sediment penetrated at most sites along the eastern transect, although a thin lower Miocene unit was encountered at the base of Hole 1131A (~590 610 mbsf). An expanded middle Miocene section at Site 1132 was accompanied by sedimentation rates ranging 14 54 m/m.y. (Fig. 6). A similar rate of 50 m/m.y. was recorded for the middle Miocene at Site 1133. The absence of middle–early Miocene biofacies from Sites 1130 and 1128 is interesting because these two sites respectively represent the intermediate and deepest water sites along the western transect. At Site 1130 (495 mbsf), the upper Miocene section was disconformably underlain by sediments of mainly early–middle Oligocene age, indicating a depositional gap of ~15 m.y. At Site 1128 (3890 mbsf), the entire middle Miocene–upper Oligocene interval corresponds to a ~15-m-thick debrite with mixed calcareous nannofossil and planktonic foraminifer assemblages of early to late Miocene age, suggesting unconformities totaling ~13 m.y. in duration. Sites 1126 and 1134, the two intermediate-water sites from the west, exhibit remarkable similarities in assemblage compositions, ages of recovered sediments, and position and number of hiatuses. These are the only sites yielding definite early Miocene calcareous nannofossils and planktonic and benthic foraminifers.

Sediments of Oligocene age and older were recovered only from the west. At Sites 1130 and 1132, the Oligocene section disconformably overlies Eocene sediments, and a hiatus of at least 2 m.y. is indicated by biostratigraphic data. However, the zonal succession of nannofossils and planktonic foraminifers is largely continuous across the Oligocene/Eocene boundary, suggesting a conformable succession at Sites 1126, 1128, and 1134. Mainly early Oligocene assemblages are present at Sites 1132, 1130, and 1128 in the west, and an expanded lower Oligocene section was indicated by nannofossils at Site 1128. Biostratigraphic resolution below 70 mbsf at Site 1128 was largely achieved by calcareous nannofossils because planktonic foraminifers were rare or barren in sediments dominated by siliceous oozes and packstones.

Holes 1126D and 1134A are the only holes containing rich calcareous microfossils of Eocene age. Poor preservation, however, impaired proper recognition of species and biozones in some intervals. Although present at all western sites, the middle Eocene is represented by poorly preserved, impoverished assemblages in various poorly recovered lithologies. It consists of a siltstone (~150 m thick) at Site 1128 with sporadic nannofossils, a calcareous packstone (~30 m thick) at Site 1126 with moderately preserved nannofossils and planktonic and benthic foraminifers, and a dark, iron-stained sand (30 m thick) at Site 1134 with rare and poorly preserved microfossil assemblages. A calcareous sandstone at Site 1130 and a bioclastic limestone at Site 1132 both contain shallow-water associations of planktonic and benthic

foraminifers. No calcareous nannofossils or foraminifers were discovered in dark green sandstone at the base of Hole 1126D, which may correspond to Cretaceous synrift sediments along the southern Australian margin.

Paleobathymetry and Paleoceanography

The succession of microfossil assemblages from Leg 182 provide an unmatched record of sea-level and circulation changes in the Great Australian Bight from the Eocene to Holocene. Expanded Pleistocene successions at Sites 1127, 1129, 1130, 1131, and 1132 contain upper bathyal benthic foraminifer assemblages with a redeposited neritic component. Apparent fluctuations in the relative proportions of neritic taxa and upper bathyal taxa indicate that downslope transport periodically varied in intensity during the Pleistocene. These changes, together with the periodic intrusion of warm-water species into temperate planktonic foraminifer assemblages, indicate responses to changing climate and oceanic circulation. Calcareous nannofossil assemblages dominated by *Braarudosphaera bigelowii* indicate that a major ecological crisis affected the planktonic ecosystem at base of the Pleistocene.

At the three shallow-water sites (Site 1129, 1131, and 1132), diversified, extremely well-preserved benthic foraminiferal assemblages, including unusually large specimens (>1 mm), are found together with abundant and well-preserved bryozoan fragments (Fig. 5). These assemblages were probably part of a highly dynamic ecosystem that became established at the seafloor during the later Pleistocene, coincident with bryozoan buildups in paleodepths of 200–300 m. A shallowing-upward trend from middle bathyal paleodepths in the middle and late Miocene to upper bathyal paleodepths in the Pleistocene is recorded at Sites 1129, 1130, and 1132 (Fig. 5). Middle bathyal faunas at these sites reflect middle and late Miocene transgressive pulses that are also expressed onshore southern Australia by thin transgressive tracts.

Middle bathyal assemblages from upper Eocene–upper Miocene successions show major changes in composition at intermediate water Sites 1126 and 1134. The most severe changes in the early Miocene probably relate to global changes in deep- and intermediate-water circulation affecting the distribution of bathyal benthic foraminifers worldwide. The composition of abyssal assemblages at Site 1128 indicates deposition above the CCD during the Pleistocene, close to lysocline in the late Oligocene–middle Eocene, and below the CCD in early–middle Eocene in the deep basin (Fig. 5). Assemblage boundaries appear to be coeval in the Eocene, Oligocene, and lower Miocene of intermediate- and deep-water Sites 1126, 1128, and 1134, suggesting that benthic foraminifer distribution was controlled by major environmental changes during these periods. Discrepancies between assemblage boundaries of deep-, intermediate-, and shallow-water sites in the middle Miocene–Pleistocene sequence relate to stratigraphic or lithological differences, and reflect distinct depositional and paleoceanographic regimes in the region.

Paleomagnetics

Previous carbonate legs have proved very unsatisfactory for paleomagnetists because the magnetic intensity of the sediments has been so low that remanence measurements were essentially unreliable. However, with the change to direct-current superconducting quantum interface devices (DC SQUIDs) in the new instrument, it was possible to measure the magnetization at most sites during Leg 182. Nevertheless, the natural remanent magnetization (NRM) of sediments from Sites 1126 and 1134 was so weak that after a coring overprint was removed the magnetization was at the noise level of the instrument for much of the hole.

Coring Experiments

During Leg 182, an experimental nonmagnetic cutting shoe was used in advanced hydraulic piston core (APC) coring. The shoe and other components of the bottom-hole assembly were used to continue investigations of anomalous magnetization observed in these cores. Comparisons were made between cores taken with standard core-barrel assemblies, with standard core-barrel assemblies and the nonmagnetic shoe, and with nonmagnetic core barrels and shoe. On some occasions, it was clear that the nonmagnetic shoe and assembly greatly improved the paleomagnetic record. On other occasions, the shoe alone improved the record compared with the core-barrel standard assemblies. However, there were also sites where neither the nonmagnetic shoe nor the whole nonmagnetic core-barrel assembly had any obvious effect. This is consistent with the intermittent nature of the anomalous magnetization experienced during past legs. Work postcruise will focus on trying to isolate other sediment properties such as grain size, porosity, or shear strength, which may affect the coring contamination.

Rock Magnetism

A common feature of the rock magnetism of the upper sections of Leg 182 holes was the extremely high ratio of anhysteretic remanent magnetization to isothermal remanent magnetization (ARM/IRM). This is a measure of the degree to which single-domain particles dominate among the magnetic phases present in the samples. This ratio generally decreased downhole and was accompanied by a decrease in intensity of magnetization and coercivity. This decrease in intensity of magnetization is generally interpreted as dissolution of the finest grained magnetic phases in the sediment. IRM acquisition suggests that magnetite and magnetic sulfides are the principal remanence carriers. The observation of a downhole decrease in ARM/IRM and intensity is consistent with diagenesis models of organic matter oxidation and sulfate reduction as the principal processes that regulate the preservation of ferromagnetic phases.

Magnetostratigraphy

Long-core and discrete sample measurements yielded a record of inclination from which a Pliocene–Pleistocene magnetostratigraphy was interpreted. Overall, deeper water records are of good to fair quality, yielding accurate estimates of the expected inclination for the present latitude. In contrast, lower intensities in the shallow-water sites result in shallow inclinations with large scatter. The Brunhes/Matuyama boundary was identified in five high-sedimentation-rate sites (Fig. 7; Table 1). The Jaramillo Subchron (C1r1n) and the top of the Olduvai Chron (C2n) were also found at three sites. The interpretation of magnetic polarity in Figure 7 implies that sedimentation rates in the early Pleistocene were considerably lower than during the Brunhes Chron. In addition, variations of the intensity of the remanence after partial demagnetization were found to oscillate on time scales comparable with those of the geocentric axial dipole. Although the intensities have not been normalized to account for variations in concentration, these sediments may provide a valuable relative paleointensity record that can be used for high-precision correlation between sites. For Sites 1126 and 1134, magnetostratigraphic data were obtained for parts of the Miocene. Site 1128 also contains a long record of the polarity sequence of the early Oligocene.

Geochemistry

The drilling of nine sites off the Eucla margin provided a unique insight into the fluid dynamics along a continental margin dominated by cool-water carbonates. With respect to this objective, the most significant discovery was the presence of a brine, varying in salinity between 80 and 105, that was present in and underlying seven of the nine sites (the exceptions being Site 1128, drilled in a water depth of 3884 m, and Site 1133). At Site 1133 (located in 1043 m of water) fluids were encountered with a salinity of 40, but recovery problems precluded the measurement of the salinities in deeper samples. The brine was present at relatively shallow depths at the deeper sites (1134 and 1126), whereas the maximum salinities were not encountered until depths $\geq$400 mbsf at the shallower sites (1127, 1129, 1130, 1131, and 1132). The impact of the brine is more readily visible along the eastern transect (Sites 1129, 1131, and 1127; see also Fig. 4). Similar processes appear to occur at Sites 1130 and 1132, although they are reduced in nature.

At Sites 1129, 1131, and 1127, a gradual increase in salinity was encountered, reaching a maximum value of ~100 at Site 1127 (farthest away from the margin) and 92 at Site 1129 (closest to the platform). A contour map of the distribution of Cl^- at the three sites is shown in Figure 8. Pore fluids in the Pleistocene portion of the sediments from these sites also possess a Na^+/Cl^- ratio exceeding that of seawater, suggesting that the fluids in the sediments were involved in the dissolution of NaCl. Although the origin of the fluids has not yet been established, a probable explanation is that they formed during the Pleistocene when the Eucla shelf was exposed numerous times during sea-level lowstands. We suggest that large

hypersaline lagoons developed during these episodes of low sea level. Because of the greater hydrostatic head, fluids with high salinity were forced into underlying strata and out onto the adjacent continental slope. During sea-level highstands high salinity fluids then diffused upward as additional sediment was deposited, and the profiles of the individual ions were modified by diagenetic reactions in the sediments. This sequence may have occurred a number of times as sea level fluctuated during the Pleistocene. This hypothesis is supported by an examination of the Cl^- distribution between the three sites (Fig. 8) which suggests that the top of the brine has a common depth below sea level and, therefore, crosscuts sequence boundaries.

All three sites exhibited high concentrations of hydrogen sulfide (H_2S) and methane, combined with high values of alkalinity. The high concentrations of H_2S are derived from the oxidation of organic material by sulfate-reducing bacteria. The relatively low concentrations of iron in carbonates, in contrast to those found in locations adjacent to continental margins with a large amount of siliciclastic input, means that the H_2S is not sequestered as iron sulfides. Consequently, concentrations of H_2S are able to reach high levels (>150,000 ppm at Site 1129). As a result of the high rate of sedimentation (>200 m/m.y.) and the position of the sites close to the continental shelf, these sites contained an initial high concentration of organic material. Under normal conditions, the organic material would be oxidized first by oxygen and then by sulfate-utilizing bacteria, thereby creating alkalinity and hydrogen sulfide. Although this process also takes place in the Eucla margin, the high-salinity brines underlying and within the Pleistocene succession provide as much as three times the normal sulfate concentrations; therefore, with sufficient organic material, significantly higher amounts of hydrogen sulfide can be formed. As the sediments are buried, the concentration of sulfate is depleted in the sediment and a gradient is established between the sediments, the overlying seawater, and the underlying brine. Because of the high sulfate concentration of the brine, the flux of sulfate diffusing into the zone of organic material remineralization is significantly greater than in a normal marine sediment, thus resulting in greater than normal sulfate reduction and higher alkalinity. In addition to H_2S, high concentrations of methane and the presence of other higher molecular-weight hydrocarbons were discovered in the sediments at Sites 1129, 1131, and 1127. At Site 1127, gas pockets in the core were found to contain as much as 73% methane and 365 ppm ethane. We suggest that these gases, including the higher molecular-weight hydrocarbons, are bacterial in origin, being generated in situ. Higher molecular-weight alkanes are generally only believed to form through thermogenic processes (Fig. 9). However, the concentration of ethane, propane, and butane did not increase with depth, but instead reached a maximum associated with the maximum in methane, suggesting that these gases also originated in this portion of the sediment and were not thermogenic in origin.

The oxidation of organic material also has an important influence on the process of carbonate recrystallization. The sediments at all the sites cored during Leg 182 initially contained a mixture

of aragonite, high-Mg calcite (HMC), and low-Mg calcite (LMC). Of these minerals, aragonite and HMC are metastable and gradually will alter to the more stable forms of LMC and dolomite. This process is evident at all the sites drilled and is greatly accelerated by the processes of sulfate reduction and the consequent formation of H_2S. During the oxidation of organic material, two important chemical reactions take place that alter the carbonate chemistry in the pore waters: (1) sulfate reduction creates two moles of alkalinity for every mole of sulfate that is consumed and (2) one mole of H_2S is produced ($2CH_2O + SO_4^{2-} = H_2S + 2HCO_3^-$). The H_2S dissociates in the pore water causing the pH to be reduced and the speciation of carbonate in the pore waters to move from being dominated by HCO_3^- to H_2CO_3. This sequence of events produces pore fluids that are undersaturated with respect to the metastable carbonate minerals. The most thermodynamically soluble form of calcium carbonate, HMC dissolves first, followed by aragonite, and LMC. This trend is followed at all of the sites. The high-alkalinity environment creates a thermodynamic regime favorable for the formation of dolomite. Dolomitization consumes Mg^{2+} from the pore waters, setting up a strong diffusive gradient into the reaction zone from the overlying seawater and the underlying brine. The formation of dolomite is well illustrated at Sites 1127, 1131, 1129 (Fig. 10), which shows concentrations of ~5% at Sites 1127 and 20% at Sites 1129 and 1131.

Although the high-salinity pore fluids were also present at other sites (Sites 1130, 1132, 1126, and 1134), these sites showed lower concentrations of H_2S and methane and consequently lower amounts of carbonate diagenesis. The controlling factor at these sites is the supply of organic material combined with the rate of sedimentation.

Petrophysical and Downhole Measurement Data

Downhole logging data were collected at eight of nine sites drilled during Leg 182. To complement these data, an extensive program of sediment physical properties measurements was undertaken. Both datasets will provide detailed information for intersite correlation, characterization of lithostratigraphic boundaries, and core-log correlation. The presence of chert, particularly in the post-Pleistocene sequences sedimentary section, resulted in low recovery. Downhole logging data will provide the information necessary to fill in recovery gaps, refine the placement of lithostratigraphic boundaries, and enable interpretation of sedimentary facies, composition, and structure within missing intervals. Checkshot surveys conducted at five sites will facilitate correlation of the drilled strata to the regional grid of high-resolution seismic data to formulate and refine models of temperate-water carbonate sedimentation and view the influence of eustatic sea-level variations on this sedimentation.

The downhole logging and physical properties measurement program undertaken during Leg 182 provided an unparalleled opportunity to investigate early and postdepositional diagenesis in a nontropical carbonate depositional system. Preliminary diagenetic characterization of

temperate-water carbonate sediments recovered during Leg 182 show distinct geochemical, mineralogic, and textural variations, despite the preconceived notion that cool-water carbonates have low diagenetic potentials because of their dominantly low-magnesium calcite mineralogy. Postcruise analysis of Formation MicroScanner (FMS) and conventional logs will provide a more detailed analysis of mineralogical and textural changes occurring during diagenetic alteration.

An important finding of Leg 182 was the discovery of distinct, possibly Milankovitch, cyclicity recorded in gamma-ray and density data from the thick Pleistocene sediment wedge drilled at numerous sites (Fig. 11). The high sedimentation rates of this deposit, in excess of 40 cm/k.y., will enable frequency analysis of the logging and physical properties datasets to assist in the refinement of the biostratigraphic ages within this time interval. FMS data collected at six of the logged holes will allow for detailed investigation of depositional facies and sedimentary structure in the sediment cycles, particularly in the intervals where recovery was poor. Correlation of the cyclicity present in the temperate-water carbonate wedge to other Pleistocene carbonate and noncarbonate marginal systems will provide important information on differences in eustatically influenced sedimentation patterns occurring on continental margins from the seafloor to the bottom of the drilled interval.

PRINCIPAL RESULTS

Site 1126

Site 1126 is located on the eastern Eyre Terrace upper slope in 783.8 m of water. This site was designed to intersect Cenozoic seismic Sequences 2, 3, 4, and lobes 1 and 3 of Sequence 6A, and to intersect as much of the upper part of the Cretaceous section as time permitted. The target depth at this site was a high-amplitude reflector of probable Cenomanian age, estimated before drilling (on the basis of stacking velocities) to be at 525 mbsf. Because this was also the first ODP site in this basin, it provided the opportunity to establish a basic stratigraphy for the Cenozoic sequences that could then be refined at later sites.

Five lithostratigraphic units were delineated at Site 1126. Unit I (0–60.2 mbsf) is a calcareous ooze with a gradational alternation between two major sediment types: (1) white gray nannofossil-rich matrix-supported ooze and (2) light gray grain-supported ooze rich in planktonic foraminifers. Unit II (60.2–116.8 mbsf) is characterized by several intervals of slumped calcareous ooze. Sediment composition in these bodies is the same as in the undisturbed sediments. The first downhole occurrence of silicified layers (porcellanite) subdivides Unit II into an upper Subunit IIA and a lower Subunit IIB. As in Unit I, intervals that are not affected by slumping display a light/dark alternation. In the lower part of Unit II, these cycles are increasingly asymmetric, with the dark portions becoming dominant. Unit III (116.8–165.5 mbsf)

consists of calcareous ooze with interbeds of silicified layers in the upper part of the unit. The lower part of the unit is porcellanite free and displays the same type of cyclicity as sediments in the overlying units. Unit IV (165.5–396.6 mbsf) coincides with an interval of low core recovery and thus cannot be described in detail. It consists of an alternation of calcareous ooze to chalk intervals and silicified pelagic limestones with some planktonic foraminifers and bioclasts. Unit V (396.6–455.9 mbsf) consists of black to green sandstones, silty sandstones, clayey siltstones, and minor granule conglomerates.

Nannofossil and planktonic foraminifer biostratigraphies show that Quaternary through middle Eocene sequences were recovered. Sandstones of probable Cenomanian age (Unit V) recovered at the base of the drilled interval are barren of marine microfossils. Sedimentation rates were relatively high in the Quaternary (31 m/m.y.) and lower Pliocene (24 m/m.y.) and slow in the remainder of the Neogene and Paleogene sections, where rates alternate between 7–8 m/m.y. and 11–15 m/m.y. with faster rates in the upper Miocene, lower Miocene, and upper Oligocene. Two intervals of slow sedimentation are present at the Miocene/Pliocene and early/middle Miocene boundaries. Benthic foraminiferal assemblages show a change in benthic environments from lower bathyal to middle bathyal in the upper part of the middle Eocene nannofossil zone, NP16. Slumps between ~55 and 110 mbsf are marked by a mixture of late Miocene and early Pliocene planktonic taxa found within a latest early Pliocene assemblage. The slump is also flagged by a mixture of a displaced upper bathyal assemblage of benthic foraminifers found within an in situ middle bathyal assemblage.

The results of paleomagnetic long-core measurements of cores from Hole 1126B and 1126C were disappointing. The NRM was dominated by a vertically downward coring contamination that was largely removed by 20 mT demagnetization, whereupon the signal was almost uniformly reduced to the noise level of the instrument. In addition, there were anomalous peaks in intensity near the tops of most cores and of several sections. These were so large that we interpret them as contamination. Only a single core gave a sequence of reversals that could be interpreted magnetostratigraphically. A comparison between whole-core and archive-half core measurements showed that the two measurements are not significantly different from each other, thereby settling a long-debated question. The nannofossil chalks gave stronger signals, but poor recovery precluded determination of a useful magnetostratigraphy. In the sandstone recovered toward the base of Hole 1126D (Unit V), normal magnetizations were observed. Their high inclination, giving a paleolatitude of ~50°S, is in accordance with northerly motion of the Australian plate as it moved away from the Antarctic-Australia spreading center. Rock magnetic properties of representative samples from the various sedimentary units differ in a manner that is consistent with the NRM variation. In the nannofossil chalk and in some of the more strongly magnetized nannofossil oozes, the magnetic carrier appears to be single-domain magnetite

consistent with a magnetotactic bacterial origin, whereas a different and harder phase dominates in the uppermost nannofossil ooze sediments.

The upper 154.0 m of sediment at Site 1126 was double cored. Construction of the composite section from Holes 1126B and 1126C indicates that a complete record of the sedimentary section was not recovered. Correlation between cores was hindered by significant differential core distortion, particularly at the very top of each core where an expanded record was indicated. Correlations were further hindered by a decrease in core recovery below 100 mbsf, resulting from the presence of multiple thick chert layers. Below 60 mcd, large data gaps and the presence of numerous slumps made correlations difficult and highly tentative. The composite section indicates gaps in the record at ~26–27, 64–65, 73–74, 86–87, 109–112, 124–125, and 130–137 mcd.

Only low concentrations of methane and ethane were detected at Site 1126. Methane ranges from 2.2 to 13.6 ppm. Ethane is present in five samples between 186.5 and 236 mbsf (1.1–2.7 ppm) but is not detected at greater depths. The carbonate content is uniformly high (80–91.2 wt%) in the upper 116 mbsf but becomes highly variable (30.6–93.2 wt%) from 116 to 254.2 mbsf. Because of poor core recovery, no samples are available in the interval from 254.2 to 348.6 mbsf. From 348.6 to 389.6 mbsf, the carbonate content returns to high levels within a narrow range (79.5–90.0 wt%), dropping again to very low values in sandstones (0.4–0.6 wt%) from 406.4 to 454.5 mbsf. Total organic carbon is low throughout the cored interval except for the bottommost sample of Hole 1126D, which has 1.33 wt% organic carbon. All other organic carbon values are less than 0.8 wt% and most are less than 0.2 wt%

Site 1126 is characterized by a large increase in salinity that manifests itself as shallowly as 10 mbsf, reaching a maximum of 106 (about three times normal salinity) by a depth of ~100 mbsf. Most of the other geochemical parameters exhibit nonconservative behavior with respect to chloride, including calcium which shows a net excess, and magnesium, sulfate, and alkalinity, all of which show net losses. The pore waters have a sodium/chloride ratio close to that of seawater. We believe that the origin of these saline fluids may relate to fossil brines that penetrated the sediments during a previous sea-level lowstand.

Physical properties data closely reflect the location of sequence boundaries and changes in lithology and mineralogy. These data were subdivided into five units on the basis of shifts in measured parameters. Physical properties (PP) Unit 1 is characterized by high natural gamma radiation (NGR) with a trend of increasing *P*-wave velocity and bulk-density measurements to the bottom of the unit. The base of PP Unit 1 roughly coincides with the late Pliocene/Pleistocene boundary. PP Unit 2 is characterized by relatively high natural gamma radiation that dramatically decreases toward the base of the unit. This decrease occurs because of the downhole disappearance of aragonite. *P*-wave velocity increases throughout PP Unit 2, as does thermal conductivity. The base of the unit coincides with the late Pliocene/early Miocene

boundary. PP Unit 3 is characterized by low variability in *P*-wave velocity and NGR. The base of this unit was not recovered in the sediments, but can be defined at 185 mbsf using downhole logs. PP Unit 4 is characterized by alternations of high-velocity porcellanite and lower velocity oozes. This high contrast of sediment induration was probably the major cause of the low recovery in this unit. The top of PP Unit 5 coincides with a major hiatus at the base of the Tertiary. PP Unit 5 shows much greater NGR values and higher *P*-wave velocities reflecting the transition from PP Unit 4 ooze into PP Unit 5 sandstone. This indicates that PP Unit 5 sediments were affected by diagenesis. Thermal conductivity co-varies with water content, bulk density, and *P*-wave velocity.

Hole 1126D was logged with three tool strings: the triple combination logging tool, Sonic/Geologic High Resolution Magnetic Tool (GHMT) combination, and the well seismic tool (WST). The FMS tool was not run with the Sonic as usual because of (1) excessive heave caused by dual swell directions that was not compensated for by the wireline heave compensator and (2) a large hole diameter as indicated by the caliper on the triple combo. The triple combo was deployed from 439 mbsf to well above the mudline. The Sonic/GHMT tool string was deployed from 430 mbsf to above the mudline. The WST was used for recording nine checkshot stations between 420 and 130 mbsf. Several zones of washed out hole affected readings made by excentric tools (e.g., neutron porosity and density), whereas readings measured by hole-centered tools (e.g., magnetic susceptibility, sonic, and resistivity logs) were little influenced by hole conditions. The magnetic susceptibility data were useful for subdividing the measured section into 10 provisional logging units, some of which correlate with the seismic stratigraphic units. In the interval below 160 mbsf where core recovery was poor, changes in several logs provide the detail and continuity necessary to further subdivide the section. The spectral gamma-ray log measured by the triple combo proved very useful for correlating the part of the section measured through pipe (upper 116 mbsf) with core measurements. In the lower siliciclastic part of the section, photoelectric effect (PEF) values indicate the presence of iron minerals.

The checkshot survey showed that the actual time-depth conversion curve fell within the narrow envelope of time-depth curves derived from stacking velocities, so depth estimates for other sites based on stacking velocity curves can be viewed with more confidence. The preliminary biostratigraphic data permitted ages of the regional Cenozoic seismic sequences to be defined, showing that Sequence 2 corresponds to the Pleistocene, Sequence 3 is of Pliocene–late Miocene age, Sequence 4 is of latest Miocene age, and Sequence 6A is of Eocene–Oligocene age.

Site 1127

Site 1127 was the first and most seaward site of a planned three-site transect through a spectacular set of late Neogene clinoforms immediately seaward of the present-day shelf edge.

Site 1127, located on the upper slope in 480.6 m of water, intersects an expanded record of the youngest clinoforms as well as the lowest, more condensed portion of the clinoform sequence. The principal objective of this transect was to collect detailed, high-resolution profiles through a late Neogene shelf-edge (high energy) to upper slope (low energy) succession deposited within a cool-water carbonate environment to determine the response of this type of depositional system to Pliocene–Pleistocene sea-level fluctuations.

At Site 1127, we recovered a 510.7-m-thick monotonous succession (Table 2) that is dominated by very fine- to fine-grained, heavily bioturbated, unlithified to partially lithified, greenish gray wackestones to packstones, made up of three units. Unit I (0–6.0 mbsf) consists of two subunits, an upper nannofossil ooze and a lower foraminiferal ooze. Unit II (6.0–464.5 mbsf) consists of alternating bioclastic wackestone- and packstone-dominated packages with thin grainstone beds, divisible into five subunits. These subunits are characterized by a lower portion composed of wackestones to packstones, grading up into wackestones, and dominated at the top by packstones with thin capping grainstones. Shallower water fauna are most abundant near the top of each subunit. The lowermost subunit (~420–464.5 mbsf) has a slumped base with abundant clasts, including bryozoan and large skeletal fragments within an ooze matrix. Unit III (464.5–510.7 mbsf) consists of an upper nannofossil ooze and a lower glauconite-rich bioclastic packstone, with minor capping grainstone beds with intraclasts.

Calcareous nannofossils and planktonic foraminifers indicate an extraordinarily expanded Pleistocene sequence of more than 450 m, with a hiatus of over 3 m.y. between basal Pleistocene (Zone NN19) and underlying Miocene sediments. Based on preliminary biostratigraphic datums, average sedimentation rates were 240 m/m.y. in the Pleistocene, and 2–8 m/m.y. in the Miocene. The thin Miocene section contains a strongly mixed planktonic foraminiferal assemblage. A well-preserved benthic Pleistocene foraminiferal assemblage is recognized down to 414.5 m. Between 414.5 and 501.1 mbsf, two benthic assemblages were identified that contain mainly upper bathyal taxa but include large numbers of abraded and corroded tests, indicating extensive mixing or reworking. Calcareous nannofossil assemblages throughout most of Zone NN19 are dominated by small forms, suggesting some sorting. Similarly, Pleistocene benthic foraminiferal assemblages display a uniformity in test size and lack of medium to large tests that is consistent with grain-size sorting and downslope redeposition. The cool temperate Pleistocene fauna is accompanied by warm-water species at various intervals, probably reflecting a combination of global climatic fluctuations and regional paleoceanographic variations, especially in relation to flow of the Leeuwin Current.

Paleomagnetic measurements revealed a long section of normal polarity to 343.4 mbsf, which we interpret as the Brunhes Chron. The mean inclination was –49.9°, with a standard deviation of 22°. It was only possible to locate a very approximate onset (380 mbsf) and end (395 mbsf) of the Jaramillo Subchron. We found intensity fluctuations within the Brunhes Chron in the NRM

after 20 mT demagnetization that appear to correlate with standard records of geomagnetic field fluctuations back to 400,000 yr. The calculated sedimentation rate for the whole Brunhes Chron is 480 m/m.y., whereas the rate for the first 400,000 yr based upon the intensity estimation is 277 m/m.y. Rock magnetism analysis revealed that the dominant magnetic phase was chemically unstable, so that the saturation remanence decayed by as much as 60% within 48 hr. This behavior is typical of the ferromagnetic sulfide greigite, which inverts sluggishly to paramagnetic pyrite. The high ARM/IRM suggests a dominant single-domain grain size and a strong magnetotactic bacteria input. However, if this suggestion is correct, the magnetotactic bacteria synthesize greigite rather than magnetite.

The most striking organic geochemical results at Site 1127 are the very high concentrations of methane and hydrogen sulfide present throughout the section. Gas pockets within the core were common from 47 to 312 mbsf, and these were sampled directly through the core liner with a gas-tight syringe (vacutainer). Methane concentrations in these gas pockets range from 165,000 to 730,000 ppm, with most values between 400,000 and 600,000 ppm. Hydrogen sulfide ranges from ~60,000 to 138,000 ppm. Methane is present at lower and highly variable concentrations in headspace samples, with the lowest values at the top and bottom of the drilled interval. Methane/ethane ratios in vacutainer samples decrease downhole from 2728 to 1309, with a decrease in the ratio to 174 in headspace samples. Carbonate content values predominantly range between 85 and 92 wt%, with a trend toward lower values with increasing depth. Organic carbon values are primarily in the range of 0.1–0.6 wt% down to ~250 mbsf, and then vary from 0.5 to 1.0 wt% to the bottom of the hole.

Although similarly influenced by high-salinity pore fluids (up to 100 in Pliocene and older portions of the section), pore-water geochemistry at Site 1127 was fundamentally different than at Site 1126 because of an extended sulfate reduction zone. Because of the more inshore location, Site 1127 not only had a higher initial organic matter content compared to Site 1126, but more of the organic material was preserved as a result of higher sedimentation rates. Because of the high sulfate concentration in the deeper, higher salinity fluids, the sulfate reduction zone is enlarged and the consequent production of hydrogen sulfide is much higher than in normal organic-rich sediments. In addition, the relatively iron-poor nature of these sediments precludes the formation of iron sulfide phases that would normally sequester hydrogen sulfide. The greatest amount of carbonate recrystallization appears to occur at the lower interface between the sulfate-depleted zone (~180 mbsf) and the underlying sediments, where sulfate is actively diffusing upward from the higher salinity fluids below. This process produces pore fluids undersaturated with respect to metastable minerals, causing the precipitation of low-Mg calcite and dolomite. Striking variations in the amount of low-Mg calcite, high-Mg calcite, aragonite and dolomite also occur throughout the succession, with presumed sea-level lowstands characterized by increased high-Mg calcite and the presence of dolomite.

Because of disruption of the sediments during degassing, laboratory physical properties measurements are of limited value for developing a downhole stratigraphy. However, the NGR measurements were only affected to a minor extent, and can be used to define three PP units: PP Unit 1, from 0 to 130 mbsf, is characterized by three high-amplitude cycles superimposed on a rising trend, and corresponds to seismic subsequence 2a. PP Unit 2 is from 130 mbsf to the Pliocene/Pleistocene boundary at 467 mbsf, which is marked by a sudden decrease in NGR values. This unit is characterized by low-amplitude, high-frequency cyclicity in NGR values and corresponds to seismic subsequences 2b and 2c. PP Unit 3 corresponds to the Pliocene sediments below the Sequence 2 boundary, which are also significantly denser than the Pleistocene sediments. Magnetic susceptibility was uniformly very low, and the data were shown to be nonreproducible at the core-section scale.

Hole conditions were excellent for logging, with most caliper readings within 10 cm of bit size. Hole 1127B was logged with three tool strings: the triple combo and FMS/Sonic to the mudline, and the GHMT to 59 mbsf. The triple combo was run without the nuclear source in the hostile environment lithodensity sonde (HLDS) because of safety concerns, and consequently density logs are not available for this site. During and after logging, close examination showed that there was no obvious damage to either the logging cable or tools from the limited H_2S exposure. Cycles and surfaces seen in the high-quality FMS data correlate well with conventional logs (gamma ray [GR], sonic, and resistivity) and indicate the presence of high-frequency cycles (10–20 m thick) in the lower part of the Pleistocene succession. Simultaneous peaks on GR, resistivity, sonic, and susceptibility logs may reflect changes in sediment lithification throughout the logged section. Because of the high quality and uniform response of the sonic log, the WST was not deployed at this site. We anticipate that a checkshot survey at one of the other sites in this transect will provide appropriate drift control on the integrated sonic log.

Site 1128

Site 1128, the deep-water component of the Leg 182 shelf-to-basin transect, is located on the upper continental rise in 3874.6 m of water. The primary goals of this site were to (1) recover pelagic ooze from the upper continental rise to compile a paleoceanographic record of the Cenozoic opening of the Southern Ocean and development of the Circum-Antarctic Current, (2) determine the history of Cenozoic and Late Cretaceous CCD fluctuations and deep-water mass variations during the evolution of the Southern Ocean, and (3) determine depositional and diagenetic facies on the upper continental rise.

The sedimentary succession intersected at Site 1128 was divided into four major lithostratigraphic units. Unit I (0–95.6 mbsf) is a pink to brown, bioturbated, calcareous nannofossil ooze punctuated by numerous thin glauconite and planktonic foraminiferal sand calciturbidites and conglomeratic sediment gravity-flow deposits. A chaotic zone of debrites and

slumped sediment (54.4–70.0 mbsf) separates this succession into three subunits containing variable proportions of resedimented material. Unit II (95.6–281.9 mbsf) is a thick section of uniform, green, variably calcareous clay and claystone that is locally interrupted, particularly in the upper parts, by several centimeter-thick turbidites composed of planktonic foraminiferal and nannofossil ooze. The relatively few carbonate particles in the sediment are etched and corroded, suggesting accumulation near the carbonate lysocline. The lower parts of this unit contain numerous well-preserved trace fossils (*Planolites, Chondrites, Zoophycos, Terebellina, and Thalassinoides*), and numerous thin chert horizons. A thin unit of green, glauconitic sand-to-carbonate nannofossil ooze turbidites forms Unit III (281.9–284.0 mbsf) and marks a sharp change in sedimentation to the coarser, green, carbonate-free silts and clays of Unit IV (284.0–452.6 mbsf). Unit IV was subdivided into an upper Subunit IVA (284.0–358.4 mbsf) composed of bioturbated clayey siltstone with minor chert and glauconitic sand turbidites, and Subunit IVB (358.4–452.6 mbsf) made up of highly burrowed sandy siltstone that grades to green silty sandstone at the base. The well-preserved siliceous microfossils and almost total lack of calcareous microfossils indicates accumulation below the CCD. The burrowed green sediment points to accumulation in dysoxic bottom waters.

Two major biostratigraphic successions were recovered at Site 1128, dated by calcareous nannofossils and planktonic foraminifers as late Miocene–Pleistocene (0–55 mbsf) and early Eocene–early Oligocene (72–427 mbsf). These intervals are separated by the debrite interval (55–72 mbsf) containing mixed upper Paleogene and Miocene nannofossils and planktonic foraminifers. Calcareous nannofossil data indicate four possible hiatuses within the Neogene succession, and a major unconformity spanning the Miocene/Oligocene boundary at ~72 mbsf. Both nannofossil and planktonic foraminifer data show that this unconformity spans a gap of at least 5 m.y., as the entire upper Oligocene is missing. Below 72 mbsf, nannofossils and planktonic foraminifers show increasing signs of dissolution and are absent at some levels, suggesting deposition near the lysocline and CCD. Sedimentation rates were 10–12 m/m.y. through the Neogene, 50–60 m/m.y. in most of the early Oligocene, and 4 m/m.y. in the late Eocene. Although characterized by poor core recovery and barren intervals, datum levels from the remainder of Eocene sediments suggest a sedimentation rate of 40–45 m/m.y. Five benthic foraminiferal assemblages are distinguished: (1) a diversified Pleistocene and Pliocene assemblage indicating abyssal paleodepths above the CCD; (2) a mixed assemblage of displaced faunas in the debrites; (3) an impoverished early Oligocene–early-late Eocene assemblage indicating lower bathyal to abyssal paleodepths close to the lysocline; (4) an impoverished early-late to late-middle Eocene calcareous assemblage indicating lower bathyal to abyssal paleodepths close to the lysocline; and (5) an impoverished late-middle to late-early Eocene agglutinated assemblage indicating deposition below the CCD.

Long-core measurements established a magnetostratigraphy for the uppermost 40 mbsf, spanning the Brunhes Chron, Matuyama Chron, and part of the Gauss Chron. Below this, the interval characterized by debris flows disrupts the record and it is not possible to recognize a magnetostratigraphy until a depth of ~60 mbsf, where the record was correlated with the early Oligocene magnetic polarity time scale. A nonmagnetic APC coring assembly was used at this site, and produced significant improvement in the declination record in shallow APC cores. Excellent records were obtained both with and without the nonmagnetic assembly toward the bottom of the intervals cored by APC.

Construction of a composite depth section from Holes 1128B and 1128C indicates that a complete Pleistocene through upper Miocene sedimentary record was recovered at Site 1128. A break in the record occurs at ~68 mcd, corresponding to a 15-m-thick debris flow separating upper Miocene from lower Oligocene sediments. The numerous turbidites in the section aided correlation. The primary lithologic parameters used to create the composite section were magnetic susceptibility, gamma-ray attenuation (GRA) wet bulk density, natural gamma emissions data acquired by the multisensor track on whole cores, and color reflectance data (400 nm) measured on split cores.

Only low concentrations of methane were detected (maximum of 6.2 ppm), with most samples having less than 3 ppm. Calcium carbonate content has a bimodal pattern with generally high values (75–90 wt%) present in the upper 50 mbsf, followed by a decrease to a low of 2.1 wt% at 138 mbsf. Between 138 and 240 mbsf, carbonate content increases to a second mode with a maximum value of 68 wt%, and then decreases downhole with very low values (0–1 wt%) below 353 mbsf. Organic carbon concentrations are generally less than 0.16 wt% down to the base of Hole 1128B. Because organic carbon values are 0 wt% from 200 to 276 mbsf, and headspace methane concentrations in this depth range are barely above background, no samples in Hole 1128D were analyzed for organic carbon. Sulfur is present in only five samples in Hole 1128B, with values ranging from 0.05 to 0.21 wt%. Nitrogen is not detectable in any sample. Sulfur and nitrogen were not analyzed in samples from Hole 1128D.

Site 1128 does not appear to be influenced by the high-salinity pore fluids observed at Sites 1126 and 1127. With the exception of the lower part of the cored interval, salinities are close to normal seawater values throughout. As a consequence of slow rates of deposition and low concentrations of organic material, pore fluids are not significantly depleted in sulfate in the upper sediments, and rates of carbonate recrystallization are relatively low. Two significant changes in pore-water chemistry occur at Site 1128, the first at 20–40 mbsf, and the second between 236.8 and 253.3 mbsf. The change in pore-water chemistry at the shallow depth is manifest as an abrupt decrease in silica concentration from values of ~570 to 350 mM, corresponding to a slump unit. Seismic imagery indicates that this unit outcrops at the seafloor, so it is possible that bottom water infiltrates the formation to cause this effect. The second major

change in pore-water chemistry, accompanied by a decrease in salinity, is evident in most of the major and minor cations and occurs between the transition from lithostratigraphic Unit II to Unit IV. Concentrations of magnesium, potassium, sulfate, and sodium show a marked decrease, whereas lithium, alkalinity, and calcium increase. Although the change in salinity is accompanied by a decrease in chlorinity, the chloride decrease is not of the magnitude expected from the salinity decrease alone, indicating that a portion of the salinity decrease is a result of the removal of cations and anions through precipitation and adsorption. Downhole logs indicate the presence of numerous relatively impermeable layers in the interval between lithostratigraphic Units II and IV, which would effectively limit vertical diffusion between these two units and allow them to geochemically evolve relatively independently of each other. The sediments in lithostratigraphic Unit IV contain very low concentrations of carbonate minerals, and reactions leading to the enrichment and depletions in the pore-water constituents principally involve clay minerals.

Sediment physical properties data at Site 1128 closely reflect lithologic variations observed in the recovered sediments and provide essential data for core-log correlation. Physical properties data were subdivided into five units on the basis of trends in the measured parameters. Unit 1 (0–70 mbsf) is characterized by high variability in all datasets, corresponding to the lithologic sequence of turbidites and debris flows interbedded with nannofossil ooze. The base of this unit is marked by abrupt shifts in all parameters measured. Unit 2 (70–139 mbsf) is characterized by low variability in all datasets, punctuated by a number of distinct data offsets (1–5 m thick) corresponding to sharply bounded intervals of redeposited nannofossil ooze. Unit 3 (139–231 mbsf) is an interval characterized by relatively low and nearly constant values for all parameters, corresponding to a sequence of monotonous clays. An increase in NGR, magnetic susceptibility (MS), GRA, discrete *P*-wave velocity, and a decrease in porosity is observed at the upper boundary of Unit 4 (231–363 mbsf), after which all parameters display increased variability reflecting alternations of indurated and nonindurated sediments. The upper boundary of Unit 5 (363–452 mbsf) is marked by a negative shift in GRA, MS, and NGR, corresponding to the transition into lithostratigraphic Subunit IVB. Other than porosity, which decreases through the unit, the other parameters measured show constant downhole trends for the rest of the recovered interval.

Site 1128 was successfully logged with the triple combo and Sonic/FMS tools. Because of time constraints, the GHMT and WST tools were not run. Downhole logging data were divided into four units, with trends closely correlating with lithologic and sediment physical properties data. Unit 1 (0–242 mbsf) is characterized by uniform values, punctuated by sharp decreases in gamma-ray values and increases in density and resistivity apparently corresponding to intervals of redeposited nannofossil ooze. Unit 2 (242–295 mbsf) is characterized by high variability in all datasets measured, corresponding to an interval of high variability in sediment physical

properties data and an interval of variable lithification in cores. The lower part of this unit corresponds to lithostratigraphic Unit III and consists of nannofossil ooze interbedded with variably indurated sandstone turbidites. These interbedded sediments are reflected in logging data as alternations of low gamma-ray, high-density, and resistive intervals corresponding to calcite-rich layers, and high gamma-ray, low-density, and conductive intervals corresponding to sandstones. Logging Unit 3 (295–362 mbsf) has low variability and nearly constant values on all logs except the gamma ray, which increases downcore. Increased concentrations of thorium and potassium correspond to an increased concentration of terrigenous sediment. Unit 4 (363–414 mbsf) has minimal variability in most parameters, with the exception of cyclic variations in gamma-ray values. Downhole measurements from Unit 5 indicate the presence of clays and quartz through the unit as shown by the recovered sediment.

Site 1128 provided the first opportunity to sample and establish a seismic stratigraphy for this thick (containing over 10 km of sediment) and laterally extensive continental rise basin. Seismic imagery shows that the thin (72 m), relatively condensed Neogene section (largely corresponding to lithostratigraphic Unit I) was deposited in a small perched sub-basin lying within a thick Paleogene and Mesozoic succession and that the Neogene sequence is thin or absent over much of the basin. Exposed Mesozoic sediments on the middle and lower slope are the presumed source of lithified material commonly present within resedimented intervals. Although not intersected because of operational time constraints, a prominent angular unconformity ~150 m below total depth at Site 1128 almost certainly marks the base of the Cenozoic. Apart from hiatuses between the lower and middle Eocene and Oligocene and Miocene, Site 1128 results indicate that the upper part of this basin contains a thick, almost continuous biosiliceous record of Southern Ocean development through the Paleogene.

Site 1129

Site 1129 was the third and proximal site of a planned three-site transect through a spectacular set of late Neogene clinoforms immediately seaward of the present-day shelf edge. Site 1129, located just seaward of the shelf edge in 202.4 m of water, intersects the most expanded record of the oldest part of the clinoform sequence. The principal objective of this transect is to collect detailed, high-resolution profiles through a late Neogene shelf-edge (high energy) to upper slope (low energy) succession deposited within a cool-water carbonate environment, to determine the response of this type of depositional system to Pliocene–Pleistocene sea-level fluctuations.

The succession recovered at Site 1129 is 604.2 m thick (Table 2) and was subdivided into three lithostratigraphic units. Unit I (0–149.8 mbsf) consists mainly of unlithified bryozoan floatstone to rudstone and bioclastic packstone to grainstone, with abundant bryozoan fragments. The floatstone and rudstone are pale yellow to light gray and have a poorly sorted, very fine to

medium sand-sized bioclastic packstone matrix. The floatstone and rudstone contain abundant granule- to pebble-sized bryozoan fragments exhibiting highly diverse growth forms. The bioclastic packstone to grainstone is pale yellow, light gray, and light olive gray, and consists of very fine to fine sand-sized bioclasts with some coarse sand- to granule-sized bryozoan fragments. The unit is subdivided into five subunits, each forming a package grading upward from bioclastic packstone at the base to bryozoan floatstone and rudstone at the top, with each subunit representing an individual mound-building episode. Unit II (149.8–556.7 mbsf) consists of thick, light gray, light olive gray, and gray bioturbated bioclastic packstone and minor grainstone and wackestone with four nannofossil chalk intervals. Lithification increases from unlithified at the top of Unit II, to partially lithified with well-lithified chalk intervals at the base. The upper part of Unit II is dominated by very fine to fine sand-sized, generally well-sorted, massive bioclastic packstone with subordinate grainstone and wackestone. The lower part is characterized by muddy bioclastic mudstone, wackestone, and packstone with abundant well-defined burrows. Unit II therefore exhibits an overall coarsening-upward trend. Unit III (556.7–604.2 mbsf), with very poor recovery, consists of dolomitized fine sand-sized bioclastic grainstone and chert fragments. It is likely that the chert fragments represent thin beds and lenses of preferentially silicified wackestone/ooze. The boundary between Units II and III is very sharp, and represents a major hiatus.

Site 1129 contains two biostratigraphic units: (1) an expanded Quaternary section, more than 554 m thick, that is underlain by a thin and conformable Pliocene section, and (2) a middle–lower Miocene section. These units are separated at 556 mbsf by an unconformity representing ~12 m.y. The unconformity is marked by a bryozoan turbidite overlying indurated sediments and chert layers. Calcareous nannofossils are generally abundant and moderately well preserved in the upper part of the section, but below 371 mbsf the preservation is poor. Preservation and abundance of planktonic foraminifers degrade more rapidly downhole than the nannofossil assemblages. Below ~68 mbsf, most characteristic features of foraminifers are obscured by carbonate cement and recrystallization. Benthic foraminifers are generally abundant and well preserved in the upper part of Hole 1129C. At a depth of ~140 mbsf, preservation and abundance deteriorate markedly. Three main assemblages are recognized at Site 1129: (1) a distinctive, well-preserved Pleistocene assemblage found in bryozoan-rich accumulations (down to ~140 mbsf); (2) a Pleistocene assemblage (140–565 mbsf), which includes a variable redeposited neritic component; and (3) a sparse Miocene assemblage. The two Pleistocene assemblages indicate upper bathyal paleodepths, whereas the Miocene assemblage indicates an upper to middle bathyal paleodepth.

Long-core measurements of Hole 1129C sediments revealed an extensive interval of normal magnetization to a depth of ~340 mbsf. Sediments record reverse polarity magnetizations below that depth, with the boundary best defined by measurements on discrete samples. This reversal is

interpreted as the Brunhes/Matuyama boundary. In Hole 1129D, a long interval of predominantly reverse-polarity magnetizations to a depth of ~540 mbsf is interpreted as the upper part of the Matuyama Chron (C1r). The Jaramillo Subchron (C1r1n) is recorded in both holes at depths of ~400–440 mbsf. Normal polarities are recorded again in Hole 1129D at depths of 540–550 mbsf, possibly representing the Olduvai Chron (C2n). This would indicate a variable sedimentation rate, with late Pleistocene sedimentation nearly triple the rate of the early Pleistocene. Rock magnetic characteristics, such as near saturation with inductions of 400 mT and median destructive fields of the IRM of 20–40 mT, suggest that magnetite and possibly magnetic sulfides are the principal remanence carriers. ARM/IRM indicate a high relative abundance of single-domain grains, possibly biogenic magnetite.

High concentrations of methane and hydrogen sulfide through much of the section are a major feature at Site 1129. Methane and H_2S concentrations at this site fall between the levels found at Sites 1127 and Site 1131. Calcium carbonate content is uniformly high, primarily in the range of 86–94 wt%. Organic carbon concentrations generally vary from 0.4 to 0.7 wt%.

Site 1129, like many other sites drilled during Leg 182, is influenced by the presence of high-salinity pore fluids within and below the cored interval. Within the cored interval, the presence of pore waters with sodium/chloride ratios significantly higher than seawater indicates the influence of fluids that have been involved in the precipitation and dissolution of halite. Site 1129 was characterized by high rates of sulfate reduction of organic material and consequent production of alkalinity. The absence of significant iron concentrations resulted in a pH less than 6. Although high concentrations of hydrogen sulfide and high alkalinity values were measured at relatively shallow depths, significant sulfate reduction did not occur until below 100 mbsf. This suggests that hydrogen sulfide is diffusing from the underlying sediments into the overlying oxic sediments, where it is oxidized to sulfate. Rates of carbonate alteration, reflected in the strontium concentration (>2 mM), were the highest yet observed during Leg 182. Dolomite is ubiquitous below a depth of 70 mbsf and reached values as high as 24 wt%.

Physical properties measurements at Site 1129 correlate well with lithologic changes observed in the sedimentary section and provide an important data set for core-log correlation. In general, Site 1129 is characterized by significant variations in NGR and GRA bulk density. In general, variations are less marked in *P*-wave velocity, porosity, and other physical properties data. A well-defined cyclicity is seen in the NGR record and can be correlated with the downhole gamma-ray logs and NGR records from Site 1127 and 1131. Physical properties data were divided into three major units. Unit 1 (0–40 mbsf) is characterized by a rapid increase in NGR, as observed at most other Leg 182 sites. The base of this unit coincides with the top of the three bryozoan mound sequences, which form the lower part of lithostratigraphic Unit I. *P*-wave velocity and bulk density also increase with depth toward the base of this unit. Unit 2 (40–258 mbsf) is characterized by a uniformly high NGR with some cyclic variations and by a slight

increase in GRA bulk density and *P*-wave velocity. A significant offset to higher values of *P*-wave velocity and bulk density can be seen at 90 mbsf in Unit 2. Unit 3 (258–558 mbsf) is characterized by increasing *P*-wave velocity (1650–2450 m/s) and bulk density and decreasing porosity, which reflects the increasing induration of the succession. Below 558 mbsf, core recovery was too low for physical properties characterization of the deeper part of the sedimentary section.

Hole 1129D was successfully logged with three logging-tool strings. The triple combo produced very good results, except for the interval between 360 and 460 mbsf, where the porosity log was affected by excessive borehole rugosity. The log patterns are very similar to the logs from Hole 1131A; the uranium gamma-ray log showed distinct cyclicity in the lower part of the Pleistocene sequence, with 18–20 individual cycles, each measuring 10–20 m in thickness. Chalk layers and firmgrounds in the Pleistocene succession, as indicated by the conventional logs, are clearly imaged by FMS data. The FMS data also provide a detailed picture of the thickness distribution of thinly bedded cherts (~20 cm) and carbonates (1–2 m) in the middle upper Miocene succession, where recovery was very poor.

The high-resolution site survey seismic data at Site 1129 clearly images the bryozoan mound complex within lithostratigraphic Unit I and shows that this or similar mound complexes have existed at and immediately below the shelf edge throughout the Pleistocene. A combination of the results from Sites 1129 and 1131, now correlated with the recognition of a distinctive motif on seismic data, confirms that development of extensive bryozoan mound complexes has been one of the characteristic features of Pleistocene cool-water carbonate sedimentation across a large area of the western Great Australian Bight.

Site 1130

Site 1130 was located to intersect and characterize Neogene cool-water carbonate shelf-edge sequences and the nearshore portion of a Paleocene?–middle Eocene progradational siliciclastic wedge (seismic Sequences 2, 4, and 6A). The principal objectives were to (1) recover a detailed record of siliciclastic progradation and aggradation to evaluate the complex interaction among Paleogene sea-level fluctuations, accommodation space, and subsidence, (2) determine the facies characteristics, sea-level response, and paleoceanographic history of a Neogene cool-water carbonate succession in a shelf-edge setting, and (3) evaluate diagenetic history and processes within the Neogene facies in a shelf-edge setting.

The sediments recovered at Site 1130 were divided into four major lithostratigraphic units. Unit I (0–261.43 mbsf) is a light gray to pale olive, strongly bioturbated, unlithified to partially lithified bioclastic packstone. This succession is punctuated by unlithified bioclastic wackestone layers and occasional nannofossil foraminiferal ooze to chalk intervals. The upper part of this unit is characterized by a repetitive uphole textural change from matrix-supported to grain-

supported sediment. Lighter intervals in the otherwise monotonous packstones are fine grained and foraminifer rich, whereas the generally coarser and darker intervals contain more bioclasts. The lower part of Unit I is typified by gradual color changes ranging from light gray to olive gray, with a few abrupt transitions. Soft sediment deformation structures interpreted as slumps are present at the base of Unit I. Unit II (261.43–328.86 mbsf) is dominated by strongly bioturbated, white to light gray nannofossil foraminiferal chalk with a wackestone to packstone texture. Disseminated black grains (pyrite, glauconite, and other unidentifiable grains) are scattered throughout the unit. Unit III (328.86–369.5 mbsf) consists of chert layers (silicified nannofossil planktonic foraminiferal ooze) interbedded with intervals of white nannofossil planktonic foraminiferal ooze. The light to dark gray, partially translucent chert fragments contain burrows filled with white, fine-grained, lithified planktonic foraminiferal packstone to grainstone. Unit IV (369.5–386.51 mbsf) is dominantly a calcareous sandstone, but with compositional and textural variability encompassing red bioclastic glauconitic wackestone, sandy bryozoan grainstone, pink, coarse-grained bivalve grainstone, and red, very coarse-grained calcareous sandstone.

Calcareous nannofossils and planktonic foraminifers indicate that three biostratigraphic successions were recovered at Site 1130: (1) Pleistocene–upper Miocene (0–327 mbsf), (2) upper–middle Oligocene (327–~355 mbsf), and (3) a sandy limestone of unknown age from the bottom of Holes 1130A and 1130C. Preliminary results indicate that part of the Pliocene section is either missing or highly condensed and that the major disconformity between upper Miocene and Oligocene sediments represents a hiatus of at least 15 m.y. The sedimentation rate for the middle–upper Oligocene was 10–30 m/m.y., although this should be viewed with caution because of poor core recovery. The rate fluctuated between 15 and 30 m/m.y. during the Pliocene–Miocene, and reached as high as 240–260 m/m.y. during most of the Pleistocene. The three benthic foraminiferal assemblages recognized correspond respectively to the Oligocene, Pliocene–Miocene, and Pleistocene and indicate a shallowing-upward trend during these time periods. The Oligocene and Pliocene–Miocene assemblages are typically cosmopolitan, middle bathyal assemblages, whereas the Pleistocene contains a mixed assemblage representing upper bathyal paleodepths and containing many well-sorted specimens from shelf environments.

Long-core measurements revealed a deep episode of normal magnetization and then a sharp reversal to normal polarity at 199.9 mbsf, interpreted as the Brunhes/Matuyama boundary. Intensities of magnetization varied from 0.01 to 1 mA/M, with an overall decreasing trend downhole. Within this general trend are fluctuations with dominant wavelengths of a few tens of meters. The ratio of ARM/IRM, a measure of the relative importance of single-domain to multidomain behavior, decreases downcore, suggesting that the role of biogenic magnetite diminishes. Coupled with the decrease in magnetization, this strongly suggests that fine-grained magnetite of biogenic origin is preferentially dissolved.

An experimental nonmagnetic cutting shoe was used for alternate cores on Cores 182-1130A-3H to 7H, and an entire nonmagnetic core-barrel assembly was used on Cores 182-1130B-3H to 7H. Both the nonmagnetic shoe and core-barrel assembly produced reductions in radial component contamination, but the effects were not as dramatic as at Site 1128.

Construction of the composite section from Holes 1130A and 1130B indicates that a continuous sedimentary record was not recovered at Site 1130. Low recovery in Core 182-1130A-3H and no recovery in Core 182-1130B-3H produced a gap at 22 24 mbsf. The record below this is apparently continuous to ~191 mcd (all Pleistocene), at which point core overlap becomes minimal to nonexistent, disrupting continuity of the spliced section. The primary lithologic parameters used for correlation at Site 1130 were natural gamma emissions and a ratio of the 700:400 nm color reflectance data.

Only low concentrations of methane were detected, with most samples having less than 7 ppm (maximum = 11.3 ppm). Calcium carbonate content ranges from 80.9 to 93.2 wt% in lithostratigraphic Units I and II, with most samples varying between 85 and 90 wt%. No carbonate analyses were conducted in Units III and IV (328.9–386.51 mbsf) because of low core recovery.

Site 1130 is influenced by high-salinity pore fluids, as was the case at Sites 1126 and 1127. The maximum rate of salinity increase, 5.7/m, is the highest observed during Leg 182. The steep gradient down to ~32 mbsf, and then the constant salinity concentration (83) below, suggest nonsteady-state conditions. In contrast to Site 1127, the sulfate reduction zone is incomplete and confined to the upper part of the profile, and the degree of sulfate reduction is ~40% less than at Site 1127. These differences are probably caused by a lower initial organic carbon content at Site 1130. As a consequence of the decreased sulfate reduction activity, interstitial waters are saturated with respect to strontium sulfate, limiting pore-water strontium concentrations.

Sediment physical properties data closely reflect Oligocene–Holocene lithologic variations observed in recovered sediments and downhole logging data. Three physical properties units were recognized primarily on the basis of trends in NGR. The homogenous bioclastic packstones of Unit 1 (0–43 mbsf) are characterized by low variability in all measured parameters. The large increase in NGR from 5 to 35 cps at the base of Unit 1 does not correlate to any lithologic change, but is roughly coincident with an increase in *P*-wave velocity variability, suggesting that it results from diagenesis. Unit 2 (43–254 mbsf) is dominated by cyclic variations in NGR that appear to be related to Milankovitch cyclicity on a 100-k.y. frequency from 43 to 175 mbsf and on a higher 41-k.y. frequency for the remainder of the unit. This change in frequency occurs near the Brunhes/Matuyama boundary and is clearly seen in downhole logging data from this site. From 199 to 254 mbsf in Unit 2, increased variability in *P*-wave velocity corresponds to a series of firmgrounds observed in the recovered sedimentary section. The upper boundary of Unit 3 (254–335 mbsf) correlates well with a distinct change in lithology (lithostratigraphic Unit II)

from packstone/wackestone to nannofossil oozes and chalks. NGR and *P*-wave velocity show low variability within Unit 3, whereas bulk density shows a general increasing trend.

Three large-scale units were identified in downhole logging data from Hole 1130C, based on shifts in conventional and FMS logs, with boundaries at 258 and 329 mbsf. The interval above 260 mbsf is characterized by a near-constant background level of gamma radiation of 20 API, with individual spikes reaching 40–45 API. The boundary at 260 mbsf is defined at a sharp downhole decrease in the uranium gamma-ray log, and the boundary at 329 mbsf corresponds to the change from carbonate sediments above to siliciclastic deposits below.

Integration of the various datasets with the regional seismic stratigraphic interpretation provides a sequential record consisting of an Eocene? progradational wedge deposited at shelf water depths, overlain, after an indefinite hiatus, by deep-water late Oligocene oozes that have since been irregularly silicified. The record then contains another hiatus of ~20 m.y., before deposition of Miocene–Pliocene oozes that pass up into a packstone unit, as a continuation of a shallowing-upward trend. A further short hiatus was then followed by rapid deposition of a thick sequence of Pleistocene wackestones and packstones at upper slope/shelf-edge depths.

Site 1131

Site 1131 was the second and intermediate site of a planned three-site transect through a spectacular set of late Neogene clinoforms immediately seaward of the present-day shelf edge. Site 1131, located on the upper slope in 333.6 m of water, intersected the best record of the middle part of the clinoform sequence. The principal objective of this transect was to collect detailed, high-resolution profiles through a late Neogene shelf-edge (high energy) to upper slope (low energy) succession deposited within a cool-water carbonate environment and to determine the response of this type of depositional system to Pliocene–Pleistocene sea-level fluctuations.

Three major lithostratigraphic units were identified at Site 1131. Unit I (0–25.0 mbsf) consists dominantly of bioclastic packstone, floatstone, and rudstone. The upper part of Unit I is composed of a massive, homogeneous, light gray to olive gray, unlithified, bioclastic packstone, which includes a significant bryozoan component. The lower part of Unit I is a heterogeneous interval of unlithified bryozoan floatstone and rudstone punctuated by thin (decimeter scale) layers of wackestone, packstone, and grainstone. Unit II (25.0–531.7 mbsf) consists of a very thick (>500 m), homogeneous succession of light gray to olive gray, bioclastic packstone, grainstone, and wackestone. In general, lithification and diversity of the bioclastic component increase downhole, and large miliolid foraminifers appear in the lower part of Unit II. Unit III (531.7–607.4 mbsf) is separated from Unit II by an unconformity representing a major hiatus. Below the unconformity, recovery was incomplete in a succession consisting of dark gray, silicified nannofossil ooze beds or lenses within olive gray, partially to strongly lithified bioclastic grainstone containing blackened grains and glauconite.

Two biostratigraphic successions were identified at Site 1131: (1) an expanded Quaternary interval more than 510 m thick, underlain by a thin and conformable Pliocene (?) interval, and (2) a middle and lower Miocene section lacking hiatuses within the resolution of available biostratigraphic data. These successions are divided by a disconformity at 532 mbsf that spans ~10 m.y. An environmental crisis produced an unusual nannofossil assemblage dominated by *Braarudosphaera bigelowii* near the base of NN19 at ~522 mbsf. A similar event was observed in the same stratigraphic interval at Site 1127. Carbonate microfossils, especially foraminifers, were strongly affected by overgrowths, cementation, and recrystallization below 60–100 mbsf. These effects are consistent with the pore-water geochemistry and the onset of lithification. One main Pleistocene upper bathyal assemblage of benthic foraminifers is recognized above 100 mbsf. This assemblage also contains a large proportion of small neritic tests (63–150 µm), probably redeposited from the shelf. Poor preservation prevented detailed faunal analysis below 100 mbsf.

Magnetic measurements of archive-half cores established a magnetostratigraphy to a depth of 320 mbsf, which includes the Brunhes and uppermost Matuyama Chrons. Below this, drilling disturbance disrupted the record and no further magnetostratigraphic data were obtained. Rock magnetic properties show minimum downhole variability and are consistent with single-domain biogenic magnetite, except for cores at intermediate depths (70–150 mbsf) that display the typical behavior of ultrafine-grained (superparamagnetic) greigite. Magnetic susceptibility is dominated by contributions from the diamagnetic carbonate matrix.

Composite section construction from Holes 1131A and 1131B indicates that a continuous record was not recovered. Overlap between cores in adjacent holes was maintained to ~55 mcd, until poor recovery in Core 182-1131C-6H resulted in a short (few centimeters) data gap. Below 70 mbsf, low recovery from extended core barrel (XCB) cores resulted in reduced core overlap and prohibited splicing below 78 mcd. The primary parameters used for correlation were natural gamma-ray emissions, GRA bulk density, and color reflectance. Comparison of data between holes revealed a low degree of similarity, making correlations difficult.

The most striking organic geochemical results from Site 1131 were the high concentrations of methane (C_1) and hydrogen sulfide in the upper part of the section. In comparison to Site 1127, gas pockets were less abundant, and the concentration of C_1 in both gas pockets and headspace samples at Site 1131 was lower. Hydrogen sulfide concentrations, however, were comparable at both sites. Atypically, C_1/C_2 values first increase and then decrease with increasing depth in Hole 1131A, essentially mirroring the methane profile as C_2 varies little throughout the section. Calcium carbonate content is uniformly high (86–94 wt%). Organic carbon is less than 0.4 wt% down to 125 mbsf, with higher values (up to 1.0 wt%) at greater depths.

Site 1131 exhibited similar inorganic geochemical features as Site 1127, with the exception of more extreme changes in pore-water geochemistry profiles because of increased oxidation of

organic material. For example, alkalinity reached a maximum value of 137 mM, compared to 106 mM at Site 1127. In contrast to Site 1127, although there was significant depletion in the concentration of sulfate, measurable concentrations remained even in the zones of highest alkalinity, suggesting that organic material was the limiting factor in the production of hydrogen sulfide at Site 1131. Excess sulfate in the upper portion of the core suggests that the oxidation of hydrogen sulfide originated lower in the section. In the upper 300 m, there was depletion in the concentration of calcium and magnesium and enrichment in Sr, indicating the recrystallization of aragonite and HMC. This was confirmed by mineralogical analyses, which showed that HMC had disappeared by 50 mbsf. Aragonite gradually decreased with increasing depth, and vanished at the Pliocene/Pleistocene boundary. Ratios of sodium to chloride were in excess of the ratio in seawater throughout the Pleistocene section, indicating that the waters responsible for the high-salinity fluids had participated in the precipitation and dissolution of halite.

Physical properties measurements at Site 1131 correlate well with lithologic changes observed in the sedimentary section and provide the basic data for core-log correlation to reconstruct poorly recovered intervals. Correlation of downhole gamma-ray logs with NGR data from the multisensor track (MST) indicates that moderate to poor recovery at Site 1131 may have aliased and concealed in cores the cyclic fluctuations that are clearly visible on downhole logs. Physical properties data indicate that the cored interval is divisible into two units. Unit 1 (0–31 mbsf) is mainly defined by a large increase in NGR toward the base of the unit, corresponding to the lower limit of the bryozoan floatstone/rudstone comprising lithostratigraphic Subunit IA. This NGR peak is also observed on downhole logs, with spectral gamma data indicating that it reflects uranium content and, accordingly, is either the result of increased organic matter content or carbonate diagenesis. *P*-wave velocity and bulk density also increase toward the base of this unit. Unit 2 (31–532 mbsf) is characterized by gradual increases in porosity, *P*-wave velocity, and bulk density, primarily reflecting increased compaction, but also showing data excursions corresponding to coarser and more lithified horizons. More indurated layers within the generally homogenous sediments of Unit 2 have increased velocities and bulk densities, and generally lower NGR. Below 532 mbsf, core recovery was too low for physical properties characterization of the deeper part of the sedimentary section.

Three successful logging-tool strings were deployed in Hole 1131A. Downhole logging data indicate that the uppermost part of the cored section (0–28 mbsf) correlates with bryozoan-rich horizons described in core. As was noted with the physical properties data, a uranium peak at the base of this unit reflects increased organic content and/or carbonate diagenesis and may indicate a firmground. The remainder of the cored section to 575 mbsf contains porosity-density crossovers that coincide with low PEF values and high resistivity and sonic values. These crossovers are interpreted as probable chert layers. In contrast, low-porosity peaks associated with density, PEF, sonic, and resistivity peaks may represent possible firmgrounds.

Integration of coring results with high-resolution site survey seismic data at Site 1131 confirms that the mounded features visible in the uppermost part of the seismic section are in fact bryozoan-dominated mounds. The spectacular clinoform geometry corresponding to the remainder of the cored interval consists of bioclastic packstone, grainstone, and wackestone, with variable lithification as the dominant factor controlling seismic data amplitude and impedance variability. The lithostratigraphic and biostratigraphic boundary toward the base of the section coincides with a major regional unconformity and sequence boundary.

Site 1132

Site 1132 was located to intersect and characterize Neogene cool-water carbonate shelf-edge sequences and the nearshore portion of a Paleocene?–middle Eocene progradational siliciclastic wedge (seismic Sequences 2, 3, 4, and 6A). The principal objectives were to (1) recover a detailed record of siliciclastic progradation and aggradation to evaluate the complex interaction between Paleogene sea-level fluctuations, accommodation space, and subsidence; (2) determine the facies characteristics, sea-level response, and paleoceanographic history of a Neogene cool-water carbonate succession in a shelf-edge setting; and (3) evaluate the diagenetic history and processes within the Neogene facies in a shelf-edge setting.

The recovered succession was subdivided into six lithostratigraphic units. Unit I (0–113.5 mbsf) consists of bryozoan floatstone and rudstone, alternating with bryozoan packstone and, in the lower part, also bioclastic wackestone with bryozoans. The abundant bryozoan fauna are highly diverse and include a great variety of growth forms. The sediments are unlithified and burrow mottled, and the color is dominantly light gray with thinner pale olive and white intervals. This unit represents a major bryozoan mound complex. Unit II (113.5–158.3 mbsf) consists of uniform bioclastic packstone with a great diversity of bryozoan growth forms. The color is light gray, with minor light olive gray and white intervals. The sediment is burrow mottled and mainly unlithified, but thin, partially lithified beds are present at 130–140 mbsf. Unit III (158.3–250.7 mbsf) consists of unlithified bioclastic packstone and minor wackestone and grainstone, with an interbedded thin package of foraminiferal ooze and chalk. The unit is strongly burrowed and mainly unlithified down to 168 mbsf and partially lithified below that level. The color is dominantly light olive gray with thinner olive, pale olive, and white intervals. Several prominent firmgrounds are the basis for subdivision into five subunits. Unit IV (255.8–437.33 mbsf) was poorly recovered; however, available data suggest that it consists of bioclastic packstone and grainstone with an interval of nannofossil foraminiferal chalk partially replaced by nodular, light to dark gray chert. Unit V (441.5–517.7 mbsf) is also characterized by poor recovery, but recovered material indicates that it consists of bioclastic packstone and grainstone and lacks chert. Glauconite is abundant, and the colors vary between very pale brown and pale yellow. Unit VI (517.7–555.95 mbsf) is topped by a prominent mineralized hardground

and consists of lithified bioclastic packstone and wackestone. It differs from overlying units in its colors, prominent firmgrounds and hardgrounds, solution seams, and centimeter-sized bioclasts. The color is pale yellow at the top and passes downward into light gray, pale yellow, red yellow, to pale and dark red at the bottom. The lowest recovered bed contains pebbles of siliciclastic sandstone, rich in lithic fragments.

Calcareous nannofossils and planktonic foraminifers indicate that drilling at Site 1132 recovered a thick Pleistocene–Eocene sequence (~550 m thick), overlying a relatively thin, barren section (~45 m). Calcareous nannofossils from the basal Pleistocene registered a nannofossil event, the "*Braarudosphaera* Event," which previously was recorded at Sites 1127, 1130, and 1131, indicating a dramatic short-lived change in surface-water conditions over a large geographic area. The thick Pleistocene section contains (~230 m) Zones NN21/NN20 and NN19, and the equally thick middle Miocene section (~300 m) contains Zones NN6 and NN5/NN4. These sections are separated by a thin interval (~20 m) with poor core recovery. Hiatuses are likely within this thin interval, where the recovered nannofossils and planktonic foraminifers suggest late Miocene age. Another similarly thin interval (~20 m) with poor core recovery, which is also likely to contain hiatuses, is recorded between the middle Miocene section and the underlying mainly lower Oligocene. An Eocene age is indicated for the section underlying the lower Oligocene, based on thin-section analysis of two samples at ~530 and ~547 mbsf, respectively. A sharp change in sedimentation rates corresponds to the condensed interval between Pleistocene and middle Miocene sections. The Pleistocene section registered an average sedimentation rate of 175 m/m.y., whereas the middle Miocene showed an average rate of 20 m/m.y. Another condensed section between the middle Miocene and Oligocene successions is indicated by the sparse biostratigraphic datums through this interval. Four main benthic foraminifer assemblages are identified. These indicate upper to middle bathyal paleodepth for the Pleistocene–Oligocene section. In the Pleistocene, a striking, well-preserved assemblage characterized by many large (>1 mm) agglutinated forms is found within bryozoan-rich accumulations. This assemblage probably reflects a diverse, highly dynamic ecosystem that became established at the seafloor at various times during the Pleistocene, corresponding to episodes of bryozoan mound growth. Changes in the composition of this assemblage may relate to sea-level or circulation fluctuations.

The Brunhes/Matuyama boundary was found at ~180 mbsf, yielding a sedimentation rate of ~230 m/m.y. There were indications of the same intensity fluctuations observed at earlier sites; therefore, there is a possibility of high-resolution stratigraphy within the Brunhes Chron after further shore-based work. The top of the Jaramillo Subchron was found at 230 mbsf, which is consistent with this sedimentation rate. Magnetic anomalies were found associated with hardgrounds with mineralized crusts, and with lithified skeletal limestones. In some cases, this suggests that diagenesis occurred extremely early, within 100,000 yr of sedimentation.

As at Sites 1126, 1128, and 1130, only low concentrations of methane were detected at Site 1132. Of the four sites, Site 1132 has the highest methane content, with a maximum value of 54 ppm. Unlike the other low-methane sites, hydrogen sulfide is present at Site 1132 in low concentrations. Calcium carbonate content is between 85 and 95 wt%, with values at the higher end of the range near the surface and declining gradually toward the lower end of the range with depth. Organic carbon values are primarily in the range of 0.3–0.6 wt%. Nitrogen concentrations are all less than 0.1 wt%, and sulfur is present, at low concentrations, in only a few samples in the upper 90 mbsf.

Site 1132, similar to the previous sites except 1128, is influenced by the presence of high-salinity fluids. However, unlike the neighboring Site 1130, the rate of salinity increase with depth is uniform and shows no evidence of nonsteady-state conditions. Site 1132 possibly had an initially higher organic carbon content, producing slightly higher sulfate reduction rates and a more extended sulfate reduction zone. In turn, carbonate diagenesis is more active, causing carbonate precipitation in the upper part of the profile, whereas the lower part is characterized by carbonate dissolution. As with Site 1131, Site 1132 displays a sodium/chloride anomaly in the upper part of the profile. Site 1132 is characterized by a constant seawater composition of both conservative and nonconservative interstitial water constituents in the upper 30 mbsf, suggesting active flushing with seawater. With the completion of the slope transect from Site 1130 to 1132, we can draw initial conclusions about the horizontal distribution of brine in this area. It appears that salinity values at Sites 1130 and 1132 stabilize at about the same depth below the sea surface, suggesting a horizontal top of the main brine body ~520 meters below sea level (mbsl).

High-quality NGR and gamma-ray attenuation porosity evaluator (GRAPE) bulk density data were obtained from the MST. Variations of NGR and GRAPE bulk density, supplemented by index properties measurements of porosity and thermal conductivity, form the basis for the five PP units recognized at Site 1132. Unit 1 (0–5 mbsf) is characterized by very low (<5 cps) NGR and a high initial bulk density (>1.9 g/cm^3), which declines rapidly with depth. This unit corresponds to a thin package of grainstones that caps lithostratigraphic Unit 1. Unit 2 (5–140 mbsf) has an overall increase in bulk density with depth (1.65–1.90 g/cm^3). There is a corresponding decrease in porosity from 55% to 43%, but with considerable variation, probably associated with lithological variability. High-amplitude cyclic variation in both NGR (>20 cps) and bulk density (0.2 g/cm^3) is also observed throughout this unit. Unit 3 (140–248 mbsf) is characterized by a decline with depth in GRAPE bulk density and porosity and by a continued but more regular cyclicity in both NGR and GRAPE bulk density. Unit 4 (~248–520 mbsf) is recognized solely on the basis of a change in NGR from 25 to <5 cps at 248 mbsf. Similar characteristics are present in limited core recovery from 516 to 520 mbsf, with cherts having the anticipated high values of *P*-wave velocity. Unit 5 (>520 mbsf) is poorly characterized because of limited recovery and drilling disturbance. NGR shows a shift back to higher values (10–20

cps), but there are considerable fluctuations associated with the much greater variety of lithologies present.

Two logging runs were attempted at Site 1132. The triple combo successfully logged 560 m, whereas hole conditions limited the FMS/Sonic tool to only 70 m. Logging data closely reflect lithologic variations observed in the upper 245 mbsf of the section. Below this depth, downhole logs enable the characterization of sedimentary sequences in low recovery intervals and assist in intersite correlations. Logging data were subdivided into four units on the basis of variations in the collected datasets. Unit 1 (0–242 mbsf) is characterized by an increase in the magnitude and variability of gamma-ray values that are mainly the result of increased uranium concentrations. High and variable uranium contents continue for the remainder of the unit, with an abrupt decrease at the boundary with Unit 2. In the open-hole logged interval below 104 mbsf, separation of the porosity and density curves indicate a somewhat higher noncarbonate fraction than is present in the remainder of the hole. This noncarbonate fraction is only slightly enriched in K and Th. The base of Unit 1 correlates well with the base of lithostratigraphic Unit III. Unit 2 (242–437 mbsf) is characterized by a return to low gamma-ray values and increased variability in the magnitude of density and porosity variations, possibly caused by chert layers. In addition, resistivity logs from Unit 2 indicate that drilling fluid invasion occurred within this partially lithified packstone interval, suggesting higher porosity than in surrounding units. In the lower part of Unit 2, both porosity and density values increase, as does the degree of fluid invasion. The base of Unit 2 correlates well with the base of lithostratigraphic Unit IV, and is characterized by increases in resistivity and decreases in gamma-ray values, porosity, and density. Unit 3 (437–524 mbsf) is characterized by nearly constant density and gamma-ray values and variable porosity. Resistivity logs show low variability and indicate that drilling fluid invasion occurred in this interval, although to a lesser extent than in the units above and below. Unit 3 correlates well with lithostratigraphic Unit V, which, despite low recovery, appears to be dominated by a homogenous interval of lithified bioclastic grainstones. The upper boundary of Unit 4 (524–537 mbsf) is marked by a sharp increase in all parameters. Within the limited section logged, resistivity measurements show increased drilling fluid invasion. The gamma-ray increase in Unit 4 is dominated by increased Th and K, indicating the presence of terrigenous minerals within the carbonate sediments. Unit 4 correlates with lithostratigraphic Unit VI.

Regional seismic stratigraphic correlation shows that the Pleistocene bryozoan mound complex, represented on seismic imagery by a distinctive mounded facies, occurs in a narrow band immediately below the shelf edge along much of the western Great Australian Bight. Lithostratigraphic data indicate that bryozoans are also important constituents of underlying nonmounded packstone and grainstone facies corresponding to the lower parts of seismic Sequence 2. Seismic Sequences 3 (middle-late Miocene) and 4 (early Oligocene–middle Miocene) are characterized by bioclastic grainstones, packstones, and wackestones, with minor

foraminiferal ooze. Increased amplitudes toward the base of Sequence 3 probably represent increased impedance contrast associated with interbedded silicified horizons, and disconformity surfaces visible on the high-resolution seismic within both sequences appear to correlate with firmgrounds and hardgrounds. Lithostratigraphic and biostratigraphic data show that the small mounds immediately overlying the distinctive Sequence 7 progradational wedge are composed of lithified bioclastic packstone and wackestone of Eocene age. The only samples recovered from Sequence 7 are carbonate-cemented sandstone fragments forming the uppermost sequence boundary, with the underlying friable sandstones being too poorly cemented for recovery.

Site 1133

Site 1133 is located on the middle-upper slope in 1037.2 m of water. It was one of two paleoceanographic sites located to intersect pelagic sections that collectively span the entire Cenozoic succession and form the deeper water component of the shelf-to-basin transect. The principal objectives at this site were to (1) recover pelagic ooze from the middle-upper slope to construct a Cenozoic paleoceanographic record of the opening of the Southern Ocean and the development of the Circum-Antarctic Current, (2) determine the history of Cenozoic CCD fluctuations and intermediate water mass variations, and (3) determine depositional and diagenetic facies on the middle-upper slope.

Sediments recovered at Site 1133 were divided into two major lithostratigraphic units. Unit I (0–28.55 mbsf) consists of gray and white, moderately to strongly bioturbated calcareous ooze with varying amounts of calcareous nannofossils and planktonic foraminifers. This unit was subdivided into three subunits based on color changes, textural differences, firmgrounds, and a scoured surface. The boundary between Unit I and II is marked by a firmground that separates overlying white nannofossil ooze from underlying unlithified bioclastic wackestone. Unit II (28.55–142.59 mbsf) consists mainly of (1) gray to light gray, poorly sorted, unlithified bioclastic wackestone, with very fine-grained silt- to sand-sized particles; (2) gray, light gray to light olive gray, uniform, unlithified to partially lithified bioclastic packstone, with poorly to well-sorted silt- to sand-sized grains; and (3) gray to dark gray chert/porcellanite (silicified wackestone). Most of the recovered sediments are pebble- to cobble-sized fragments. Some porcellanite/chert fragments are draped with a thin layer of unlithified to partially lithified bioclastic packstone. It is likely that the entire unit consists of bioclastic packstone or wackestone containing beds or lenses of preferentially silicified limestone (formerly nannofossil planktonic foraminiferal ooze/chalk).

Drilling at Site 1133 revealed the presence of two major biostratigraphic units, dated by nannofossils and planktonic foraminifers as Pleistocene and middle–early Miocene. The Pleistocene sequence extends down to 21.49 mbsf and overlies a thin, highly condensed interval with upper Miocene assemblages. This disconformity represents a hiatus of at least 3 m.y., and a

second disconformity at 28.55 mbsf separates upper Miocene from lower–middle Miocene (Zone NN5/NN4). Three main benthic foraminifer assemblages are recognized—a diversified Pleistocene calcareous assemblage, a diversified upper Miocene assemblage, and an impoverished middle–lower Miocene assemblage. All three assemblages indicate middle to lower bathyal paleodepths.

Magnetic measurements of archive-half cores establish a tentative Pleistocene magnetostratigraphy to 40 mbsf in Hole 1133B, which includes the Brunhes Chron (0–12 mbsf), Matuyama Chron (12–24 mbsf), and Gauss Chron (24–? mbsf). The interpretation is problematic because the same result was not reproduced in Hole 1133A, which yielded uniform normal polarity magnetizations to a depth of 20 mbsf and anomalously shallow magnetizations of both polarities below this depth. Intensities are low; after demagnetization to 20 mT, median values are ~7×10^{5} A/m. Intensity fluctuations are closely correlated with lithology in both holes but appear to be inversely correlated with magnetic susceptibility. Anomalously high intensities and susceptibilities are observed in both holes at ~30 mbsf. Rock magnetic properties are consistent with single-domain biogenic magnetite or greigite as the remanence carrier. Magnetic susceptibility is dominated by contributions from the diamagnetic carbonate matrix.

Construction of the composite and spliced section from Holes 1133B and 1133C indicates that a complete record of the cored interval between 0 and 39 mcd (34 mbsf) was recovered. This depth interval includes Holocene and Pleistocene–early Miocene age sediments. Distinctive high-amplitude events occur in the reflectance and GRA density records, enabling easy correlation between holes. Difficulties in correlation result from a slumped interval at ~20–32 mcd; however, the base of the slumped interval is clearly defined and provides a good correlation horizon.

Except for two samples with slightly higher methane contents, generally low concentrations of methane (<12 ppm) were detected at Site 1133. Calcium carbonate content ranges from 78.5 to 94.4 wt%, with most samples between 85 and 92 wt%. Organic carbon values are <0.4 wt%.

Seven interstitial water samples were collected at Site 1133. These data indicate that Site 1133 may be, as was the case with most other sites, underlain by high-salinity fluids, although the maximum salinity value measured was 41 at 123.4 mbsf. Compared to shallower sites, the sulfate reduction rate is substantially reduced and the resulting maximum alkalinity values are <5.24 mM. This, together with the small variations in excess calcium, suggests that the rate of carbonate diagenesis is slower than at other Leg 182 sites.

Physical properties measurements at Site 1133 were limited because of poor core recovery. Data were divided into two units, with the boundary correlating with the base of the Pleistocene. Unit 1 (0–21.8 mbsf) is characterized by increasing NGR (5–22 cps), bulk density (1.65–1.95 g/cm^3), velocity (1.57–1.62 km/s), and decreasing porosity (62%–45%). At the base of Unit 1, NGR values decrease to 5 cps, bulk density decreases to 1.8 g/cm^3, and porosity shows a general

increase to 58%. Unit 2 (21.8–152.1 mbsf) is mainly composed of neritic carbonate with low NGR values (~5 cps), variable density, and variable velocities, correlating with an alternation between high-velocity silicified limestones and packstones and lower velocity partially lithified/unlithified packstones.

Site 1134

Site 1134 is located on the eastern Eyre Terrace upper slope in 701 m of water. This site was designed to intersect Cenozoic seismic Sequences 2, 3, and 4 and lobes 2 and 3 of Sequence 6A (Feary and James, 1998), and as much of the upper part of the Cretaceous section as time permitted. The principal objectives at this site were to (1) collect a detailed record of Paleogene–early Neogene temperate to subtropical mid-latitude sedimentation in an upper-slope environment and (2) recover a record of marine flooding of the evolving rift basin in the Cenomanian. The target depth at this site was just below a high-amplitude reflector of probable Cenomanian age, estimated before drilling to be 520 mbsf (on the basis of stacking velocities).

Site 1134 contained a 397.1-m-thick record (Table 2) of middle Eocene–middle Pleistocene sedimentation that was subdivided into six units. Unit I (0–33 mbsf) consists of calcareous nannofossil ooze with varying amounts of planktonic foraminifers. In general, whitish matrix-supported intervals, consisting of planktonic foraminifers, sponge spicules, bioclasts, benthic foraminifers, radiolarians, and minor tunicate spicules in the >63-µm fraction, alternate with darker, grainier, light gray intervals that contain echinoid spines as well as rare glauconite, pyrite, and unidentified black grains. Unit II (33–66 mbsf) is characterized by soft-sediment deformation interpreted as slumping. Two slumped intervals were identified, with the lower interval defining the boundary between Units II and III. Unit II consists of white to light gray, calcareous nannofossil ooze and calcareous nannofossil foraminifer ooze, as well as unlithified wackestones, packstones, floatstones, and rudstones. The light gray wackestones to rudstones contain a wide variety of coarse components such as various bryozoans (robust and delicate branching, arborescent, and fenestrate growth forms), bioclasts, sponge and tunicate spicules, as well as pellets. Pebble-sized lumps of calcareous nannofossil ooze, which are interpreted to be reworked clasts, are observed in packstones and floatstones. Unit III (66–152 mbsf) consists of calcareous nannofossil ooze and calcareous nannofossil foraminifer ooze. In the lower part of the unit, there are short-term alternations between unlithified and lithified sediment that are too rapid to be solely related to sediment compaction. The lower limit of alternating lithification corresponds to the base of Sequence 3 and thus may reflect condensed sedimentation related to this sequence boundary. The lower limit of Unit III is marked by a change from dominantly pelagic sediments to partially lithified wackestones of Unit IV. Unit IV (152–214.3 mbsf) consists of unlithified to partially lithified wackestone/packstone, foraminifer chalk, and very minor packstone. The style of deposition is uniform throughout the unit, characterized by meter-

scale alternations of light gray foraminifer chalk and light gray to gray wackestone/packstone. The unlithified to partially lithified wackestone/packstone contains similar components to the chalk, but it is richer in glauconite and dominated by bioclasts. Some of these layers have a sharp base and are normally graded, and thus are interpreted as turbidites. The lower boundary of Unit IV has been placed at the top of a white foraminifer chalk. In Unit V (214.3–368.2 mbsf), two main lithologies were recovered: (1) strongly bioturbated calcareous nannofossil chalk and (2) fragments of porcellanite and chert. The matrix of white chalk is dominated by calcareous nannofossils with common sponge spicules as well as trace amounts of bioclasts and dolomite, whereas the coarse fraction consists of planktonic and benthic foraminifers. The gray and green porcellanite are silicified chalk. Only 30 cm of the lowermost Unit VI (368.2–397.1 mbsf) was recovered. The sediments within this unit are coarse sand-sized, brown limonitic sandstones with quartz, limonite, glauconite, mica, and abundant skeletal grains, as well as minor planktonic foraminifers.

Calcareous nannofossils and planktonic foraminifers indicate that sediments recovered at Site 1134 range from Quaternary to middle Eocene in age. Two hiatuses are indicated: the first occurs within the Pliocene (nannofossil Zones NN18–NN13 missing at ~57 mbsf) and the second in the middle–upper Miocene (nannofossil Zones NN9–NN7 missing at ~114 mbsf). Planktonic foraminifers also indicate hiatuses at approximately the same depths. A third hiatus may be present in the Eocene section as nannofossil Zone NP17 was not recognized; however, poor core recovery makes confirmation of this hiatus difficult. Calcareous nannofossils are moderately well preserved above ~200 mbsf, with decreasing preservation below this level. Planktonic foraminifers are moderately well preserved throughout most of Hole 1134A, with preservation deteriorating only in the lowermost 30 m of the hole. Benthic foraminifers are generally rare compared to planktonic foraminifers, decreasing in abundance in the lower 130 m of Hole 1134A. Preservation of benthic foraminifers is comparable to that of the planktonic foraminifers. The five main assemblages of benthic foraminifers can be correlated with coevel assemblages at Site 1126 and indicate middle bathyal paleodepths.

Long-core measurements at Site 1134 indicate that the intensity of magnetization is extremely weak in the uppermost 100 mbsf, similar to that at Site 1126. However, discrete measurements revealed that a stable remanence is present, and the Brunhes/Matuyama boundary was identified in both holes. Magnetization intensity decreases to a minimum near 110 mbsf in a manner characteristic of the dissolution of fine magnetic particles. There is a marked increase in intensity to 120 mbsf, which coincides with the first appearance of chert at Site 1134. A brief magnetostratigraphy was determined within the Anomaly 5 sequence. Whole-core measurements and nonmagnetic coring experiments were continued, but the intensity of magnetization was so weak that further analysis is required from shore-based work.

Construction of a composite section for Site 1134 indicates that recovery of Holocene–middle Miocene sediments was complete to a depth of 151.7 mcd. The composite section was constructed primarily using 400 nm color reflectance, the 700:400 nm color reflectance ratio, and GRA bulk density data from Holes 1134A and 1134B. The mcd scale at Site 1134 is expanded by ~6% relative to the mbsf scale. The upper 35 m of sediment (lithostratigraphic Unit I) exhibits cyclic oscillations in color reflectance, which are distinctively correlatable between holes. Lithostratigraphic Unit II (34.7–68.9 mcd) contains two slumped intervals that yield excellent correlative horizons at their tops and bases. Lithostratigraphic Unit III (>68.9 mcd) is more difficult to correlate because of dissimilarities in the records of each hole, which may be a result of differential lithification and diagenesis.

Methane concentrations at Site 1134 were low with maximum concentrations of 7.7 ppm and average concentrations less than 5 ppm. Calcium carbonate contents range from 58 to 94 wt%, averaging 80–92 wt%.

Site 1134 was characterized by a very steep gradient in pore-water salinity, reaching values of 97 by a depth of 65.90 mbsf. This salinity gradient is similar to that measured at Sites 1130 and 1126 and is consistent with the idea that the brine has a common level beneath all sites and is controlled by the level of the hydrostatic head during sea-level lowstands. Because of the low initial concentration and accumulation of organic material at Site 1134, oxidation rates of organic material and carbonate diagenesis are reduced compared to the more proximal sites. Significant geochemical reactions appear to take place only in the upper 40 mbsf at Site 1134. In this interval, there is a decrease in the concentration of metastable minerals such as aragonite and HMC and in the appearance of small concentrations of dolomite. As a result, there is only a small increase in strontium with depth an increase that is quickly swamped by increases associated with greater salinity. The concentration of iron in interstitial waters from Site 1134 is higher than at shallow-water hydrogen sulfide-dominated sites, reaching concentrations >60 mM.

Sediment physical properties measurements closely reflect lithologic variations and provide essential data for core-log correlation. These data were subdivided into four units based on variations in measured parameters. Unit I (0–33 mbsf) is characterized by a sharp decrease in porosity (50%–30%) and increase in bulk density (1.7–2.0 g/cm^3) and *P*-wave velocity (1.6–1.8 km/s) that corresponds to the nannofossil ooze succession of lithostratigraphic Unit I. The top of Unit 2 is defined by an abrupt increase in bulk density and NGR and correlates with the transition from nannofossil ooze to unlithified bioclastic wackestone. Unit 2 (33–66 mbsf) is typified by high variability in *P*-wave velocity, bulk density, and NGR that correlates with intervals of soft sediment deformation interpreted as slumps. Unit 3 (66–145 mbsf) is characterized by a gradual decrease in bulk density and *P*-wave velocity, and a sharp decrease in NGR (10–2 cps). The lower part of the unit shows a marked increase in magnetic susceptibility (negative values to ~10×10^{-6} SI units) and porosity. The base of Unit 3 is defined by an increase

in NGR and a sharp decrease in magnetic susceptibility. Unit 4 (145–368 mbsf) shows highly variable *P*-wave velocity, bulk density, and porosity, which results from alternation of nannofossil oozes and wackestones/packstones in the upper part, and alternations between chalk and chert in the lower part of the unit.

Three logging strings were successfully deployed in Hole 1134A. Overall, downhole measurement trends are similar to those at Site 1126C, but gamma-ray values at Site 1134 display markedly higher values than at Site 1126C. The sedimentary succession at Site 1134 was divided into six logging units based on trends in the data that reflect lithologic alternations between calcareous ooze, wackestones, grainstones, and thin chert interbeds. Positive density and porosity separation and relatively high PEF values indicate the presence of dolomite toward the top of Unit 1. Narrow separation of density and porosity and relatively low PEF values indicate the presence of quartz in the carbonates of Unit 2. The presence of blackened grains in recovered cores coincides with higher gamma-ray values, indicating a possible phosphatic and/or glauconitic composition. Downhole logs also identify an interval of unusually low potassium concentrations in Unit 3, the significance of which is still to be established. Density, PEF, caliper, and resistivity were the only logs acquired in the sandstones at the base of the succession (Unit 6). High density and high PEF peaks are consistent with the small amount of limonitic sandstone recovered from this horizon, which may correspond to Unit 8 at Hole 1126C. Seven checkshot stations were recorded, with individual stations situated near the estimated depths of significant reflectors.

REFERENCES

Bein, J., and Taylor, M.L., 1981. The Eyre Sub-basin: recent exploration results. *APEA J.*, 21:91–98.

Bone, Y., James, N.P., and Kyser, T.K., 1992. Syn-sedimentary detrital dolomite in Quaternary cool-water carbonate sediments, Lacepede Shelf, south Australia. *Geology,* 20:109–112.

Boreen, T.D., and James, N.P., 1993. Holocene sediment dynamics on a cool-water carbonate shelf, southeastern Australia. *J. Sediment. Petrol.,* 63:574–588.

Davies, H.L., Clarke, J.L.A., Stagg, H.M.J., Shafik, S., McGowran, B., and Willcox, J.B., 1989. Maastrichtian and younger sediments from the Great Australian Bight. *Bur. Miner. Resour. Aust. Rec.,* 288.

Feary, D.A., 1995. Proposal for an ODP site survey cruise by the R/V Rig Seismic in the western Great Australian Bight. *Geol. Surv. Aust.*, 67.

Feary, D.A., and James, N.P., 1995. Cenozoic biogenic mounds and buried Miocene (?) barrier reef on a predominantly cool-water carbonate continental margin, Eucla Basin, western Great Australian Bight. *Geology,* 23:427–430.

Feary, D.A., and James, N.P., 1998. Seismic stratigraphy and geological evolution of the Cenozoic, cool-water, Eucla Platform, Great Australian Bight. *AAPG Bull.,* 82:792–816.

Feary, D.A., James, N.P., and McGowran, B., 1994. Cenozoic cool-water carbonates of the Great Australian Bight: reading the record of Southern Ocean evolution, sea level, paleoclimate, and biogenic production. *Geol. Surv. Aust.*, 62.

Haq, B.U., Hardenbol, J., and Vail, P.R., 1987. The chronology of fluctuating sea level since the Triassic. *Science,* 235:1156–1167.

Hegarty, K.A., Weissel, J.K., and Mutter, J.C., 1988. Subsidence history of Australia's southern margin: constraints on basin models. *AAPG Bull.,* 72:615–633.

James, J.M., 1992. Corrosion par melange des eaux dans les grottes de la plaine de Nullarbor, Australie. *Karst Evol. Climat.,* 333–348.

James, J.M., Rogers, P., and Spate, A.P., 1989. Genesis of the caves of the Nullarbor Plain, Australia. *Proc. 10th Int. Congr. Speleol.:* Budapest, 263–265.

James, N.P., Bone, Y., and Kyser, T.K., 1993. Shallow burial dolomitization of Cenozoic cool-water calcitic deep shelf limestones, southern Australia. *J. Sediment. Petrol.*, 63:528–538.

James, N.P., and Kendall, A.C., 1992. Introduction to carbonate and evaporite facies models. *In* Walker, R.G., and James, N.P. (Eds.), *Facies Models, Response to Sea Level Change:* St. Johns, NF (Geol. Assoc. Can.), 265–276.

James, N.P., and von der Borch, C.C., 1991. Carbonate shelf edge off southern Australia: a prograding open-platform margin. *Geology,* 19:1005–1008.

Kendall, C.G.St.C., and Schlager, W., 1981. Carbonates and relative changes in sea level. *In* Cita, M.B., and Ryan, W.B.F. (Eds.), Carbonate platforms of the passive-type continental margins. *Mar. Geol.,* 44:181–212.

Kennett, J.P., 1982. *Marine Geology:* Englewood Cliffs (Prentice-Hall).

Kennett, J.P., and Barker, P.F., 1990. Latest Cretaceous to Cenozoic climate and oceanographic developments in the Weddell Sea, Antarctica: an ocean-drilling perspective. *In* Barker, P.F., Kennett, J.P. et al., *Proc. ODP, Sci. Results,* Leg 113: College Station, TX (Ocean Drilling Program), 937–960.

Kennett, J.P., and Barron, J.A., 1992. Introduction. In Kennett, J.P., and Warnke, D.A. (Eds.), The Antarctic Paleoenvironment: A Perspective on Global Change. *Am. Geophys. Union,* 56:1–6.

Marshall, J.F., 1986. Regional distribution of submarine cements within an epicontinental reef system: Central Great Barrier Reef, Australia. *In* Schroeder, J.H., and Purser, B.H. (Eds.), *Reef Diagenesis:* New York (Springer-Verlag), 8–26.

McKenzie, J.A., Isern, A., Elderfield, H., Williams, A., and Swart, P., 1993. Strontium isotope dating of paleoceanographic, lithologic, and dolomitization events on the northeastern Australian margin, Leg 133. *In* McKenzie, J.A., Davies, P.J., Palmer-Julson, A., et al., *Proc. ODP, Sci. Results,* 133: College Station, TX (Ocean Drilling Program), 489–498.

Miller, K.G., Fairbanks, R.G., and Mountain, G.S., 1987. Tertiary oxygen isotope synthesis, sea level history, and continental margin erosion. *Paleoceanography,* 2:1–19.

Nelson, C.S., 1988. An introductory perspective on non-tropical shelf carbonates. Sediment. Geol., 60:3 12. Reeckmann, S.A., 1988. Diagenetic alterations in temperate shelf carbonates from southeastern Australia. *In* Nelson, C.S., (Ed.), Non-tropical shelf carbonates: modern and ancient. *Sediment. Geol.,* 60:209–219.

Rockford, D.J., 1986. Seasonal changes in the distribution of Leeuwin Current waters off southern Australia. *Aust. J. Mar. Freshwater Res.,* 37:1–10.

Sarg, J.F., 1988. Carbonate sequence stratigraphy. *In* Wilgus, C.K., Hastings, B.S., Kendall, C.G.St.C., Posamentier, H., Ross, C.A., and Van Wagoner, J. (Eds.), *Sea-Level Changes: An Integrated Approach.* Spec. Publ. Soc. Econ. Paleontol. Mineral., 42:155–181.

Simms, M., 1984. Dolomitization by groundwater-flow systems in carbonate platforms. *Trans. Gulf Coast Assoc. Geol. Soc.,* 34:411–420.

Stagg, H.M.J., Cockshell, C.D., Willcox, J.B., Hill, A.J., Needham, D.J.L., Thomas, B., O'Brien, G.W., and Hough, L.P., 1990. Basins of the Great Australian Bight region: geology and petroleum potential. *Bur. Miner. Resour. Aust. Rec.,* 5.

Vahrenkamp, V.C., Swart, P.K., and Ruiz, J., 1991. Episodic dolomitization of late Cenozoic carbonates in the Bahamas: evidence from strontium isotopes. *J. Sediment. Petrol.,* 61:1002–1014.

Willcox, J.B., Stagg, H.M.J., Davies, H.L., et al., 1988. Rig Seismic research cruises 10 & 11: geology of the Central Great Australian Bight region. *Rep. Bur. Mineral Resour. Geol. Geophys. (Aust.),* 286.

TABLE CAPTIONS

Table 1. Summary of Pleistocene magnetostratigraphy.

Table 2. Summary of operations.

FIGURE CAPTIONS

Figure 1. Location of the Leg 182 drill sites in the western Great Australian Bight.

Figure 2. Schematic North-South diagram from the Nullarbor Plain to the upper continental slope across the Eyre Terrace (along longitude 128°E), showing the distribution and internal relationships of seven Cenozoic sequences (unshaded) defined from seismic data, overlying Mesozoic synrift siliciclastic sequences, and Precambrian crystalline basement (after Feary and James, 1998). Vertical scales are approximate.

Figure 3. Lithostratigraphic summary of the western transect. Inset is schematic north-south diagram showing the location of the western transect sites.

Figure 4. Lithostratigraphic summary of the eastern transect. Inset is interpreted seismic line showing the location of the eastern transect sites.

Figure 5. Major biostratigraphic units, unconformities, and paleobathymetric units recorded at Leg 182 sites.

Figure 6. Age-depth plots of biostratigraphic datum levels, showing major hiatuses and estimated sedimentation rates. Datum controls are weaker in stratigraphically older sections, due partly to poor preservation and partly to the temperate nannofossil and foraminifer assemblages that contain few age-diagnostic species.

Figure 7. Summary of paleomagnetic data (inclination) and interpreted magnetostratigraphy for sites on the **(A)** eastern and **(B)** western shelf-slope transects of Leg 182. Cross symbols are long-core measurements at 5–10 cm intervals, whereas discrete samples and lithified core fragments are shown as open symbols. The interpreted magnetostratigraphy is the same for Holes 1130A and 1130B.

Figure 8. Contour map of Cl^- concentration at Sites 1127, 1131, and 1129 overlying the interpretation of the seismic line joining the three sites. Note that the concentrations of equal Cl^- concentration crosscut the seismic sequences and appear to originate from a subhorizontal brine. Cl^- concentrations are given in millimoles per liter (mM). Normal sea water concentration is 559 mM.

Figure 9. Concentration of methane (triangles), ethane (circles), and propane (diamonds) in headspace samples from Site 1129. Note the maximum in concentration of all three gaseous species occurs between 200 and 500 mbsf. This is particularly significant for the higher weight alkanes and suggests that they are not migrating from deeper in the section.

Figure 10. Concentration of dolomite at Sites 1127, 1131, and 1129. The highest sustained concentrations (10–15 wt%) occur at Sites 1129 and 1131, although samples with values as high as 35 wt% were measured at Site 1127. The dolomitization is principally associated with the Pleistocene sediments.

Figure 11. JNOC seismic line JA90-31 for the eastern drilling transect, overlain with spectral gamma radiation (right curve at each site), bulk density (left curve at Sites 1131 and 1129), and porosity (left curve at Site 1127) from the downhole logs. Because of high H_2S in the drill hole at Site 1127, the nuclear source of the HLDS was not used. Thus, there are no bulk density estimates for this site. All data were converted to two-way traveltime using a linear interpolation of traveltime from the seafloor to the bottom of the drilled interval.

Polarity events and age	Chron boundaries	Site 1127 Depth (mbsf)	Site 1128 Depth (mbsf)	Site 1129 Depth (mbsf)	Site 1130 Depth (mbsf)	Site 1131 Depth (mbsf)	Site 1132 Depth (mbsf)	Site 1133 Depth (mbsf)	Site 1134 Depth (mbsf)
Brunhes/Matuyama	C1n/C1r1r	343.4	14	340	200	293-295	170-181	12	32
0.78 Ma		1127B-37X-4	1128B-2H-4	1129C-37X-3	1130B-22X-4	1131A-33X-3, 4	1132B-19X-21X	1133B-3H-1	1134A-4H-6
Termination Jaramillo	C1r1r/C1r1n	380.7	20	392-402	210	303	186		37
0.99 Ma		1127B-41X-4	1128B-3H-2	1129D-5R-6R	1130B-23X-4	1131A-34X-3	1132B-21X-3		1134A-5H-4
Onset Jaramillo	C1r1n/C1r2r1r	393-395	22	435-445	212		193		41
1.07 Ma		1127B-42X-5, 6	1128B-3H-4	1129D-9R-10R	1130B-23X-6		1132B-22X-2		1134A-5H-6
Termination Olduvai	C1r2r2r/C2n		28	540	215		222-229		
1.77 Ma			1128B-4H-1	1129D-20R-3	1130B-24X-1		1132B-25X, 26X		
Onset of Olduvai	C2n/C2r		32		220				
1.95 Ma			1128B-4H-4		1130B-24X-5				
Termination of Gauss	C2r/C2An		40						
2.5 Ma			1128B-5H-3						

Note: Section numbers identify location of chron boundaries for each site.

Table 1

Hole	Latitude	Longitude	Water depth (mbsf)	Number of cores	Length cored (m)	Length recovered (m)	Recovery (%)	Interval drilled (m)	Total penetration (mbsf)	Time on site (days)
1126A	33° 30.5615' S	128° 03.9957' E	784.8	1	9.5	9.69	102.0%	0.0	9.5	0.3
1126B	33° 30.5613' S	128° 03.9922' E	783.7	30	253.5	162.55	64.1%	9.8	263.3	1.3
1126C	33° 30.5638' S	128° 04.0101' E	783.8	17	154.0	138.52	89.9%	0.0	154.0	0.7
1126D	33° 30.5613'S	128° 03.9844'E	783.8	33	313.3	40.47	12.9%	150.0	463.3	2.4
		Site 1126 totals:		**81**	**730.3**	**351.23**	**48.1%**	**159.8**	**890.1**	**4.7**
1127A	33° 21.4457'S	128° 28.8780'E	478.7	1	9.5	9.68	101.9%	0.0	9.5	0.1
1127B	33° 21.4504'S	128° 28.8765'E	479.3	55	510.7	440.36	86.2%	0.0	510.7	3.2
		Site 1127 totals:		**56**	**520.2**	**450.04**	**86.5%**	**0.0**	**520.2**	**3.4**
1128A	34° 23.4686'S	127° 35.4419'E	3875.8	1	9.5	9.31	98.0%	0.0	9.5	0.4
1128B	34° 23.4706'S	127° 35.4455'E	3874.6	30	280.7	231.57	82.5%	0.0	280.7	1.8
1128C	34° 23.4633'S	127° 35.4619'E	3874.3	26	240.1	232.84	97.0%	0.0	240.1	1.5
1128D	34° 23.4563'S	127° 35.4554'E	3874.3	23	221.4	79.08	35.7%	231.2	452.6	3.9
		Site 1128 totals:		**80**	**751.7**	**552.80**	**73.5%**	**231.2**	**982.9**	**7.6**
1129A	33° 17.3857'S	128° 28.8718'E	202.9	2	13.8	13.27	96.2%	9.5	23.3	0.3
1129B	33° 17.3783'S	128° 28.8606'E	202.3	2	19.0	10.24	53.9%	22.0	41.0	0.3
1129C	33° 17.7942'S	128° 28.8785'E	202.5	48	451.6	322.89	71.5%	0.0	451.6	0.8
1129D	33° 17.7887'S	128° 28.8675'E	202.1	26	250.6	76.72	30.6%	353.6	604.2	2.2
		Site 1129 totals:		**78**	**735.0**	**423.12**	**57.6%**	**385.1**	**1120.1**	**3.6**
1130A	33° 25.2113'S	127° 36.1398'E	486.7	41	380.4	312.47	82.1%	0.0	380.4	1.9
1130B	33° 25.2091'S	127° 36.1249'E	488.2	33	310.4	300.80	96.9%	0.0	310.4	0.8
1130C	33° 25.1988'S	127° 36.1248'E	488.1	10	96.0	23.30	24.3%	299.2	395.2	1.7
		Site 1130 totals:		**84**	**786.8**	**636.57**	**80.9%**	**299.2**	**1086.0**	**4.4**
1131A	33° 19.5655'S	128° 28.8721'E	333.6	66	616.9	371.69	60.3%	0.0	616.9	3.2
1131B	33° 19.5541'S	128° 28.8528'E	331.4	12	105.8	95.14	89.9%	0.0	105.8	0.6
		Site 1131 totals:		**78**	**722.7**	**466.83**	**64.6%**	**0.0**	**722.7**	**3.8**
1132A	33° 18.9569'S	127° 36.1304'E	218.0	1	9.3	9.23	99.2%	0.0	9.3	0.1
1132B	33° 18.9713'S	127° 36.1322'E	218.5	32	284.6	217.35	76.4%	0.0	284.6	1.1
1132C	33° 18.9624'S	127° 36.1235'E	218.5	39	366.2	22.42	6.1%	237.0	603.2	2.6
		Site 1132 totals:		**72**	**660.1**	**249.00**	**37.7%**	**237.0**	**897.1**	**3.8**
1133A	33° 32.3694'S	128° 54.3063'E	1037.2	1	9.5	9.78	102.9%	0.0	9.5	0.2
1133B	33° 32.3783'S	128° 54.3173'E	1037.2	19	152.1	48.59	31.9%	0.0	152.1	0.8
1133C	33° 32.3887'S	128° 54.32098'E	1036.8	6	53.3	37.26	69.9%	0.0	53.3	0.6
		Site 1133 totals:		**26**	**214.9**	**95.63**	**44.5%**	**0.0**	**214.9**	**1.6**
1134A	33° 31.7244'S	127° 15.8400'E	701.0	43	397.1	195.54	49.2%	0.0	397.1	2.4
1134B	33° 31.7388'S	127° 15.8377'E	699.9	25	234.8	158.76	67.6%	0.0	234.8	0.9
		Site 1134 totals:		**68**	**631.9**	**354.30**	**56.1%**	**0.0**	**631.9**	**3.3**
		Leg 182 totals:		**623**	**5753.6**	**3579.52**	**62.2%**	**1312.3**	**7065.9**	**36.3**

Table 2

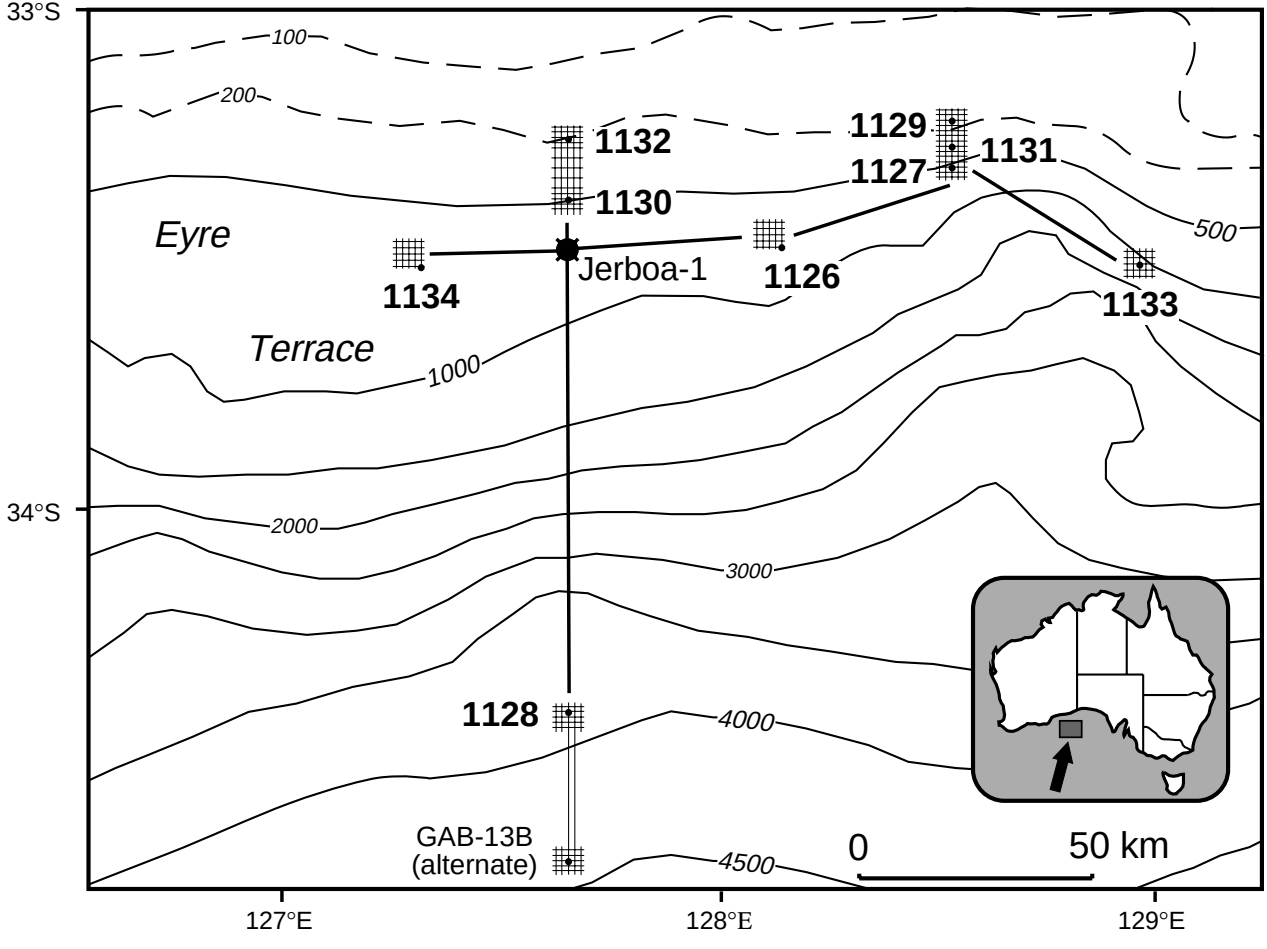
33°S
34°S
127°E
128°E
129°E
100
200
500
1000
2000
3000
4000
4500
1132
1129
1131
1127
1130
1126
1133
1134
1128
Jerboa-1
GAB-13B
(alternate)
Eyre
Terrace
0
50 km

Figure 1

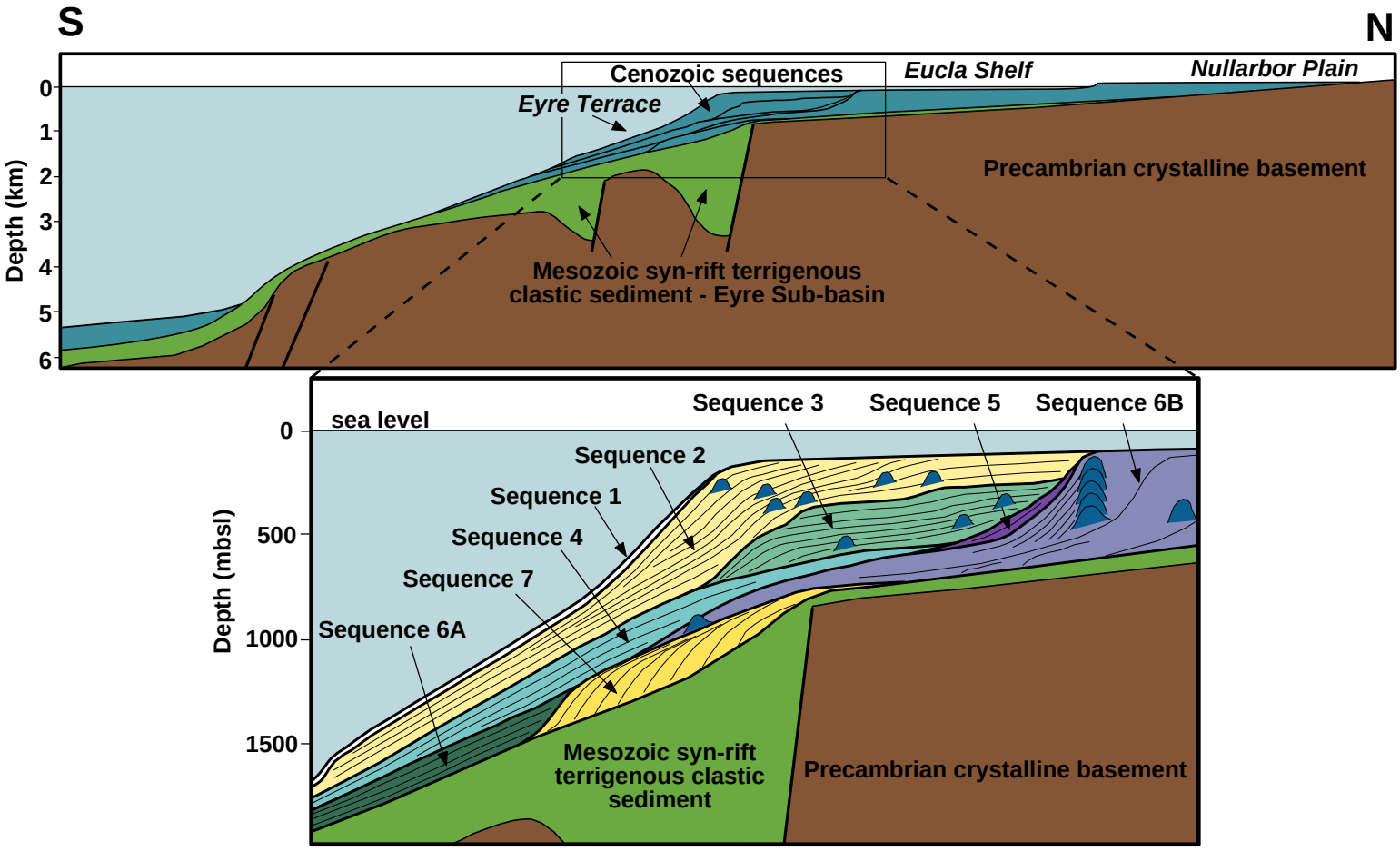
S
N
Cenozoic sequences
Eucla Shelf
Nullarbor Plain
Eyre Terrace
Depth (km)
0
1
2
3
4
5
6
Precambrian crystalline basement
Mesozoic syn-rift terrigenous
clastic sediment - Eyre Sub-basin
sea level
Sequence 3
Sequence 5
Sequence 6B
Sequence 2
Sequence 1
Sequence 4
Sequence 7
Sequence 6A
Depth (mbsl)
0
500
1000
1500
Mesozoic syn-rift
terrigenous clastic
sediment
Precambrian crystalline basement

Figure 2

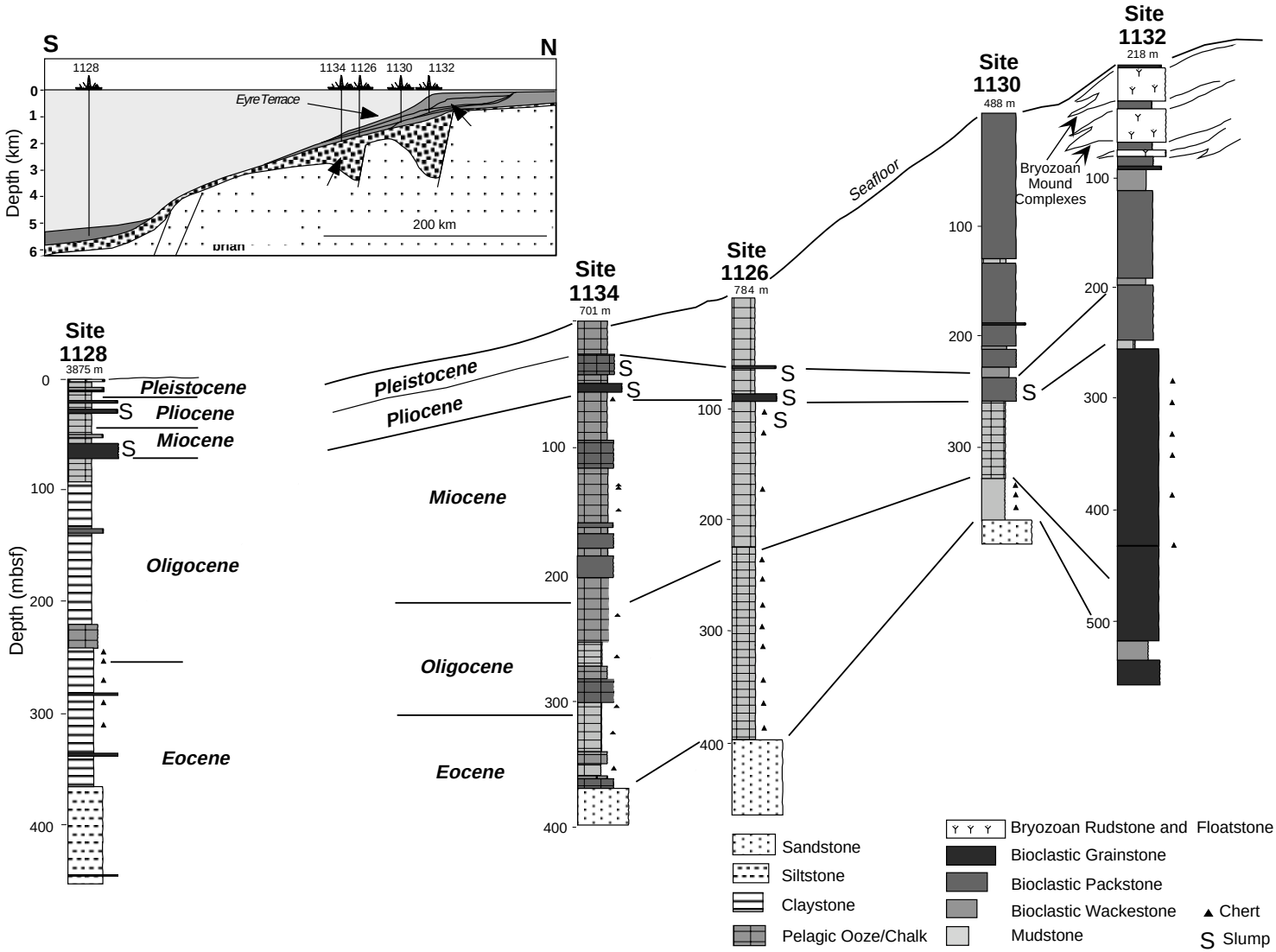
S
N
1128
1134 1126 1130 1132
Eyre Terrace
Depth (km)
200 km
Site 1128
3875 m
Site 1134
701 m
Site 1126
784 m
Site 1130
488 m
Site 1132
218 m
Seafloor
Bryozoan Mound Complexes
Pleistocene
Pliocene
Miocene
Oligocene
Eocene
Depth (mbsf)
Sandstone
Siltstone
Claystone
Pelagic Ooze/Chalk
Bryozoan Rudstone and Floatstone
Bioclastic Grainstone
Bioclastic Packstone
Bioclastic Wackestone
Mudstone
Chert
Slump

Figure 3

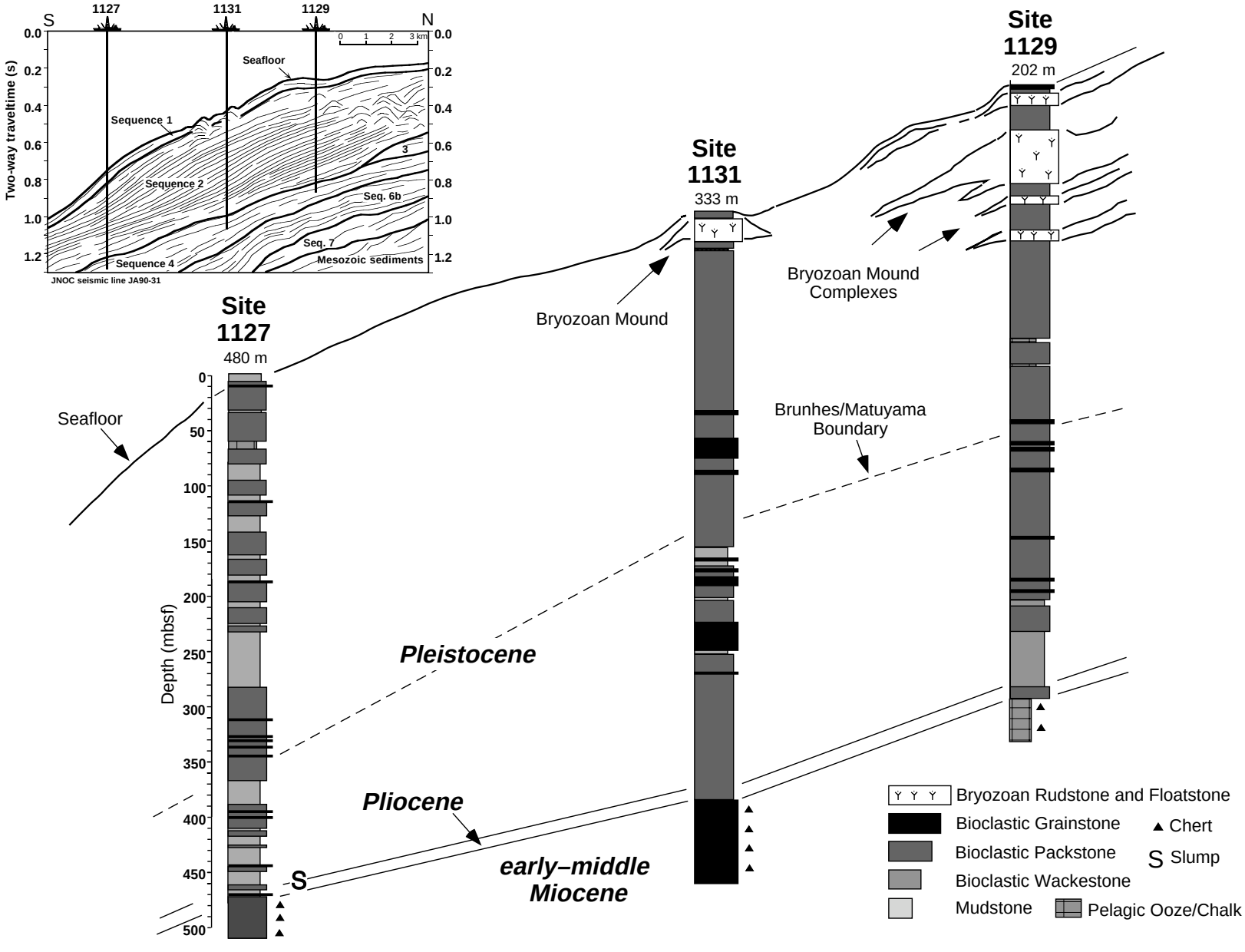
S
1127
1131
1129
N
0 1 2 3 km
Seafloor
Sequence 1
Sequence 2
3
Seq. 6b
Seq. 7
Sequence 4
Mesozoic sediments
Two-way traveltime (s)
JNOC seismic line JA90-31
Site 1127
480 m
Site 1131
333 m
Site 1129
202 m
Bryozoan Mound
Bryozoan Mound Complexes
Seafloor
Brunhes/Matuyama Boundary
Depth (mbsf)
Pleistocene
Pliocene
early–middle Miocene
S
Bryozoan Rudstone and Floatstone
Bioclastic Grainstone
Bioclastic Packstone
Bioclastic Wackestone
Mudstone
Chert
Slump
Pelagic Ooze/Chalk

Figure 4

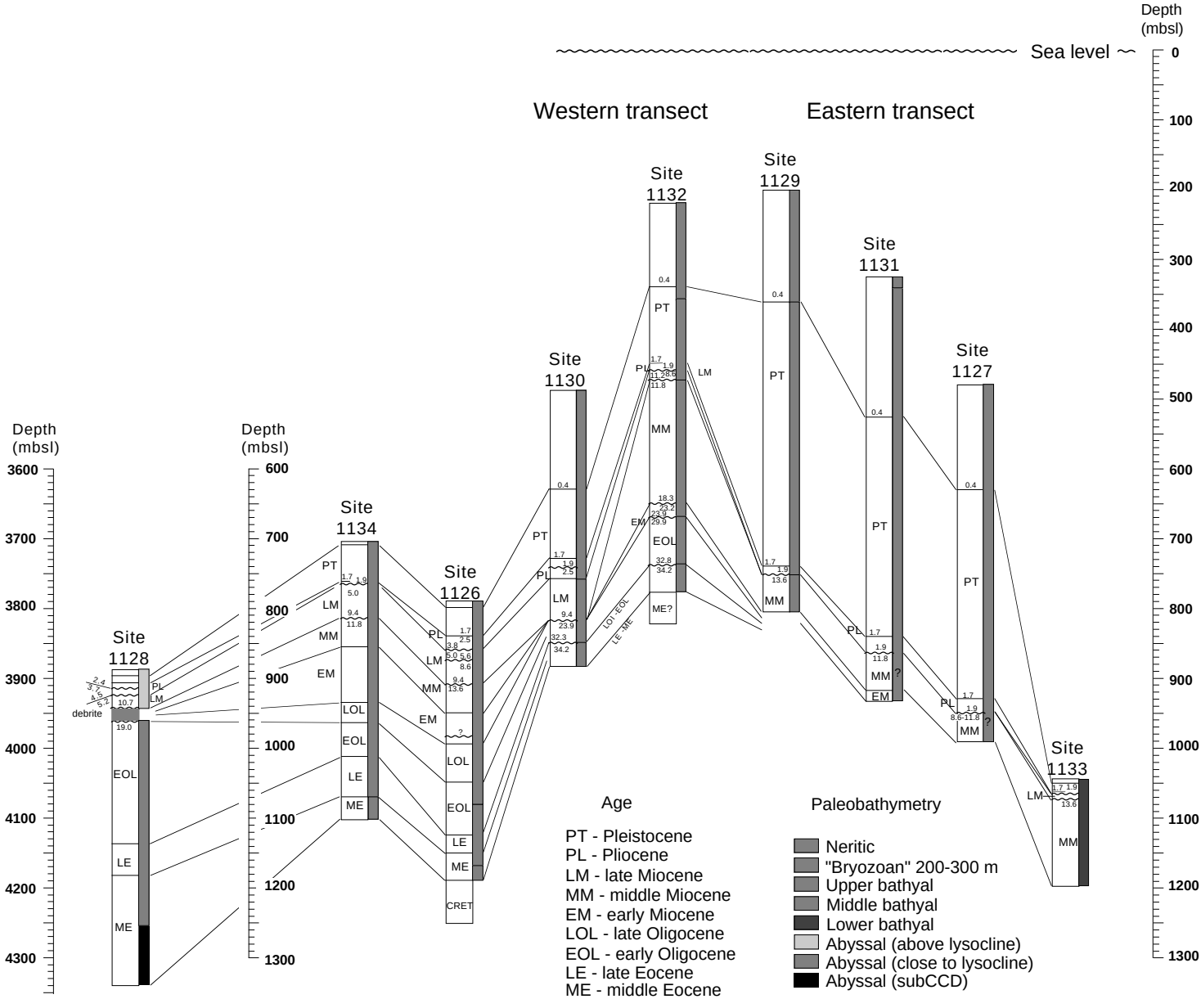
Depth (mbsl)
Sea level
Western transect
Eastern transect
Site 1128
Site 1134
Site 1126
Site 1130
Site 1132
Site 1129
Site 1131
Site 1127
Site 1133
debrite
PT
PL
LM
MM
EM
LOL
EOL
LE
ME
CRET
LOL-EOL
LE-ME
Age
PT - Pleistocene
PL - Pliocene
LM - late Miocene
MM - middle Miocene
EM - early Miocene
LOL - late Oligocene
EOL - early Oligocene
LE - late Eocene
ME - middle Eocene
Paleobathymetry
Neritic
"Bryozoan" 200-300 m
Upper bathyal
Middle bathyal
Lower bathyal
Abyssal (above lysocline)
Abyssal (close to lysocline)
Abyssal (subCCD)

Figure 5

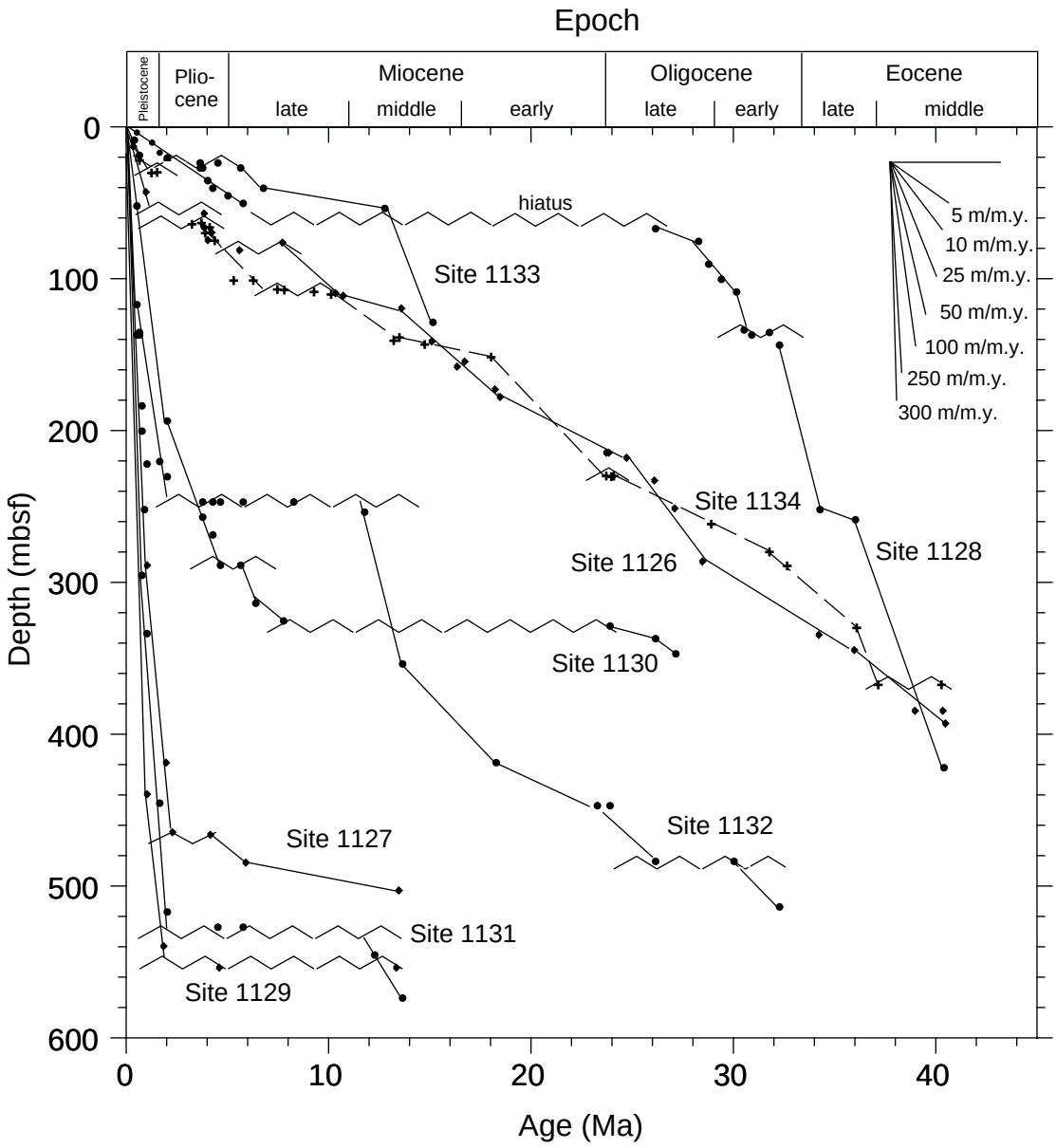
Epoch
Pleistocene
Plio-
cene
Miocene
late
middle
early
Oligocene
late
early
Eocene
late
middle
hiatus
Site 1133
Site 1134
Site 1128
Site 1126
Site 1130
Site 1132
Site 1127
Site 1131
Site 1129
5 m/m.y.
10 m/m.y.
25 m/m.y.
50 m/m.y.
100 m/m.y.
250 m/m.y.
300 m/m.y.
Depth (mbsf)
0
100
200
300
400
500
600
0
10
20
30
40
Age (Ma)

Figure 6

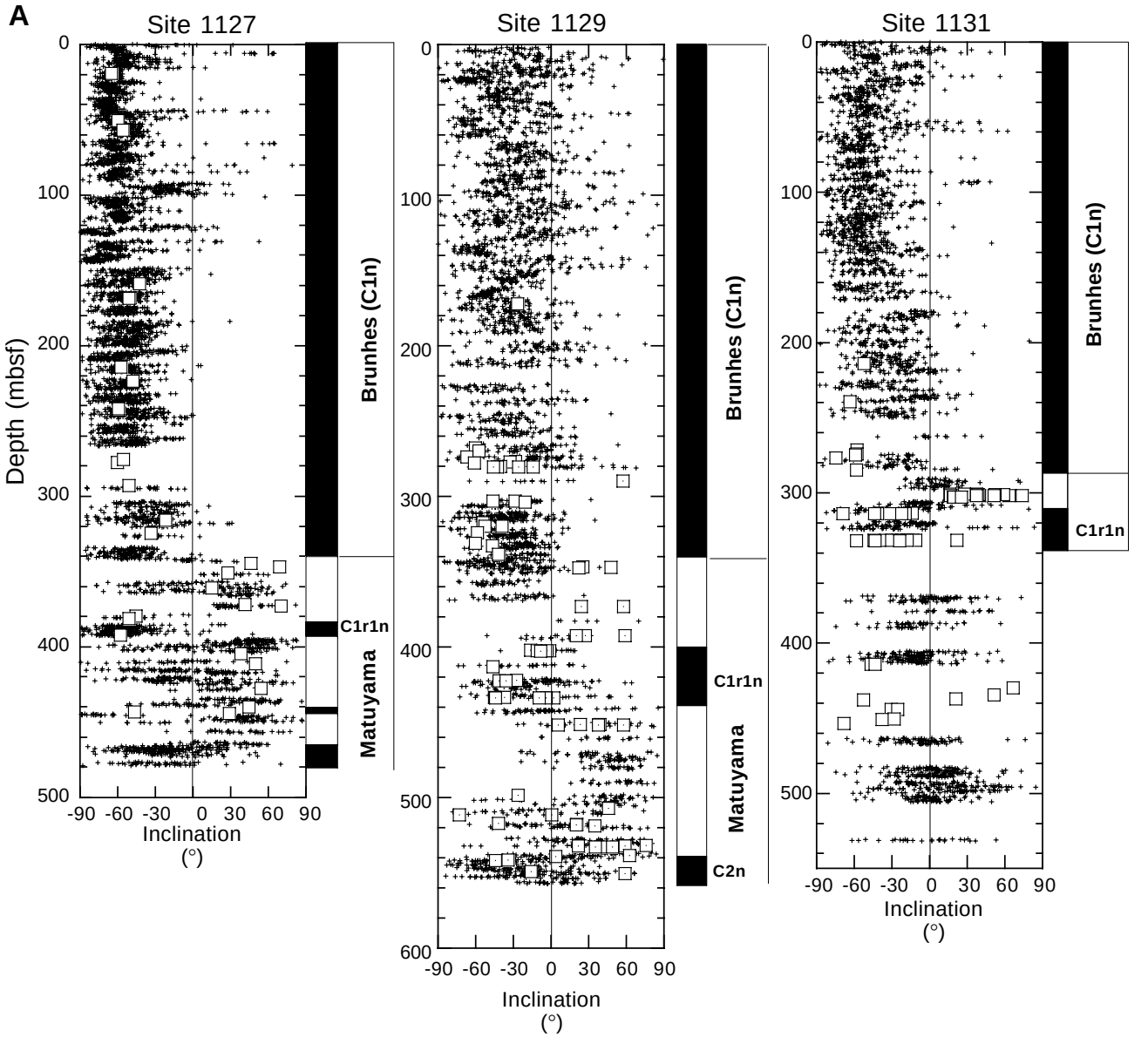
A
Site 1127
Site 1129
Site 1131
Depth (mbsf)
Inclination (°)
Brunhes (C1n)
C1r1n
Matuyama
C2n

Figure 7A

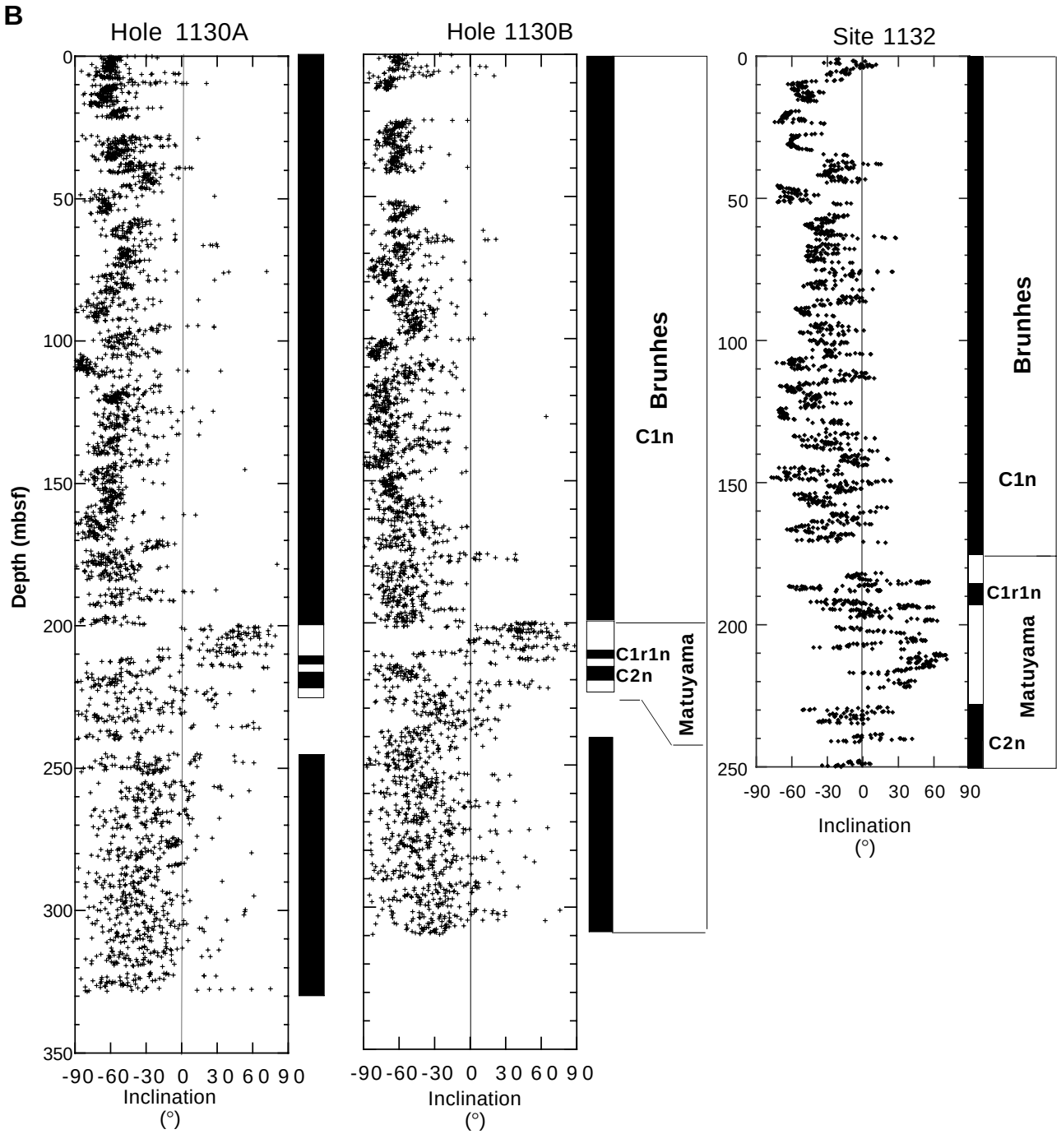
B
Hole 1130A
Hole 1130B
Site 1132
Depth (mbsf)
0
50
100
150
200
250
300
350
-90 -60 -30 0 30 60 90
Inclination
(°)
Brunhes
C1n
C1r1n
C2n
Matuyama

Figure 7B

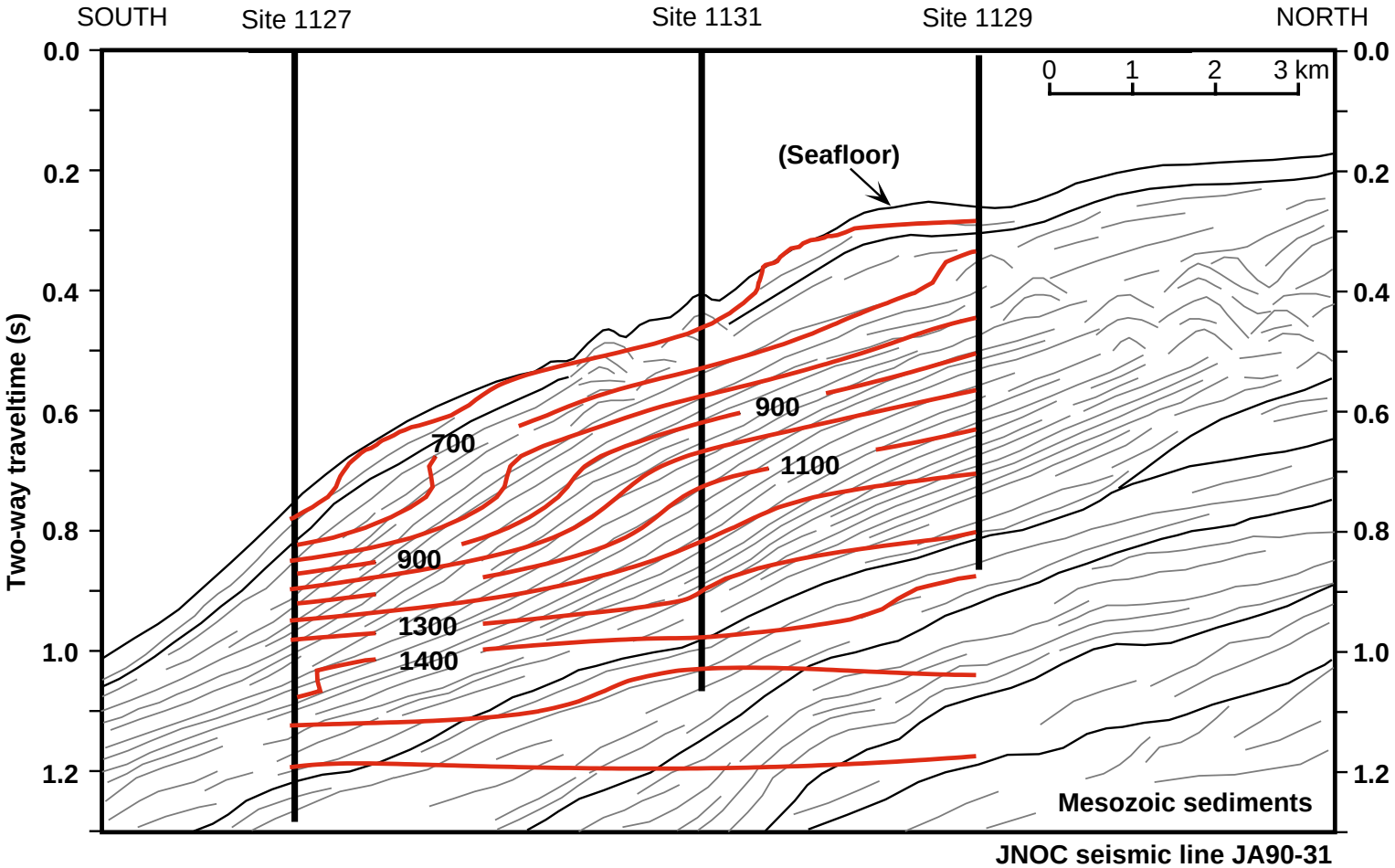
SOUTH
Site 1127
Site 1131
Site 1129
NORTH
0.0
0.2
0.4
0.6
0.8
1.0
1.2
Two-way traveltime (s)
0 1 2 3 km
(Seafloor)
700
900
1100
900
1300
1400
Mesozoic sediments
JNOC seismic line JA90-31

Figure 8

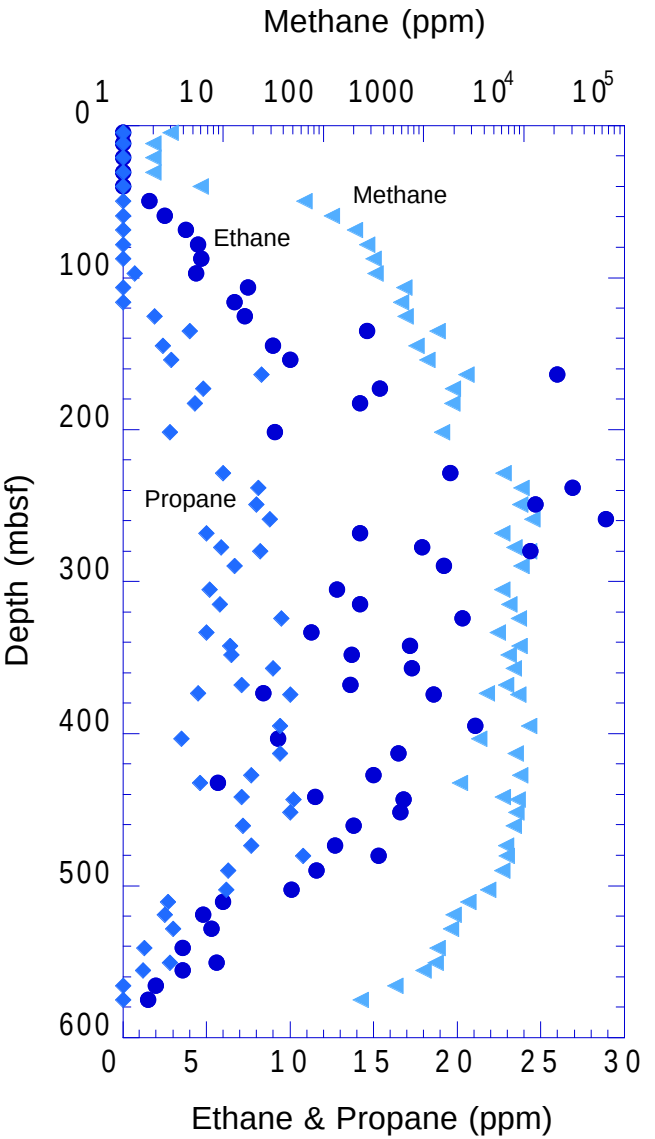
Methane (ppm)
1
10
100
1000
10^4
10^5
0
100
200
300
400
500
600
Depth (mbsf)
Methane
Ethane
Propane
0
5
10
15
20
25
30
Ethane & Propane (ppm)

Figure 9

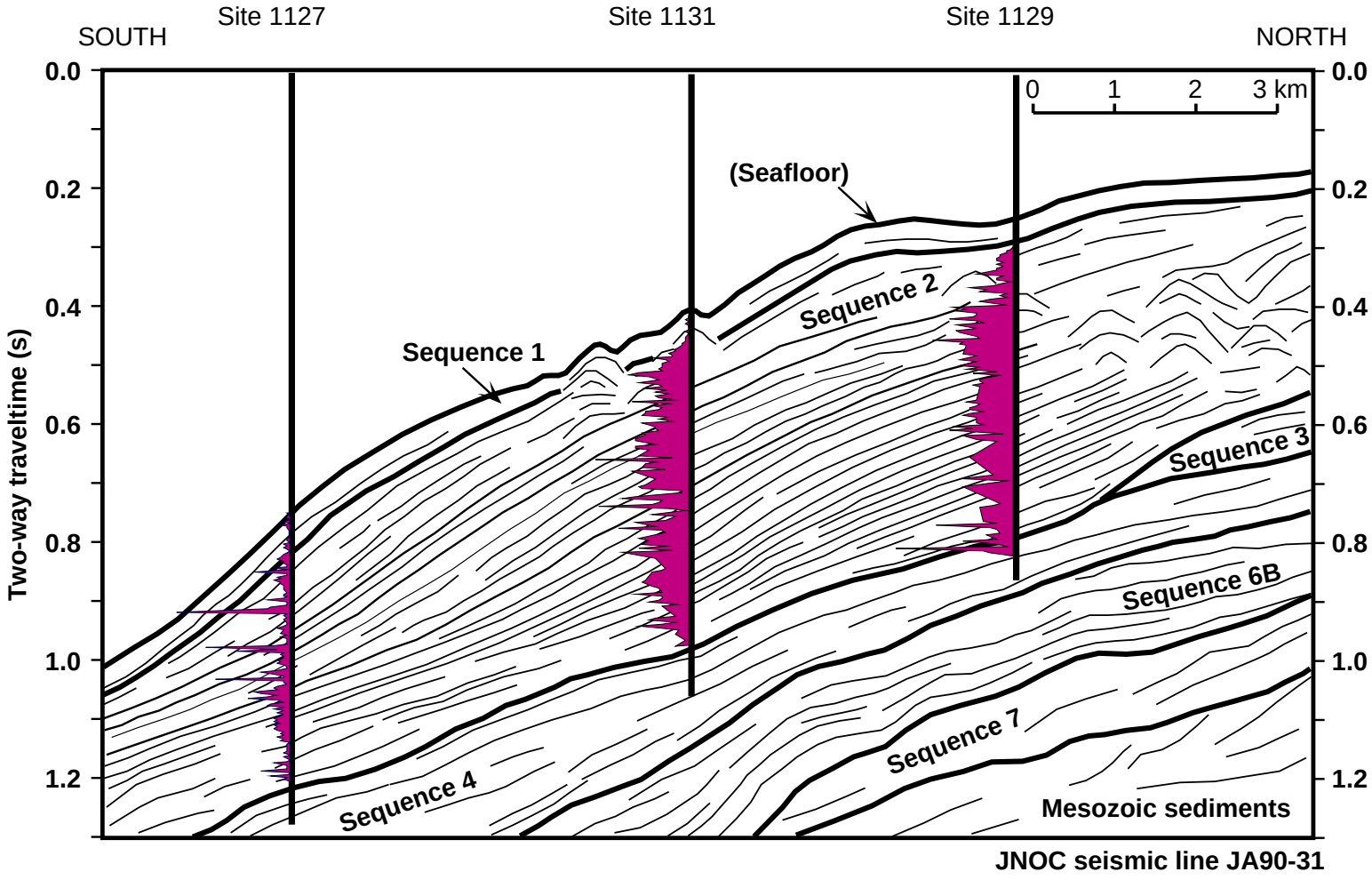
Site 1127
Site 1131
Site 1129
SOUTH
NORTH
0.0
0.2
0.4
0.6
0.8
1.0
1.2
Two-way traveltime (s)
0
1
2
3 km
(Seafloor)
Sequence 1
Sequence 2
Sequence 3
Sequence 4
Sequence 6B
Sequence 7
Mesozoic sediments
JNOC seismic line JA90-31

Figure 10

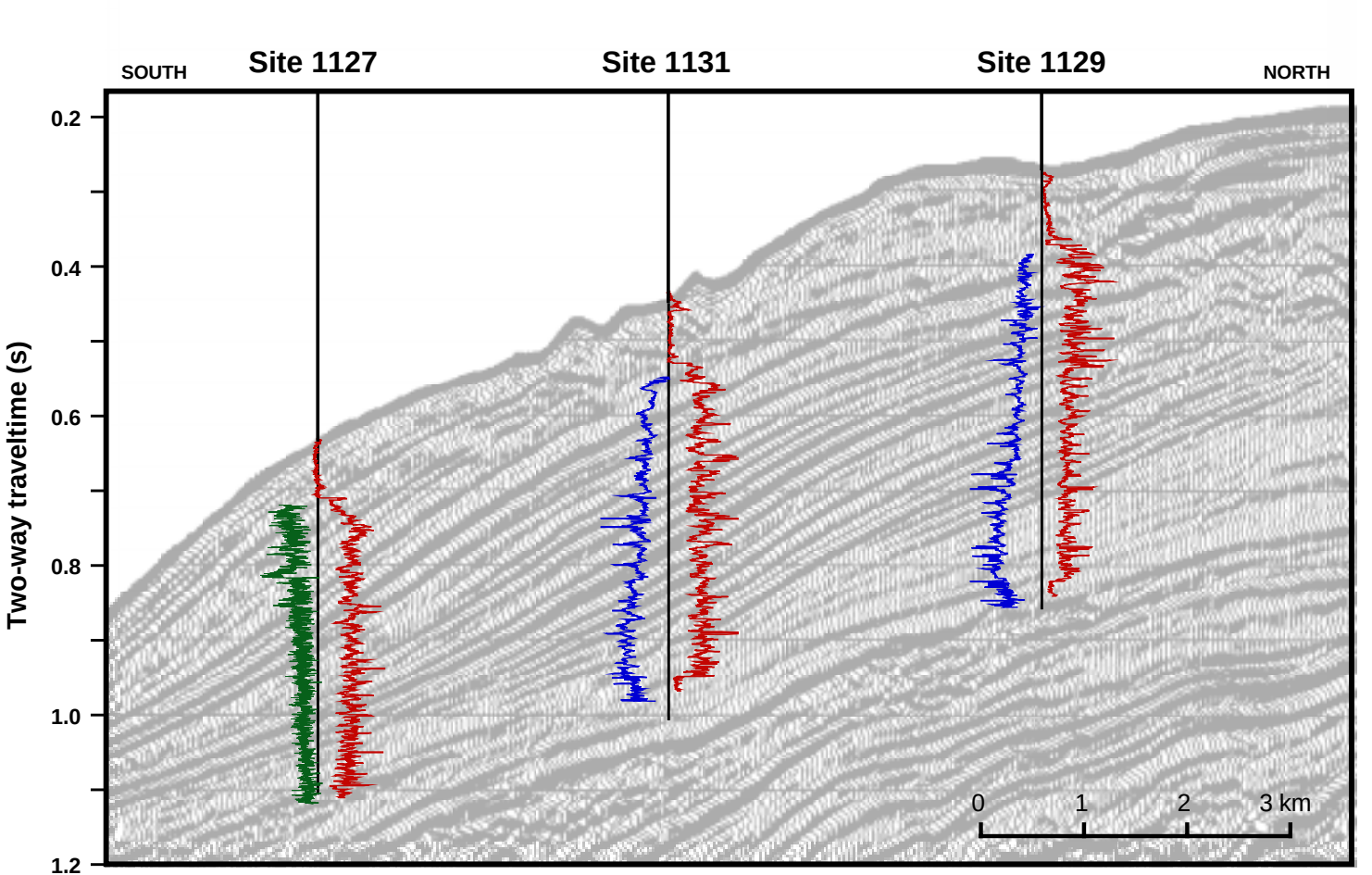
SOUTH
Site 1127
Site 1131
Site 1129
NORTH
Two-way traveltime (s)
0.2
0.4
0.6
0.8
1.0
1.2
0
1
2
3 km

Figure 11

OPERATIONS SYNOPSIS

The operations and engineering personnel aboard *JOIDES Resolution* for Leg 182 were:

ODP Operations Manager:	Gene Pollard
Schlumberger Engineer:	Robert Laronga

SUMMARY OF LEG 182 ENGINEERING AND DRILLING OPERATIONS

Port Call Activities and Transit to Site 1126 (GAB-04B)

Leg 182 officially began at 1000 hr on 8 October 1998 with the first line ashore in Wellington, New Zealand, ending Leg 181. All subsequent times in this volume are local time (e.g., Universal Time Coordinated [UTC] + 8 hr for the Leg 182 operational area), unless otherwise noted. Leg 181 had been extended 12 hr, shortening the time available to complete port call activities for Leg 182, despite the vessel's eventual early arrival. After completion of most of the port call activities, the ship's departure was scheduled for 0800 hr on 13 October. However, we were delayed further by a storm with sustained winds of 45 kt, gusting to 60 kt.

The storm moderated overnight to 25-kt winds with 35-kt gusts and the ship departed at 0809 hr on 14 October. We quickly encountered the first of numerous gale-force storms, and the ship's course was diverted several times to the north to avoid the strength of the storms and to maintain speed. Much of the transit across the Tasman Sea encountered nearly continuous high seas and swells (as high as 9 m) with green water and spray over the bow, and an opposing current (~1 kt) and winds (25–50 kt). The weather did not moderate for more than a few hours at a time until the ship passed through Bass Strait into the Great Australian Bight. Propulsion motor P-17B failed with armature problems on the transit and was inoperable for the rest of the leg. The 2375-nmi sea voyage required 11.8 days (8.4 kt average) instead of the 8.7 days (at 10.5 kt) that was projected precruise. The longer transit time, combined with the extra day spent in Wellington waiting on the weather, forced the decision to shift the initial site from GAB-03B to GAB-04B. GAB-03B was dropped to alternate status.

Hole 1126A

A positioning beacon was launched at 2257 hr on 25 October to start Site 1126. The ship was stabilized on position, and an advanced hydraulic piston core/extended core barrel (APC/XCB) bottom-hole assembly (BHA) was run to 796 meters below rig floor (mbrf) and Hole 1126A was spudded at 0530 hr on 26 October. Core 1H recovered 9.69 m, which was not appropriate for establishing a good mudline. The bit was repositioned to take another mudline core, ending Hole 1126A at 0600 hr on 26 October.

Hole 1126B

The ship was not moved, and Hole 1126B was spudded at 0630 hr on 26 October. The bit was positioned at 792 mbrf, and Core 1H recovered 6.56 m, indicating the seafloor was at 783.8 meters below sea level (mbsl). APC coring advanced to 104.0 meters below seafloor (mbsf), orienting Cores 3H to 11H. Cores 10H to 12H encountered chert horizons, causing only partial strokes of the piston. The APC shoe was damaged during firing of Core 12H, bending the cutting shoe and plugging the nozzles in the core bit. The next APC coring attempt failed despite firing

pressures of 3000 psi with the bit at 1 m off bottom; therefore, an XCB bit was dropped to deplug the throat of the drilling bit. This configuration allows water to circulate through the XCB core barrel during drilling and wash away any soft material. Thus, Core 13W (104.0–109.5 mbsf) was considered a wash interval; however, a few pieces of chert were recovered (0.2 m) and curated.

APC coring resumed from 109.5 to 124.5 mbsf with Core 15H encountering chert layers and bending another APC shoe. The XCB bit was dropped again and the chert interval (124.5–128.8 mbsf) was washed with no recovery. APC coring advanced to 160.3 mbsf (Core 20H) before penetration was again prevented by chert horizons. The Davis-Villinger Temperature Probe (DVTP) was deployed after Core 19H, but the ship's heave prevented quality data collection. Coring continued with the XCB to 263.3 mbsf (Core 32X) and was terminated when the last four coring runs destroyed both hard and soft XCB cutting shoes. The bit was pulled and cleared the seafloor at 1415 hr on 27 October.

Hole 1126C

The ship was moved 20 m east of Hole 1126B, and Hole 1126C was spudded at 1540 hr on 27 October. The bit was positioned at 794 mbrf, and Core 1H recovered 8.48 m, indicating a water depth of 783.8 m. APC coring advanced to the approximate depth of the chert horizons found in Hole 1126A. Cores 3H through 9H were oriented and Adara tool heat-flow measurements were made during Cores 4H, 6H, and 8H. As with the DVTP, the heave from long-period swell disturbed all three Adara tool runs. Coring continued with the XCB from 84.5 to 138.4 mbsf through the chert-rich intervals. We switched back to APC coring for Core 16H; however, the core was a partial stroke (6.0 m) and the APC shoe had been dented severely. A final XCB core (17X) was cut from 144.4 to154.0 mbsf with 46% recovery. The bit was pulled and cleared the rotary at 0615 hr on 28 October, ending Hole 1126C.

Hole 1126D

A rotary core barrel (RCB) BHA was run to the seafloor, which was tagged at 795.0 mbrf (783.8 mbsl). The hole was drilled from 0 to 150.0 mbsf at 42.9 m/hr with a center bit in place. The interval from 150.0 to 463.3 mbsf was RCB cored (Cores 1R–33R) with 12.9% recovery. Recovery was poorest in soft nannofossil oozes interbedded with chert because of chert blocking the throat of the bit or jamming in the core catcher, preventing softer material from entering the core barrel. The recovery increased to ~22% below 350 mbsf as the induration increased.

After coring was terminated, the hole was prepared for logging. This preparation included a wiper trip to 107 mbsf, circulation of a sepiolite mud pill, and release of the bit. The drill pipe was pulled to 117 mbsf, which placed the end of pipe below the first prominent chert layer to protect the logging tools and wireline in anticipated high-heave conditions. The triple

combination log was run from 441 mbsf (22 m off bottom) to the end of pipe at 117 mbsf. During logging, the wireline heave compensator occasionally reached its maximum stroke of 6 m. The caliper on the triple combo logging tool showed that hole conditions were poor with prominent washouts. To protect the tool from damage, the formation microscanner (FMS) was not deployed in these conditions. Therefore, the sonic tool was combined with the Geologic High Resolution Magnetic Tool (GHMT; magnetic susceptibility only; total field was inoperable), and the tool string was run from 440 mbsf to the mudline. In the final logging run, the generator-injector (GI) air gun and the well seismic logging tool (WST) were deployed for a check-shot survey. The drill pipe cleared the rig floor at 1530 on 30 October, ending operations at Site 1126.

Transit to Site 1127

The 23-nmi transit to Site 1127 was completed in 2.5 hr at 9.2 kt. A beacon was deployed at 1800 hr on 30 October, initiating operations at Site 1127. A second beacon was dropped to provide another working beacon for shallow-water operations, but it produced an erratic signal and was subsequently observed floating away, apparently self-released. A third beacon was deployed and the ship was stabilized on position.

Hole 1127A

An APC/XCB BHA was run to the seafloor, and Hole 1127A was spudded at 2110 hr on 30 October, recovering 9.68 m. Core 1H was curated, but the hole was terminated because recovery was inappropriate for establishment of a good mudline. The bit was repositioned for another mudline core, ending Hole 1127A at 2130 hr on 30 October.

Hole 1127B

The ship was not moved, and Hole 1127B was spudded at 2130 hr on 30 October. The bit was positioned at 487 mbrf, and Core 1H recovered 5.86 m, which indicated a water depth of 479.3 mbsl. APC coring advanced to 148.4 mbsf, orienting Cores 3H–16H. A noticeable odor of H_2S was detected in Core 1H. H_2S concentrations were first measured with a handheld device on Core 4H, which reached the maximum capability (2000 ppm) of the instrument. Core 6H (46.9 mbsf) had H_2S concentrations of 94,953 ppm (gas chromatograph) measured from a gas void in the core (vacutainer). Coring operations were suspended for 2.5 hr while H_2S safety procedures were implemented. These procedures included prepping crews, deploying safety equipment (e.g., Scott air packs), posting notices, installing curtains and a suction hose in the laboratory cutting room, deploying fans and fixed sensors, and increasing interior laboratory ventilation. The ship heading was rotated to maintain maximum air flow over the core handling area and air suction for the accommodation. Once a section was judged safe to enter the laboratories (Foss and Julson, 1993), it was run through the multisensor track (MST), split, and allowed to degas under

the vacuum in the splitting room. Ten more cores were taken with little entry of cores into the laboratories. Coring was suspended again to determine an improved method for more rapid degassing of the cores. Sections were run through the MST, split, carried out to the catwalk, and opened there to allow safer and more rapid venting. When the super saw was required to cut cores, sections were split and dressed out in the splitting room and then carried outside for continued venting. APC coring continued thereafter on a core-by-core basis. The coring rate had to be slowed to maintain proper handling and racking of the core, recharging of air packs, and cleaning and airing of core to reduce the ambient H_2S level.

Core 16H had 60K lb overpull with high H_2S concentrations. Therefore, coring was switched to the XCB system for the potential reduction in gas volumes typically observed in switching to XCB coring. Cores 17X and 18X were cut from 148.4 to 164.5 mbsf with good recovery; however, H_2S readings remained ~10^5 ppm. Coring continued with the XCB from 164.5 to 510.7 mbsf (Cores 19X–55X) on a core-by-core basis. Experience proved that coring more rapidly than ~45 min/core exceeded our capacity to process the core on the catwalk while wearing full protective gear.

The hole was prepared for logging with a wiper trip to 100 mbsf, and the bottom was tagged at 510.7 mbsf with no fill. The hole was filled with 180 bbl of sepiolite mud to protect logging tools from potential H_2S exposure, and the logging cable was coated with a 50/50 mixture of Marvel Mystery Oil and diesel. The bit was pulled up to the logging depth at 87 mbsf. The triple combo (without radioactive sources), FMS-Sonic, and GHMT logs were run to 510.7 mbsf. The WST was not required because in this thick, uniform sequence, the Sonic log proved to be adequate. The hole was plugged with 40 bbl of 10.5-ppg mud, and the pipe was pulled. The rig was secured for transit at 0230 hr on 3 November, ending Site 1127.

Transit to Site 1128

The 76-nmi transit to Site 1128 required 8.5 hr at an average speed of 8.9 kt. A beacon was launched at 1100 hr on 3 November initiating Site 1128. Its signal was erratic, however, and another beacon was deployed.

Hole 1128A

The ship was stabilized on position and an APC/XCB BHA was run to the seafloor. Hole 1128A was spudded at 1900 hr on 3 November, recovering 9.31 m in Core 1H. The hole was terminated at 1930 hr on 3 November because the recovery was excessive for establishment of a good mudline.

Hole 1128B

The ship was not moved, and Hole 1128B was spudded at 1955 hr on 3 November. The bit

was positioned at 3882 mbrf and Core 1H recovered 5.66 m, indicating a water depth of 3874.6 mbsl. APC coring advanced to 137.8 mbsf and ceased when a partial stroke on Core 15H bent the APC shoe. Cores 3H–15H were oriented, and coring continued with the XCB advancing from 137.8 to 280.6 mbsf. The DVTP temperature probe was deployed after Core 16X at 145.8 mbsf. It became apparent that the jet nozzles in the bit were plugged sometime after running the DVTP. The resulting increased pump pressure required to maintain circulation may have caused reduced recovery in Cores 17X and 18X. Recovery dropped to 28.9% in the last four XCB cores (27X–30X), probably as a result of the bit overheating, despite attempts to increase circulation and pressure. Coring was terminated because of the low recovery in the last four cores and increasing drilling times. The bit cleared the seafloor at 1515 hr on 5 November, ending Hole 1128B.

Hole 1128C

The ship was moved 20 m east, and Hole 1128C was spudded with the APC at 1640 hr on 5 November. The bit was positioned at 3884 mbrf, and Core 1H recovered 7.95 m, indicating a water depth of 3874.3 mbsl. APC coring advanced to 138.3 mbsf, ceasing again with a partial stroke at Core 15H and a bent APC shoe. Cores 3H–15H were oriented and Adara tool heat-flow measurements were taken at Cores 4H, 8H, and 12H. A special nonmagnetic assembly was run on the bottom two-thirds of the APC inner core barrel on Cores 3H, 5H, 7H, 9H, 11H, and 13H. Coring resumed with the XCB to the depth objective of 240.1 mbsf. The drill string was recovered at 0330 hr on 7 November, terminating Hole 1128C.

Hole 1128D

The ship was moved 20 m north of Hole 1128C, and an RCB BHA was run to the seafloor. Hole 1128D was spudded at 1115 hr on 7 November, and the hole was drilled ahead with a center bit to 231.2 mbsf. RCB coring advanced from 231.1 to 452.6 mbsf with 35.7% recovery. Coring was terminated when drilling times increased and recovery decreased to unacceptable levels. The hole was prepped for logging, and the end of the drill pipe was placed at 92 mbsf. The triple combo tool string was run but was unable to pass 96 mbsf. The tool was pulled out, and the pipe run to 112 mbsf. The triple combo was rerun through a tight spot at ~250 mbsf from 428 mbsf (24 m off bottom) to the mudline. The FMS/Sonic tool string was deployed and logged from 424 mbsf to the end of the pipe. Operational time constraints precluded deployment of the WST. The hole was displaced with mud, the drill string retrieved and secured, and the ship was under way to Site 1129 at 0130 on 11 November.

Transit to Site 1129

The 80-nmi transit to Site 1129 required 8.5 hr at an average speed of 9.4 kt. A beacon was

launched at 1030 hr on 11 November, initiating Site 1129. A second beacon was deployed a few minutes later. Although the sea state was marginal for shallow-water rotary operations, the weather forecast was favorable, and an attempt was made to APC core.

Hole 1129A

The ship was stabilized on position, and Hole 1129A was spudded at 1330 hr on 11 November. The bit was positioned at 209 m, and Core 1H recovered 4.35 m, indicating a water depth of 202.9 mbsl. Core 1H recovered coarse-grained, unlithified bryozoan grainstones. Attempts to deepen the hole resulted in the drill string standing up in the elevators on the coarse-grained bottom. With these conditions, attempts to make a pipe connection were difficult. Thus, the hole was drilled down from 4.3 to 13.8 mbsf in an attempt to deepen the hole below the unstable section. Core 2H was taken from 13.8 to 23.3 mbsf; however, the pipe continued to stand up in the elevators and the heave caused the bit to pound on bottom. Hence, drilling was terminated because of shallow-water operational limitations. The pipe was pulled, both beacons were recovered, and the rig was secured for transit to Site 1130 at 1700 hr on 11 November.

Transit to Site 1129 (Hole 1129B)

Hole 1129A was terminated because of the combination of coarse-grained sediments and the marginal sea conditions for shallow-water drilling. With an improving weather forecast, the vessel returned to Site 1129 to attempt another hole. The ship was moved in dynamic positioning (DP) mode from Site 1131 back to Site 1129, and the 2-nmi transit required 0.6 hr at 3.3 kt. A beacon was dropped at 1820 hr on 19 November, followed by a second beacon, and the ship was positioned ~20 m east of Hole 1129A.

Hole 1129B

By drilling in approximately two to three joints and cleaning out the coarse-grained material with frequent mud sweeps, we thought it was possible to establish a stable hole. Hole 1129B was spudded at 2030 hr on 19 November and drilled from 0 to 22.0 mbsf with two, 20-bbl mud sweeps circulated on each connection. However, the bit required 40 kilo-pounds (kips) overpull to pull up on the second connection, and 5 m of fill was noted immediately after running back to bottom. The procedure was repeated with 5 m of fill noted again. APC coring deepened the hole from 22.0 to 41.0 mbsf, recovering unlithified bryozoan grainstones and rudstones. Despite pumping three more 20-bbl mud sweeps, the hole conditions remained unstable. Thus, Hole 1129B was abandoned, the drill string retrieved, and one beacon was recovered. The second beacon released but was never sighted. The rig was secured for transit back to Site 1131 at 0230 hr on 20 November.

Transit to Site 1129 (Hole 1129C)

The second attempt to core at Site 1129 suggested that the unlithified coarse-grained deposits at the top of the section were too unstable for successful coring while maintaining hole integrity. A reexamination of the seismic data indicated that a finer grained surficial succession might exist only 0.43 nmi south of Hole 1129B, at the intersection of seismic Lines 169/05a and 169/05m. Approval was requested and received to spud Hole 1129C in these presumably finer grained sediments. The 44-nmi sea voyage from Site 1132 back to Site 1129 required 4.75 hr at 9.3 kt. A beacon was dropped at 2324 hr on 24 November, initiating operations.

Hole 1129C

The bit was positioned at 212.0 m, and Hole 1129C was spudded successfully at 0200 hr on 24 November. Core 1H recovered 7.29 m, indicating a water depth of 202.4 mbsl. APC coring advanced to 216.3 mbsf with 96.2% recovery. Cores 3H–23H were oriented and Adara tool heat-flow measurements were made on Cores 4H, 8H, 10H, and 20H. The nonmagnetic APC cutting shoe was run with a standard steel flapper and 10-finger core catcher on Cores 3H, 5H, 7H, 9H, 11H, and 13H. A 20-bbl mud sweep was circulated after every fifth core. H_2S gas was detected in the core barrel on the rig floor on Core 6H, and H_2S alert procedures were implemented. The last two APC cores were partial strokes, and the last three cores had shattered liners, prompting the switch to the XCB system. XCB coring deepened the hole from 216.3 to 451.6 mbsf with 48.7% recovery. Coring had to be terminated because of deteriorating weather conditions, which caused heave to exceed shallow-water limitations. The hole was abandoned with 150 bbl of mud. The drill string was retrieved, and the rig floor was secured for transit at 1830 hr on 26 November.

Transit to Site 1129 (Hole 1129D)

Improving weather conditions provided the opportunity to complete operations near Hole 1129C with an RCB hole and logging. The 26-nmi transit from Site 1133 to Site 1129 required 2.5 hr at an average speed of 10.4 kt. A beacon was deployed at 1642 hr on 28 November, and the ship was positioned on location.

Hole 1129D

A standard RCB BHA was run to the seafloor, and Hole 1129D was spudded at 1915 hr on 28 November. The hole was drilled with a center bit from 0 to 280.0 mbsf in 7 hr. RCB spot cores were taken from 280.0 to 299.6 mbsf with 16.1% recovery. After H_2S was detected in Core 1R, H_2S alert procedures were implemented. The hole was drilled again with a center bit from 299.6 to 373.2 mbsf in 2.75 hr., and RCB coring resumed from 373.2 to 604.2 mbsf with overall recovery of 30.6%. A wiper trip was performed in preparation for logging, noting 1 m of fill on bottom, and the bit was released with the mechanical bit release (MBR). The hole was filled with

mud, and the end of pipe was positioned at 100 mbsf. The following logging tool strings were run from 604 mbsf: (1) triple combo, (2) FMS-Sonic, and (3) WST in a 10-station check-shot survey. The pipe was run in to 150 mbsf, and the hole was abandoned with 50 bbl of mud. Both beacons were recovered, and the rig floor was secured for transit at 2215 hr on 29 November, ending operations at Site 1129.

Transit to Site 1130

The 45-nmi transit to Site 1130 required 4.5 hr at an average speed of 10.0 kt. A beacon was launched at 2207 hr on 11 November, followed by a second beacon, initiating Site 1130.

Hole 1130A

The ship was stabilized on position and an APC BHA was run to 476 mbrf, based on the readings from the precision depth recorder (PDR). The first two attempts to spud the hole resulted in no recovery, indicating that the PDR depth was inaccurate. The PDR computer was reinitialized and the bit was positioned at 497 mbrf, closer to the estimated water depth in the leg prospectus. Hole 1130A was spudded at 0200 hr on 11 November, and Core 1H recovered 8.48 m, indicating a water depth of 486.7 mbsl. APC coring advanced to 170.0 mbsf, ceasing when 90 kips could not dislodge Core 18H, which required drilling over the core barrel to release it. The nonmagnetic shoe, flapper, and liner seal sub were deployed on Cores 3H, 5H, 7H, and 9H. The bottom portion of Core 3H was lost when the single, nonmagnetic flapper core catcher failed. Cores 3H–18H were oriented and Adara tool heat-flow measurements were taken on Cores 4H and 8H. The DVTP temperature probe was deployed after Core 12H at 113.0 mbsf.

Coring resumed with the XCB from 170.0 to 380.5 mbsf. The last six cores (Cores 36X–41X) had 3.4% recovery in interbedded cherts and chalks. Two soft-formation XCB shoes were destroyed when chert beveled out the throat of each shoe. As a safety precaution before penetrating Sequence 7 sandstones, operations were slowed (after Core 33X) to allow hydrocarbon gas monitoring to be completed before proceeding with each succeeding core. Only background levels of gas were detected. The pipe became stuck at 378 mbsf after Core 41X; however, it was pulled free with 70 kips overpull. Hole 1130A was terminated because of poor recovery in the sandstones with the XCB system. The hole was filled with mud, and the drill string was recovered, clearing the seafloor at 1815 hr on 13 November.

Hole 1130B

The ship was moved 20 m west and Hole 1130B was spudded at 1915 hr on 13 November. The bit was positioned at 494 mbrf, and Core 1H recovered 3.93 m, indicating a water depth of 488.1 mbsl. APC coring advanced to 156.0 mbsf. Cores 3H–17H were oriented and an Adara tool heat-flow measurement was taken on Core 6H. The nonmagnetic core barrel assembly was

deployed on Cores 3H, 5H, 7H, 9H, 11H, and 13H. Core 3H was lost when it slipped past the single nonmagnetic flapper catcher; thus, a steel 10-finger core catcher was added to the nonmagnetic core barrel assembly thereafter. XCB coring was advanced to the depth objective of 310.4 mbsf with 101.2% recovery in chalk. After plugging the hole with mud, the drill string was recovered, clearing the rig floor at 1530 hr on 14 November.

Hole 1130C

The ship was moved 20 m north and Hole 1130C was spudded with the RCB at 1830 hr on 14 November. The interval from 0 to 299.2 mbsf was drilled, followed by a one-stand wiper trip to 331 mbsf to condition the hole. Coring resumed with the RCB from 299.2 to 395.2 mbsf. The rotary stalled while cutting Core 9R; however, the pipe was worked free in 15 min with 50 kips overpull. Rotation and circulation were regained, and a mud sweep was circulated. Core 10R was cut from 385.6 to 395.2 mbsf, after which the pipe became stuck again in presumably friable and variably indurated sandstones. The pipe could not be freed, so the bit was released with the MBR. The pipe was worked free after 2.5 hr, and circulation and rotation were reestablished. However, coring operations were terminated because hole conditions were too unstable to continue under shallow-water operational guidelines. The end of pipe was pulled to 106 mbsf in preparation for logging. Logging tools were run in the following order: (1) triple combo (368.5 mbsf, 26.7 m off bottom, to the mudline) in two runs because of failure of the wireline heave compensator on the first run; (2) FMS/Sonic (368.9–90.5 mbsf) in two runs; and (3) well seismic tool (WST; 363.5 mbsf to the end of the pipe) with eight stations ~30 m apart. After conclusion of logging operations, the hole was plugged with mud, the rig secured for transit, and the vessel departed for Site 1131 at 0845 hr on November 16.

Transit to Site 1131

Because of long-period swell (~3 m high) and the resulting heave, which averaged 1.5 m with excursions over 2.0 m, operations in water depths less than 300 m were precluded. Thus, we proceeded to alternate Site GAB-08A. The 46-nmi transit required 4.6 hr at an average speed of 10.0 kt. A beacon was launched at 1338 hr on 16 November, initiating Site 1131. A second beacon was deployed, as required for shallow-water operations.

Hole 1131A

The ship was stabilized on position, and an APC/XCB BHA was run to the seafloor. Hole 1131A was spudded at 1605 hr on 16 November. The bit was positioned at 339 mbrf, and Core 1H recovered 3.39 m, indicating a water depth of 333.6 mbsl. APC coring advanced to 60.4 mbsf. Cores 3H–7H were oriented, and an Adara tool heat-flow measurement was made during Core 4H. A nonmagnetic cutting shoe and a steel 10-finger core catcher were run on Cores 3H,

5H, and 7H. Recovery of Core 7H required 70 kips overpull; therefore, APC coring was terminated in favor of the XCB system. H_2S (86 ppm; headspace analysis) was detected in Core 4H (26.9 mbsf). H_2S alert procedures were implemented, including use of breathing apparatus. H_2S concentrations reached a maximum of 156,600 ppm in a vacutainer sample (359.6 mbsf), but ambient air readings remained below 10 ppm. No H_2S was detected below Core 56X (>511.3 mbsf)

XCB coring advanced from 60.4 to 616.9 mbsf with 56.3% recovery. Recovery was minimal below 540.2 mbsf in presumed mixed chalk and chert, and five XCB hard-formation shoes were destroyed. Hydrocarbon gases up to C_5 were detected beginning with Core 38X (338.3 mbsf), and the coring rate was controlled to allow proper gas monitoring. However, C_{2+} volumes were extremely low and subsequently diminished downhole; C_1/C_2 varied primarily as a function of methane fluctuation. Coring was terminated near the depth objective because of poor recovery in cherts.

Hole conditions appeared to be excellent, and the bit was pulled to 102 mbsf without a conditioning trip for logging. Logging tools were run in the following order (depths of penetration are included): (1) triple combo from 578 mbsf, 39 m off bottom, to the mudline in two passes; (2) FMS-Sonic from 573 mbsf to the end of pipe; and (3) WST tool from 567 mbsf to the end of pipe, recording eight check-shot stations. With an improving forecast and diminishing long-period swell, continued operations at Site 1131 were postponed for a return to Site 1129. After plugging the hole with mud, the drill string was retrieved, both beacons were recovered, and the rig was secured for transit at 1800 hr on 19 November, ending Hole 1131A.

Transit Back to Site 1131 (Hole 1131B)

The ship was moved in DP mode from Site 1129 back to Site 1131 to complete a second APC/XCB hole. The 2-nmi transit required 1 hr at 2 kt. A beacon was dropped at 0335 hr on 20 November, and the ship was positioned ~40 m north of Hole 1131A.

Hole 1131B

Hole 1131B was spudded at 0545 hr on 20 November. The bit was positioned at 342.0 mbrf, and Core 1H recovered 8.40 m, which indicated a water depth of 331.4 mbsl. APC coring advanced to 65.4 mbsf with 94.0% recovery. Cores 3H–7H were oriented and an Adara tool heat-flow measurement was taken on Core 6H. The nonmagnetic shoe and flapper core catcher with a steel 10-finger core catcher were deployed on Cores 3H, 5H, and 7H. H_2S was detected in Core 5H at 46 mbsf, and H_2S alert procedures were implemented. XCB coring extended the hole from 65.4 to 105.8 mbsf with 83.3% recovery. A DVTP was deployed after Core 12X at 105.8 mbsf. The hole was plugged with mud, the beacon recovered, the rig secured for transit, and the vessel was under way for Site 1132 at 1730 hr, on 20 November.

Transit to Site 1132

The 44-nmi sea voyage to Site 1132 required 4.25 hr at 10.4 kt. A beacon was deployed at 2221 hr on 20 November, initiating Site 1132.

Hole 1132A

The ship was stabilized on position, and Hole 1132A was spudded at 0100 hr on 21 November. The bit was positioned at 229.5 m, and Core 1H recovered 9.22 m. However, the excessive recovery was not appropriate for the establishment of a good mudline and the hole was terminated.

Hole 1132B

The ship was not moved and the bit was positioned at 227.5 m, and Hole 1132B was spudded at 0130 hr on 21 November. Core 1H recovered 6.78 m, indicating a water depth of 218.5 mbsl, which suggests the previous assessment of an inappropriate mudline in Hole 1132A was correct. APC coring advanced to 168.3 mbsf, ceasing after four of the five last APC cores were recovered with split liners. Cores 3H–18H were oriented and Adara tool heat-flow measurements were taken on Cores 4H, 8H, and 12H. The nonmagnetic shoe and flapper core catcher with a steel 10-finger core catcher were run on Cores 3H, 5H, 7H, 9H, 11H, and 13H. A DVTP temperature probe was deployed after Core 18H at 168.3 mbsf. XCB cores deepened the hole from 168.3 to 284.6 mbsf. Drilling times increased after Core 24X (219.5 mbsf) and recovery was poor below Core 28X (257 mbsf), thus Hole 1132B was terminated four cores later. The fishing vessel *Bolzano* was hired to deliver to the *Resolution* six self-contained breathing apparatus, two air-tank filler fittings, and 10 air-filling station filters. The *Bolzano* arrived at Site 1132 at 0200 hr on 21 November, discharged its cargo in four crane lifts, and departed at 0315 hr. The hole was plugged with mud, and the drill string was pulled to the rig floor at 0425 hr on 22 November, ending Hole 1132B.

Hole 1132C

The ship was moved 20 m northwest, and the standard RCB/BHA was run to the seafloor, spudding Hole 1132C at 0735 hr on 22 November. The hole was drilled to 161.6 mbsf with a center bit in 3.5 hr. The center bit was retrieved and RCB Cores 1R and 2R were cut from 161.6 to 180.4 mbsf in a successful effort to sample a low recovery interval from Hole 1132B. The hole was then drilled from 180.4 to 255.8 mbsf in 3.25 hr. Coring resumed with the RCB from 255.8 to 603.2 mbsf with low recovery in interbedded cherts and packstones. With no recovery in the last four cores and vigorous backflow occurring on pipe connections, a precautionary wiper trip was made to verify hole conditions. The pipe was pulled up to 535 mbsf with heavy backflow. The bit deplugger was dropped in case the annulus was plugged with debris, causing the

backflow. The bottom was tagged at 574 mbsf, indicating 29 m of fill in the bottom of the hole. The hole was cleaned to continue coring, ultimately clearing out 9 m of the fill. However, the pipe became stuck with 40 kips overpull, stalling the rotary. The pipe was worked free, and another mud sweep was circulated. A full wiper trip was made to 105 mbsf with heavy backflow and fill was tagged at 560 mbsf (43 m off the bottom). With these unstable conditions, it appeared unlikely that the hole could be safely deepened at these shallow-water depths. Thus, coring was terminated and another mud sweep was circulated, the bit was dropped with the MBR, and the sleeve was closed. The hole was loaded with 150 bbl of mud in an effort to stabilize the hole.

The end of pipe was pulled to 105 mbsf for logging. The Triple combo log was run from 470 to 397 mbsf and rerun from 560 mbsf to the mud line. The FMS-Sonic tool could not be worked past 163 mbsf, so it was run from 163 to 80 mbsf. The open-ended pipe was advanced from 105 to 89 mbsf to guide the logging tool through a presumed ledge; however, the FMS-Sonic tool could not pass 203 mbsf. The pipe was advanced again to 242 mbsf to push past any obstructions, where it stopped with 25 kips weight on the pipe. The drill string started hydraulically lifting when an attempt was made to circulate, which suggested that it was buried in fill. The end of pipe was pulled up to 105 mbsf and the FMS-Sonic tool was rerun in attempt to log the upper portion of the hole. However, the tool could not pass 180 mbsf, and the log was run from that depth. The hole was plugged with mud, the drill string retrieved, and both beacons recovered. The rig was secured for transit and the vessel was under way at 1815 hr on 24 November.

Transit to Site 1133

The 26-nmi sea voyage to Site 1133 required 3.0 hr at 8.7 kt. A beacon was dropped at 2200 hr on 26 November, initiating Site 1133.

Hole 1133A

The ship was stabilized on position and Hole 1133A was spudded at 0215 hr on 27 November. The bit was positioned at 1049 mbrf, and Core 1H recovered 9.78 m. However, the excessive recovery was not appropriate for the establishment of a good mudline, and the hole was terminated.

Hole 1133B

The ship was not moved, the bit was repositioned at 1042 mbrf, and Hole 1133B was spudded at 0245 hr on 27 November. Core 1H recovered 2.40 m, indicating a water depth of 1037.2 mbsl. APC coring advanced to 50.9 mbsf, with Cores 3H–7H oriented and an Adara tool heat-flow measurement on Core 4H. The nonmagnetic core barrel assembly was run on Cores

3H, 5H, and 7H. XCB coring deepened the hole from 50.9 to 152.1 mbsf. Recovery was very poor after Core 8X in mixed chert and unlithified bioclastic wackestones and packstones. While attempting to start the next core, the circulating pressure jumped to 2000 psi and the torque became erratic, indicating that the hole had caved in and was packing off the bit. The pipe was worked free, but the hole was judged unstable and operations were terminated. The bit cleared the seafloor at 2200 hr on 27 November.

Hole 1133C

The ship was moved 20 m south, and Hole 1133C was spudded at 2200 hr on 27 November. Core 1H was taken with the bit at 1045 mbrf and recovery was 5.74 m, indicating a water depth of 1036.8 mbsl. APC coring advanced to 53.3 mbsf with 69.9% recovery. The APC/XCB and RCB BHAs were inspected in 6 hr on the trip out, and no defects were noted. Both beacons were recovered, and the ship was secured for transit at 1330 hr on 28 November, ending Site 1133. A helicopter was dispatched to remove an ODP crew member because of a death in the family. The helicopter arrived at 1354 hr on 28 November and departed 2 min later, and the vessel was under way.

Transit to Site 1134

The 63-nmi transit required 6.25 hr at 10.1 kt. A beacon was dropped at 0430 hr on 1 December, initiating operations at Site 1134.

Hole 1134A

The ship was stabilized on position and the bit was positioned at 708 mbrf. Hole 1134A was spudded at 0840 hr on 1 December, recovering 4.50 m in Core 1H, which indicated a water depth of 701.0 mbsl. APC coring advanced to 126.0 mbsf, ceasing after a liner shattered and the regular APC cutting shoe was damaged upon striking a presumed chert interval on Core 14H. Cores 3H–14H were oriented and an Adara tool heat-flow measurement was performed on Core 4H. The nonmagnetic cutting shoe and flapper core catcher, with a steel 10-finger core catcher, were deployed on Cores 3H, 5H, 7H, 9H, 11H, and 13H. XCB coring deepened the hole from 126.0 to 397.1 mbsf, with 25.0% recovery. A short wiper trip was made to 348 mbsf to check hole conditions, and 13 m of fill was noted on bottom. Consequently, a hole-conditioning trip was made to 105 mbsf; however, 20 m of fill was noted when bottom was tagged again. Coring was terminated because of the unstable hole conditions. The hole was cleaned out to bottom, filled with mud, and then the bit was pulled up to 105 mbsf in preparation for logging. The following logs were run from 388 mbsf: (1) Triple combo, (2) FMS-Sonic, and (3) WST tool, recording seven check-shot stations. The pipe was retrieved, clearing the seafloor at 1335 hr on 3 December, ending Hole 1134A.

Hole 1134B

The ship was moved 20 m north, and the bit was positioned at 711 mbrf. Hole 1134B was spudded at 1455 hr on 3 December, recovering 8.60 m in Core 1H, which indicated a water depth of 699.9 mbsl. APC coring advanced to 122.6 mbsf and Cores 3H–13H were oriented. The nonmagnetic cutting shoe, flapper core catcher with a steel 10-finger core catcher, and nonmagnetic core barrel were run on Cores 3H, 5H, 7H, 9H, 11H, and 13H. XCB coring deepened the hole from 122.6 to 234.8 mbsf, after which coring was terminated because available operational time was depleted. The drill string was retrieved, the rig was secured for transit, and the vessel was under way at 1130 hr on 4 December.

Transit to Fremantle

The 820-nmi sea voyage to Fremantle, Australia, required 79.9 hr at an average speed of 10.3 kt. The first line was ashore at Fremantle Harbor Dock at 1925 hr on 7 December, ending Leg 182.

REFERENCES

Foss, G.N., and Julson, B.D., 1993. Revised hydrogen sulfide drilling contingency plan–*JOIDES Resolution. ODP Tech. Note,* 19.